Journal of Hazardous Materials Advances 23 (2026) 101258

Contents lists available at ScienceDirect

Journal of Hazardous Materials Advances

journal homepage: www.elsevier.com/locate/hazadv

Agricultural pollution mitigation using iron-enriched biochar

Shahidul Islam [1,2,*]

USDA Regulatory Science Center, School of Agriculture, Fisheries and Human Sciences, University of Arkansas at Pine Bluff, 1200 North University Drive, 148 Woodard Hall, Mail Slot 4913, Pine Bluff, AR 71601, USA

ARTICLE INFO

Keywords:
Iron-enriched biochar
Agricultural pollution
Heavy metal immobilization
Nutrient retention
Soil remediation
Circular economy
Fenton-like catalysis

ABSTRACT

Agricultural pollution remains one of the most serious environmental issues of the Anthropocene, driven by intensive farming practices that release excess nutrients, heavy metals, pesticides, and emerging contaminants into land and water ecosystems. Iron-enriched biochar (Fe-BC), a carbon-rich material produced by adding iron during or after pyrolysis, has emerged as a promising solution that combines biochar's natural physicochemical properties with iron's redox reactivity and pollutant-binding capacity. This detailed review examines recent research on Fe-BC, including its production, pollutant-reducing capabilities, performance in real-world agricultural settings, and role in sustainable farming. Fe-BC shows a remarkable ability to immobilize toxic heavy metals (such as Cd, Pb, As, Cr) through surface complexation, precipitation, and redox reactions, while also helping to retain nitrogen and phosphorus via ligand exchange and electrostatic interactions, thereby reducing eutrophication. Additionally, Fe-BC promotes the breakdown of persistent organic pollutants via Fenton-like reactions and facilitates electron transfer, thereby enhancing microbial degradation. Beyond reducing pollution, Fe-BC improves soil health, increases water retention, boosts crop yields, and contributes to climate change mitigation through carbon storage and lowered greenhouse gas emissions. However, challenges remain, including optimizing production costs, managing performance differences across various environments, evaluating potential ecological risks, establishing standardized regulations, and conducting long-term field studies. This review highlights recent advances, identifies key knowledge gaps, and suggests research priorities related to material design, environmental behavior, farming practices, and policy. With targeted investment in cross-disciplinary research and global cooperation, Fe-BC has the potential to become a key technology for sustainable agriculture, a circular economy, and environmental recovery worldwide.

1. Introduction

1.1. The global agricultural pollution crisis

Agriculture is both the foundation of human civilization and a major source of environmental damage worldwide. Since the Green Revolution began in the mid-20th century, global food production has tripled, largely due to the widespread use of synthetic fertilizers, pesticides, and irrigation (Tilman et al., 2011). However, this substantial increase in agricultural output has led to significant environmental issues. Current farming practices release about 14.5 million tons of nitrogen and 4.5 million tons of phosphorus each year into freshwater ecosystems, causing eutrophication and over 500 coastal hypoxic zones globally (Breitburg et al., 2018; Wang and Shui, 2021). The Gulf of Mexico, Baltic Sea, and South China Sea are key examples where seasonal dead zones have destroyed fisheries and disrupted marine food webs (Díaz and Rosenberg, 2008). At the same time, heavy metal contamination, especially cadmium, lead, arsenic, and chromium, affects nearly 35% of global agricultural soils, originating from sources such as phosphate fertilizers, industrial effluents, atmospheric deposition, and wastewater irrigation (Ali et al., 2019). Phosphate fertilizers, derived from rock phosphates that contain high levels of cadmium, are a primary pathway for cadmium contamination, contributing an estimated 3,000-10,000 tons of cadmium annually to soils worldwide (Lugon-Moulin et al., 2006). These contaminants not only lower crop yields but also enter food chains, with the World Health Organization estimating that heavy

* Corresponding author at: USDA Regulatory Science Center, University of Arkansas at Pine Bluff, School of Agriculture, Fisheries and Human Sciences, 1200 North University Drive, Mail Slot 4913, Pine Bluff, AR 71601, USA.
E-mail address: islams@uapb.edu.
[1] https://scholar.google.com/citations?user=rby07UAAAAAJ&hl=en.
[2] https://www.linkedin.com/in/shahidul-islam-74306317/.

https://doi.org/10.1016/j.hazadv.2026.101258
Received 15 April 2026; Received in revised form 11 May 2026; Accepted 27 May 2026
Available online 28 May 2026

metal exposure causes over 1.5 million premature deaths each year (WHO, 2024). The carcinogenic properties of cadmium, arsenic, and chromium(VI) have led to their classification as Group 1 carcinogens by the International Agency for Research on Cancer (IARC, 2012).

In addition to these issues, pesticide residues are found in about 64% of the world's agricultural soils, with neonicotinoids, organophosphates, and glyphosate detected at levels that exceed environmental safety limits (Silva et al., 2019; Tang et al., 2021). The widespread use of glyphosate, the most widely used herbicide, has raised concerns about its potential to cause cancer, disrupt hormones, and affect soil microbiomes (Myers et al., 2016). Organophosphate insecticides, which inhibit acetylcholinesterase in insects and mammals, have been associated with neurodevelopmental issues in children exposed before birth (Bouchard et al., 2011). Additionally, the accumulation of pesticide residues in agricultural soils threatens beneficial insects, including pollinators, and disrupts soil food webs (Goulson, 2013).

Emerging contaminants, including antibiotics, microplastics, and antibiotic resistance genes (ARGs), present an increasing challenge in agricultural pollution. Globally, over 100,000 tons of antibiotics are used each year in livestock production, with roughly 30-90% excreted unchanged in manure and later applied to farmland (Van Boeckel et al., 2015; Chen et al., 2019). This practice promotes the development of antibiotic-resistant bacteria and facilitates the horizontal transfer of ARGs, contributing to the antimicrobial resistance crisis, which is estimated to cause 700,000 deaths annually (O'Neill, 2016). Microplastics, defined as plastic particles smaller than 5 mm, have been found in agricultural soils at levels ranging from 0.5 to 10 g/kg. They originate from plastic mulch films, biosolids, and irrigation water (Huang et al., 2026; Mukherjee et al., 2022). These particles can adsorb co-contaminants, disrupt soil structure, and be absorbed by crops, potentially entering food chains (Wang et al., 2026). Overall, these pollutants harm soil health, degrade water quality, diminish biodiversity, and threaten the long-term sustainability of food production systems.

1.2. Limitations of conventional remediation approaches

Traditional remediation strategies have proven insufficient for tackling the complexity and scale of agricultural pollution. Best management practices (cover cropping, buffer strips, precision fertilization) help reduce pollutant losses but do not fully eliminate them, usually decreasing nutrient runoff by 20-40% (Hussain et al., 2025). While beneficial, these methods cannot address legacy contamination or manage heavy metals, and persistent organic pollutants already present in soils. Physical remediation techniques (soil excavation, washing, encapsulation) are extremely expensive at scale, costing between $100,000 and $1,000,000 per hectare for excavation and replacement (Khalid et al., 2017). Soil washing, which employs chemical solutions to remove contaminants, produces large volumes of wastewater that need treatment and disposal (Dermont et al., 2008). Chemical approaches (precipitation, oxidation, stabilization) may generate secondary pollutants and harm soil ecological functions. For instance, phosphate-based stabilization of heavy metals can lead to eutrophication if the metals become mobilized (Guo et al., 2023). Permeable reactive barriers with zero-valent iron are effective at remediating groundwater plumes but are not suitable for widespread agricultural pollution (Obiri-Nyarko et al., 2014).

Biological remediation using hyperaccumulator plants or microbial consortia offers environmental compatibility but is limited by slow rates of progress, climate constraints, and a narrow focus on pollutants (Rajendran et al., 2022). Hyperaccumulator species such as Thlaspi caerulescens (cadmium/zinc) and Pteris vittata (arsenic) need several growing seasons to significantly remove metals, during which the land cannot be used for food production (Van der Ent et al., 2013). Phytoremediation also produces contaminated biomass requiring proper disposal, creating secondary waste (Ghosh and Singh, 2005). Microbial remediation faces challenges such as competition with native soil microbes, sensitivity to environmental conditions, and difficulty maintaining active populations over time (Glick, 2010). Therefore, there is an urgent, unmet need for affordable, scalable, multifunctional technologies that can simultaneously remediate multiple pollutants and boost agricultural productivity.

1.3. Biochar as a foundational remediation platform

Biochar, a carbon-rich product of biomass pyrolysis, has gained notable research interest as a sustainable soil amendment and environmental sorbent (Lehmann and Joseph, 2015). Pyrolysis, which involves the thermal decomposition of organic material at 300-800°C under oxygen-limited conditions, converts labile biomass carbon into stable aromatic structures resistant to microbial mineralization (Xu et al., 2019). The resulting biochar features a highly porous structure, a large surface area (typically 50-1500 m^2/g), abundant oxygen-containing functional groups (such as carboxyl, hydroxyl, and carbonyl), and an alkaline pH (generally 7-11) (Xiang et al., 2020). These features give biochar an exceptional ability to adsorb cationic heavy metals, organic pollutants, and ammonium via electrostatic attraction, hydrophobic partitioning, and π- π stacking interactions (Ying et al., 2024). Beyond adsorption, biochar improves soil fertility through several mechanisms: (i) increasing cation exchange capacity (CEC) due to surface functional groups; (ii) enhancing water holding capacity because of pore space; (iii) improving soil aggregation and aeration; (iv) slowly releasing nutrients such as potassium, phosphorus, and calcium; (v) buffering pH in acidic soils; and (vi) providing habitat and substrates for beneficial microorganisms (Fanyue et al., 2025; Jatav, 2025). The long-term stability of biochar in soil, with average residence times ranging from 100 to 1000 years depending on pyrolysis temperature and environmental conditions, supports long-term carbon sequestration (Wang et al., 2023). Meta-analyses show that biochar application reduces greenhouse gas emissions by 30-50% for nitrous oxide and 40-60% for methane, while increasing soil organic carbon by 20-40% (Cayuela et al., 2014; Jeffery et al., 2011).

However, pristine biochar has inherent limitations that limit its effectiveness in remediation. First, its ability to attract anionic contaminants such as phosphate, nitrate, and arsenate is relatively weak due to electrostatic repulsion from negatively charged surfaces at typical soil pH (Ying et al., 2024). The point of zero charge (PZC) of pristine biochar typically ranges from 2 to 4, indicating that surfaces remain negatively charged at pH values above 4, thereby repelling anions. Second, its capacity for redox-mediated pollutant transformation is limited, reducing the breakdown of organic contaminants and the reduction of toxic metal species, such as Cr(VI) to Cr(III). Although some biochars contain redox-active quinone/hydroquinone groups, electron-transfer rates are generally slower than those of iron-bearing minerals (Klüpfel et al., 2014). Third, the performance of pristine biochar varies widely with feedstock type and pyrolysis conditions, often requiring case-specific optimization, which complicates standardization (Cardenas-Aguir et al., 2024). Fourth, pristine biochar lacks magnetic properties, which prevents its recovery and reuse from contaminated sites (Yi et al., 2020). These limitations have spurred the development of engineered biochars with enhanced functionality.

1.4. Iron enrichment: A paradigm shift in biochar engineering

Among biochar modification strategies, iron enrichment has become particularly promising due to iron's abundance (5% of Earth's crust), environmental friendliness, and versatile redox chemistry (Meng et al., 2025). Iron-enriched biochar (Fe-BC) combines biochar's structural benefits with iron's reactive properties, including (i) strong affinity for anionic pollutants through ligand exchange with iron (oxyhydr)oxide surfaces; (ii) Fenton-like catalytic activity for breaking down organic contaminants; (iii) redox buffering capacity for transforming heavy

metals; (iv) magnetic properties that facilitate recovery and reuse; (v) increased surface area and pore structure; and (vi) added nutrient value, as iron is an essential micronutrient for plants (Zhang et al., 2025b; Huang et al., 2026). Fe-BC production can be achieved through pre-pyrolysis (impregnating iron into biomass before pyrolysis) or post-pyrolysis (loading iron onto pre-formed biochar) methods, each offering unique advantages in iron distribution, stability, and cost (Feng et al., 2020). Pre-pyrolysis impregnation typically results in more stable iron incorporation, as iron species become embedded within the carbon matrix during pyrolysis, but it can also promote thermal decomposition and lower biochar yield (Zhou et al., 2022). Post-pyrolysis techniques preserve biochar structure but may result in less uniform iron distribution and increased leaching (Gross et al., 2024). Co-precipitation methods, in which iron salts are precipitated as iron oxides onto biochar surfaces using an alkali, produce magnetic Fe-BC suitable for recovery (Yi et al., 2020). The schematic representation of biochar production and iron enrichment is presented in Figure 1.

The speciation of iron in Fe-BC, whether as magnetite (Fe_3O_4), maghemite (γ-Fe_2O_3), hematite (α-Fe_2O_3), goethite (α-FeOOH), or zero-valent iron (Fe^0), significantly influences how pollutants interact with it (Feng et al., 2020). Zero-valent iron, typically produced under reducing pyrolysis atmospheres or via chemical reduction, exhibits the highest reduction potential for Cr(VI) and chlorinated organic compounds but is also most susceptible to oxidation and passivation (Li et al., 2024). Iron oxides provide stable surface hydroxyl groups for ligand exchange and complexation, while magnetite aids in magnetic separation (Yi et al., 2020). The ideal iron loading generally ranges from 10-20 wt%, as higher loadings can decrease surface area due to pore blocking and lead to iron aggregation (Zhou et al., 2022). These complementary features make Fe-BC a multifunctional platform capable of addressing various agricultural pollutants through integrated physical, chemical, and biological mechanisms. This review systematically examines the synthesis, characterization, mechanisms, applications, co-benefits, challenges, and prospects of Fe-BC in reducing agricultural pollution.

1.5. Scope and objectives of this review

The rapidly growing body of literature on Fe-BC, with over 1,500 publications since 2015, calls for a thorough review that critically assesses current knowledge, identifies gaps, and outlines strategic research priorities. This review aims to: (1) systematically analyze Fe-BC synthesis methods and their effects on material properties; (2) clarify the mechanisms behind heavy metal immobilization, nutrient retention, and organic pollutant breakdown; (3) carefully evaluate evidence of performance from laboratory, greenhouse, and field studies; (4) assess co-benefits and potential risks of Fe-BC use; (5) identify challenges that limit practical application; (6) recommend integrated research and policy strategies to move Fe-BC from laboratory research to agricultural practice. The conceptual illustration of Fe-BC multifunctionality in agricultural systems is shown in Fig. 2. By combining insights from materials science, environmental chemistry, soil microbiology, and agronomy, this review offers a comprehensive foundation for researchers, practitioners, and policymakers involved in sustainable agriculture.

2. Synthesis and characterization of iron-enriched biochar

2.1. Scenario-based selection of Fe-BC synthesis parameters

The selection of Fe-BC synthesis parameters should be tailored to the target agricultural pollution scenario and soil conditions. Lower

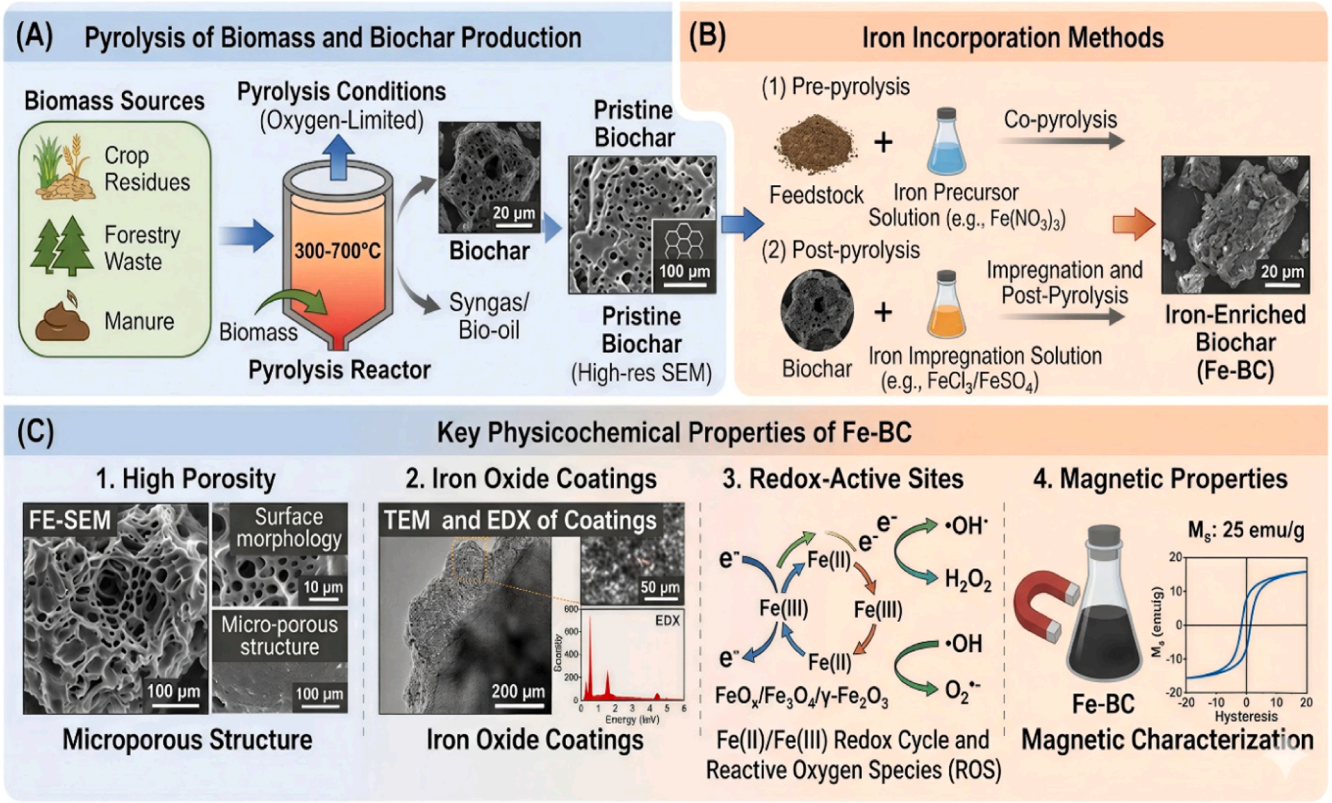

Fig. 1. Schematic representation of biochar production and iron enrichment. (A) Pyrolysis of biomass (crop residues, forestry waste, manure) under oxygen-limited conditions produces pristine biochar. (B) Iron incorporation via pre- or post-pyrolysis methods generates Fe-BC with enhanced functionality. (C) Key physicochemical properties of Fe-BC: high porosity, iron oxide coatings, redox-active sites, and magnetic properties.

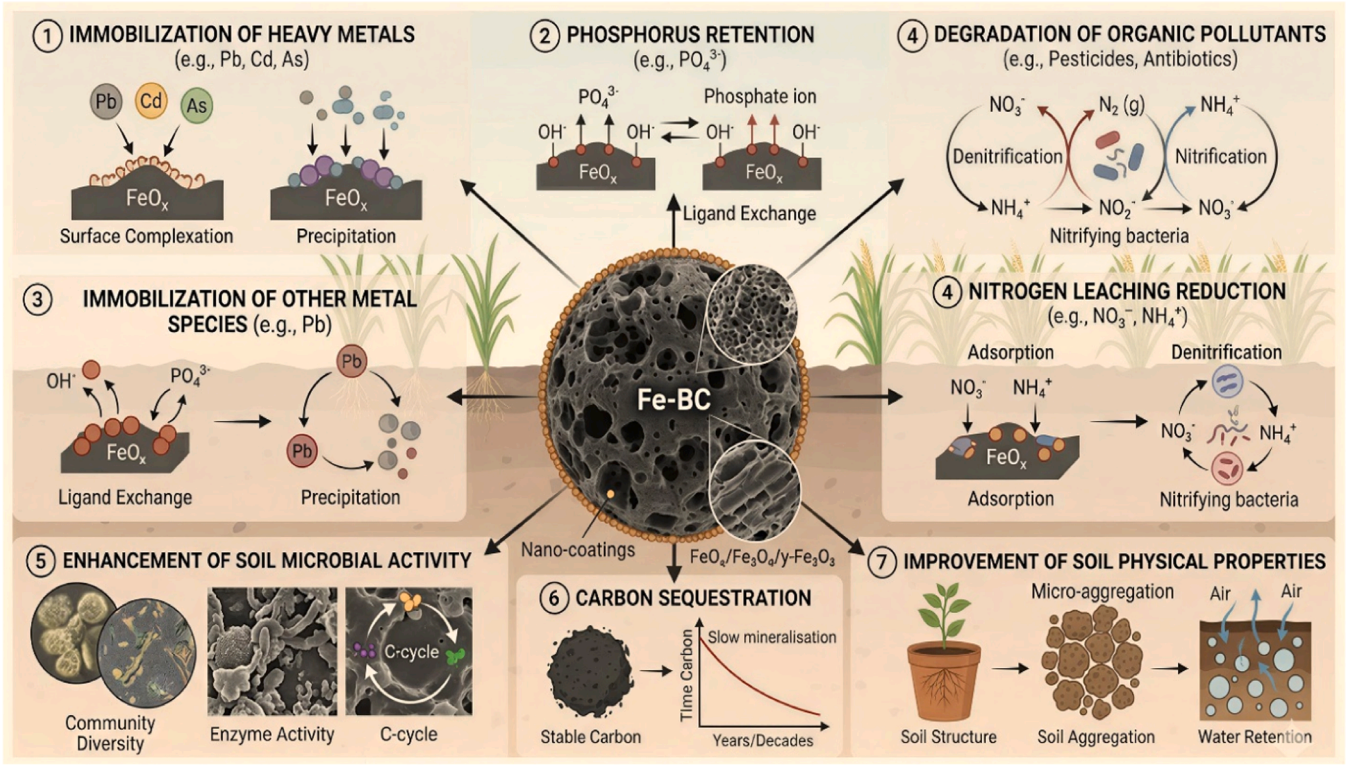

Fig. 2. Conceptual illustration of Fe-BC multifunctionality in agricultural systems. Fe-BC simultaneously: (1) immobilizes heavy metals via surface complexation and precipitation; (2) retains phosphorus through ligand exchange on iron oxide surfaces; (3) degrades organic pollutants via Fenton-like reactions; (4) reduces nitrogen leaching through adsorption and denitrification; (5) enhances soil microbial activity; (6) sequesters carbon; and (7) improves soil physical properties.

pyrolysis temperatures (350–500°C) generally preserve oxygen-containing functional groups and enhance phosphate retention and cation exchange capacity, making them better suited to acidic soils and nutrient management applications. In contrast, higher pyrolysis temperatures (600–750°C) increase aromaticity, electrical conductivity, and graphitic structure, thereby enhancing electron transfer, catalytic activity, and the degradation of organic pollutants. Similarly, co-precipitation methods often produce highly dispersed iron oxide phases that favor phosphate and arsenate immobilization, whereas ball milling and one-pot pyrolysis approaches are better suited to large-scale, low-cost production and catalytic remediation systems. Therefore, synthesis strategies should be selected based on contaminant chemistry, soil properties, economic feasibility, and the desired Fe-BC functionality.

2.2. Feedstock selection and pyrolysis conditions

The physicochemical properties of Fe-BC mainly depend on feedstock type, pyrolysis conditions, and how iron is added. Common feedstocks include agricultural residues like rice husk, wheat straw, corn stover, and sugarcane bagasse; forestry waste such as sawdust and wood chips; animal manure; and municipal organic waste (Saharudin et al., 2024). The choice of feedstock affects biochar yield, ash content, surface properties, and pore structure. Lignocellulosic biomass (wood, straw) generally produces biochars with higher carbon content (60-80%) and porosity (surface area 200-800 m^2/g), whereas manure-based biochars usually contain essential minerals like P, K, Ca, and Mg that can work with iron for pollutant removal but have lower carbon levels (30-50%) and higher ash content (20-40%) (Jatav, 2025; Yuan et al., 2014). Pyrolysis temperature plays a key role in biochar characteristics: lower temperatures (300-450°C) help retain more oxygen-based functional groups (carboxyl, hydroxyl) but result in a lower surface area (50-200 m^2/g) and less carbonization, while higher temperatures (550-800°C) create biochar's with increased porosity (300-1500 m^2/g), higher aromaticity, and better electrical conductivity, although functional group density decreases (Xiang et al., 2020; Chen et al., 2019). Temperatures between 500 and 650°C are often optimal for balancing surface functionality and structural stability in Fe-BC. Residence time (around 0.5-4 hours) influences biochar features: longer times enhance carbonization and surface area but reduce yield and functional groups (Manyà, 2012). The heating rate also affects the process: slow pyrolysis (5-15°C/min) favors bio-oil production (25-35%), whereas fast pyrolysis (above 100°C/min) increases bio-oil yield (Bridgwater, 2012). The principal methods of iron incorporation, each with distinct advantages and limitations, are shown in Table 1.

2.3. Iron incorporation strategies

Recent advances include green synthesis methods using plant extracts (such as tea, eucalyptus, and green tea) to produce Fe nanoparticles via reduction of Fe^{3+} to Fe^0, thereby eliminating the need for chemical reducing agents. Dual-metal doping (Fe-Mn, Fe-Cu, Fe-Zn, Fe-Al) creates synergistic effects, with Fe-Mn binary oxides demonstrating improved arsenic removal due to Mn-mediated oxidation of As(III) to As (V), followed by Fe-mediated adsorption (Yin et al., 2020). Template-assisted synthesis utilizing silica or polymer templates develops hierarchical porosity (micro-, meso-, and macropores) that enhances mass transport and pollutant access to reactive sites (Duan et al., 2022). The schematic approach of Fe-BC synthesis methods is presented in Fig. 3.

2.4. Iron speciation and surface chemistry

The speciation of iron in Fe-BC critically affects mechanisms of pollutant interaction. X-ray diffraction (XRD), Mössbauer spectroscopy, and X-ray photoelectron spectroscopy (XPS) analyses show that iron mainly exists as magnetite (Fe_3O_4), maghemite (γ-Fe_2O_3), hematite (α-Fe_2O_3), goethite (α-FeOOH), or zero-valent iron (Fe^0), depending on

Table 1
Principal methods of iron incorporation, distinct advantages, and limitations.

Method	Procedure	Advantages	Limitations	Optimal Applications
Pre-pyrolysis impregnation	Biomass soaked in Fe salt solution before pyrolysis	Uniform Fe distribution; stable incorporation; Fe embedded in carbon matrix	Fe may catalyze thermal decomposition, potential pore blockage, and yield reduction	High-performance sorbents requiring stable Fe anchoring
Post-pyrolysis impregnation	Biochar immersed in Fe solution, then dried/calcined	Simple; preserves biochar structure; no pyrolysis modification	Fe leaching risk; less uniform distribution; surface-only loading	Rapid, cost-effective modification
Co-precipitation	Fe^{2+}/Fe^{3+} salts precipitated as Fe oxides on biochar using alkali	High Fe loading; magnetic properties; well-crystallized Fe oxides	pH control critical; potential secondary contamination; multiple steps	Magnetic recoverable Fe-BC
Chemical vapor deposition	Volatile Fe precursors ($Fe(CO)_5$) decomposed on biochar surface	High-purity Fe coating; controlled thickness; uniform nanoscale coating	Specialized equipment; hazardous precursors; high cost	Precision-engineered Fe coatings
Ball milling	Mechanical grinding of biochar with Fe particles or salts	Green synthesis; no solvents; high dispersion; scalable	Energy intensive; potential Fe oxidation; particle size reduction	Large-scale, solvent-free production
Hydrothermal carbonization	Biomass + Fe source processed in subcritical water (180-250°C)	Low temperature; high functional group retention; processes wet biomass	Lower surface area; batch processing; pressure equipment	Fe-BC from wet biomass
One-pot pyrolysis with Fe salts	Fe salts mixed with biomass and pyrolyzed simultaneously	Simplest; industrially scalable; minimal steps	Less control over Fe Specification; potential uneven distribution	Commercial Fe-BC production
Electrochemical deposition	Fe electrodeposited on conductive biochar	Precise Fe loading control; uniform coating	Requires conductive biochar; specialized equipment	Research applications

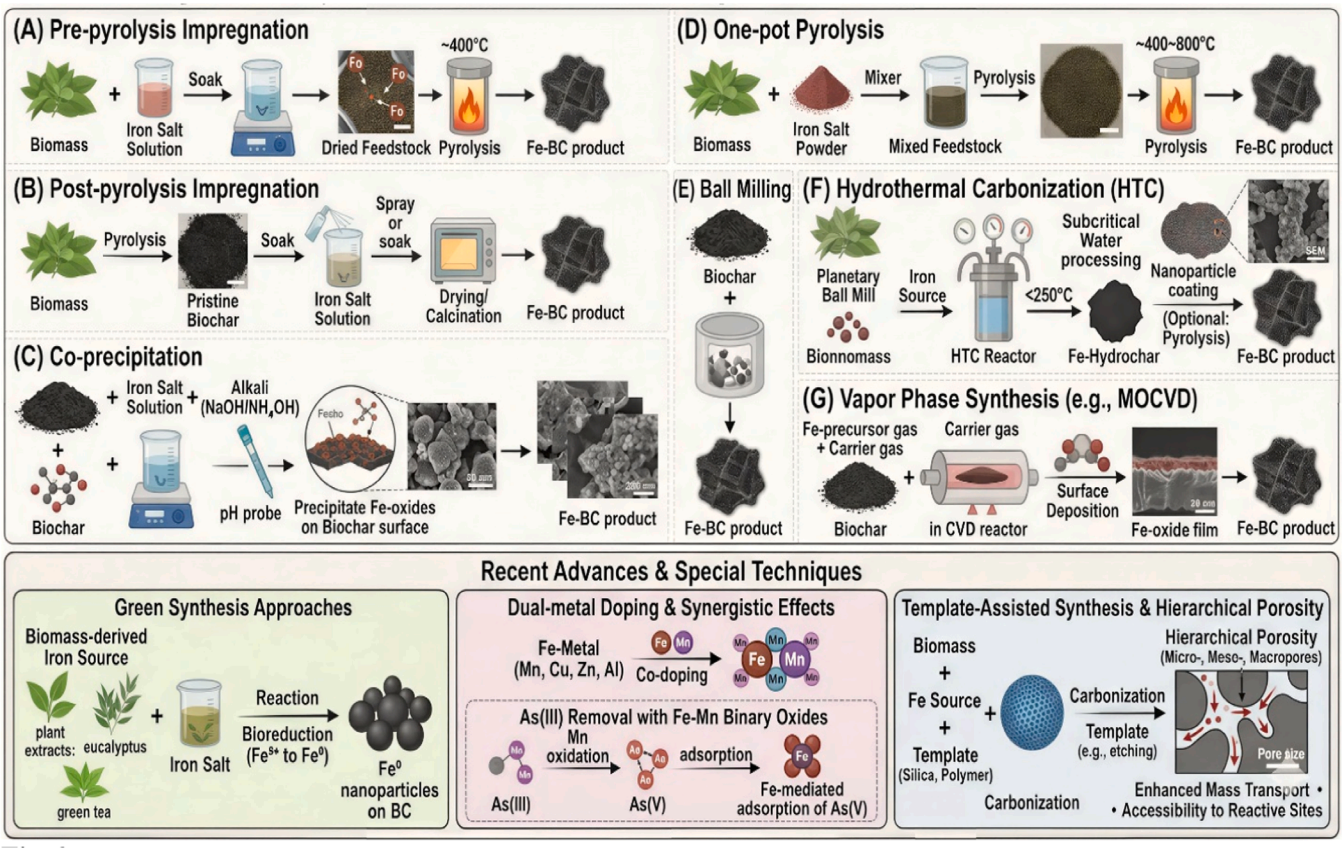

Fig. 3. Schematic diagram of Fe-BC synthesis methods. (A) Pre-pyrolysis impregnation: biomass is soaked in an iron salt solution, dried, then pyrolyzed. (B) Post-pyrolysis impregnation: pristine biochar is treated with an iron solution followed by drying and calcination. (C) Co-precipitation: iron salts are precipitated as iron oxides on biochar surfaces using an alkali (NaOH or NH_4OH). (D) One-pot pyrolysis: iron salts are mixed with biomass and pyrolyzed simultaneously. (E) Ball milling: mechanical grinding of biochar with iron particles in a planetary mill. (F) Hydrothermal carbonization: biomass and iron source processed in subcritical water under autogenous pressure.

synthesis conditions (Wang et al., 2020; Feng et al., 2020). Reducing pyrolysis atmospheres (N_2, Ar, or CO_2) or hydrogen reduction after synthesis favors Fe^0 formation, whereas oxidizing environments (air) produce ferric oxides. The Fe^{2+}/Fe^{3+} ratio influences redox reactivity, with mixed-valence magnetite offering the highest electron transfer rates due to electron hopping between octahedral Fe^{2+} and Fe^{3+} sites (Chen et al., 2025). Iron loading levels generally range from 5-30 wt.%, with optimal pollutant removal observed at 10-20%. When loading drops below 5%, there are insufficient active iron sites for effective pollutant removal. When it exceeds 25%, iron nanoparticles tend to cluster, reducing the effective surface area and blocking biochar pores. Mössbauer spectroscopy can distinguish among different iron phases and measure their relative amounts. Superparamagnetic Fe^{3+} often dominates at lower loadings (<10%), while ferromagnetic Fe_3O_4 or α-Fe_2O_3 are common at higher loadings (Wang et al., 2024). Table 2 presents essential characterization methods for a comprehensive

Table 2
Characterization methods for comprehensive Fe-BC evaluation.

Property	Technique	Information Provided	Sample Preparation Requirements	Detection Limit	Reference
Surface area & porosity	N_2-BET, BJH analysis	Specific surface area (m^2/g), pore volume, pore size distribution	Samples should be oven-dried (60–105°C) and degassed under vacuum or inert gas to remove moisture and volatile compounds prior to analysis.	0.1 m^2/g	Brunauer et al. (1938)
Morphology	SEM, TEM, HR-TEM	Particle size, shape, surface texture, Fe distribution (EDS mapping)	Samples should be finely powdered and mounted on conductive carbon tape; a conductive coating (Au/Pt/C) is often required for SEM, whereas TEM requires an ultrathin dispersion on copper grids.	1 nm (TEM)	Goldstein et al. (2017)
Crystalline phases	XRD	Iron mineralogy (Fe_3O_4, α-Fe_2O_3, Fe^0), graphitic carbon (002 peak)	Samples should be finely ground into homogeneous powders; pellet preparation or flat-surface mounting is recommended to minimize preferred orientation effects.	1–5 wt%	Cullity & Stock (2008)
Surface functional groups	FTIR, Raman	Oxygen groups (C=O, C–O, –OH), Fe–O bonds, D/G band ratio (carbon disorder)	Samples should be dried and finely homogenized; FTIR commonly requires KBr pellet preparation, whereas Raman analysis requires smooth and contamination-free surfaces.	1–5%	Socrates (2004)
Elemental composition	EDX, XRF, ICP-OES	Bulk and surface elemental analysis, Fe loading, trace metals	ICP-OES requires acid digestion (HNO_3/HCl/HF mixtures), while XRF commonly requires pelletized or fused bead samples; EDX requires conductive mounting.	0.1–1 wt%	Beckhoff et al. (2006)
Iron oxidation state	XPS, Mössbauer	Fe^{2+}/Fe^{3+} ratio, Fe^0 content, coordination environment	XPS requires ultra-high vacuum and contamination-free sample surfaces; Mössbauer spectroscopy often requires inert atmosphere or cryogenic handling to minimize oxidation artifacts.	0.5–1%	Moulder et al. (1992)
Magnetic properties	VSM	Saturation magnetization (Ms), coercivity (Hc), remanence (Mr), superparamagnetism	Dry powdered samples should be uniformly packed into nonmagnetic holders to ensure accurate magnetic measurements.	0.1 emu/g	Cullity and Graham (2008)
Surface charge	Zeta potential, pHpzc	Electrostatic interaction potential, pH-dependent surface charge	Samples should be uniformly dispersed in the electrolyte solution by sonication to prevent particle aggregation during analysis.	N/A	Hunter (2013)
Thermal stability	TGA-DSC	Decomposition temperature, mass loss, Fe oxidation behavior	Samples should be finely ground and dried prior to thermal analysis; inert gas purging (N_2 or Ar) is commonly required during measurements.	0.1 μg	Brown (2001)
Chemical stability	Leaching tests (TCLP, EN12457)	Iron and heavy metal leachability under environmental conditions	Samples should be homogenized and mixed with extraction fluids under standardized liquid-to-solid ratios and agitation conditions.	1 μg/L	USEPA (1992)
Pollutant binding	XANES, EXAFS	Bond distances, coordination numbers, binding geometry	Samples should be finely homogenized and often cryogenically preserved or sealed under inert atmosphere to prevent oxidation during synchrotron analysis.	0.01 Å	Newville (2014)

evaluation of Fe-BC.

Fourier-transform infrared spectroscopy (FTIR) and XPS reveal that Fe incorporation introduces Fe-O stretching vibrations (~550-600 cm^{-1}) and changes surface charge. The point of zero charge (pHpzc) generally rises from 2-4 (pristine biochar) to 6-9 (Fe-BC), enhancing affinity for anionic pollutants at typical soil pH (6-7) (Ying et al., 2024; Gross et al., 2024). XPS also detects Fe-bound oxygen functional groups (Fe-O, Fe-OH) and carbon-bound iron (C-Fe) species, with the latter indicating direct iron-carbon bonding that increases stability (Feng et al., 2020). Additionally, Fe-BC exhibits superparamagnetic behavior when Fe_3O_4 loadings exceed 10%, with saturation magnetization (Ms) values ranging from 10 to 50 emu/g. This enables magnetic separation and recovery using external magnetic fields (Yi et al., 2020). This property is especially useful for retrieving Fe-BC from water treatment systems or for concentrating Fe-BC after soil application. The magnetic moment arises from unpaired electrons in Fe^{3+} (d^5, S=5/2) and Fe^{2+} (d^6, S=2) within the inverse spinel structure of magnetite (Cullity and Graham, 2008).

2.5. Material heterogeneity and characterization uncertainty

An important but underexplored research gap concerns the heterogeneity of Fe-BC materials. Many reported Fe-BC systems likely consist of heterogeneous mixtures with multiple iron phases, uneven iron distribution, and variable surface chemistry arising from feedstock variability and synthesis conditions. This heterogeneity introduces uncertainty about reproducibility, mechanistic interpretation, and large-scale application performance. Furthermore, characterization techniques such as TEM, SEM, and XPS typically analyze highly localized regions and may not adequately represent bulk material properties. Results may also be influenced by sample preparation procedures and operator-dependent selection bias. Future studies should therefore incorporate statistically representative multi-point characterization, combined bulk–surface analytical approaches, and standardized protocols that link laboratory characterization with field-scale performance evaluation.

2.6. Characterization techniques and quality assurance

SEM images show a highly porous carbon structure with uniformly dispersed iron oxide nanoparticles (20–50 nm) on the biochar surface. XRD patterns confirm the presence of magnetite (Fe_3O_4, JCPDS 19-0629) and hematite (α-Fe_2O_3, JCPDS 33-0664), along with a broad carbon peak at $2\theta \approx 23^\circ$ indicative of amorphous/graphitic carbon. FTIR spectra reveal Fe–O stretching vibrations at 550–600 cm^{-1} and oxygen-containing functional groups (C=O at 1700 cm^{-1}, C–O at 1100 cm^{-1}). N_2 adsorption-desorption isotherms exhibit a type IV curve with an H3 hysteresis loop, characteristic of a mesoporous structure. VSM analysis shows superparamagnetic behavior with a saturation magnetization of 35 emu/g and negligible coercivity. High-resolution XPS Fe 2p spectra indicate a Fe^{2+}/Fe^{3+} ratio of 0.4, with satellite peaks confirming Fe_3O_4. These results demonstrate that Fe-BC has a porous carbon matrix with well-dispersed iron oxides, abundant surface functionality, mesoporosity, superparamagnetism, and mixed-valence iron states, all of which are suitable for environmental and catalytic applications. Fig. 4 is representative of the physicochemical and magnetic characterization of iron-modified biochar (Fe-BC).

(A) SEM image depicting the highly porous carbonaceous skeleton of the biochar, with iron oxide nanoparticles (shown as bright spherical spots, 20–50 nm) uniformly anchored on the surface and within the macropores. (B) XRD patterns confirming the successful synthesis of iron phases; the diffraction peaks correspond to magnetite (Fe3O4, JCPDS

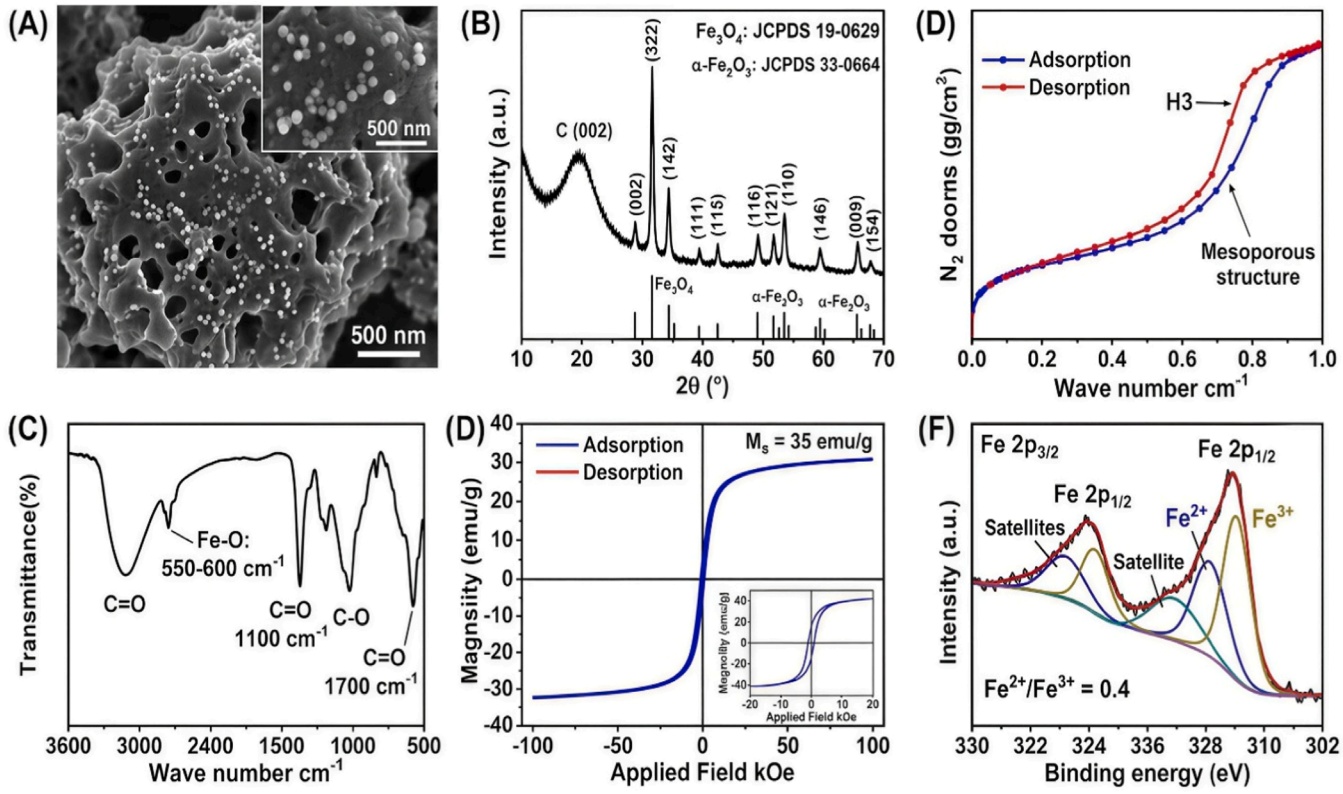

Fig. 4. Physicochemical and magnetic characterization of iron-modified biochar (Fe-BC).

19-0629) and hematite α - Fe2O3, JCPDS 33-0664), while the broad reflection at 2Θ-230 indicates the amorphous nature of the carbon matrix (Lu et al., 2020). (C) FTIR spectra revealing characteristic Fe - O stretching vibrations in the 550–$600 cm-1 region, alongside oxygen-containing functional groups such as C = O (1700cm^{-1}) and C - O (1100 cm-1), which facilitate iron binding and pollutant interaction (Chen et al., 2022). (D) N2 adsorption-desorption isotherms exhibiting a Type IV curve with an H3 hysteresis loop, indicative of a well-developed mesoporous structure and slit-like pores (Thommes et al., 2015). (E) VSM magnetization curve demonstrating superparamagnetic behavior with a saturation magnetization (Ms) of 35 emu/g, ensuring rapid magnetic separation from aqueous phases (Reddy et al., 2014). (F) High-resolution XPS Fe 2p spectrum showing Fe 2p3/2 and Fe 2p1/2 peaks with an Fe2+/Fe3+ ratio of approximately 0.4; the presence of distinct satellite peaks confirms the coexistence of multiple iron oxidation states characteristic of Fe3O4 (Zhu et al., 2020).

3. Pollutant immobilization and transformation mechanisms

3.1. Competitive interactions

In real-world agricultural systems, multiple pollutants and competing ions coexist, substantially influencing Fe-BC remediation performance. For example, phosphate and arsenate compete strongly for iron oxide adsorption sites because both form inner-sphere complexes on Fe hydroxyl surfaces. Elevated phosphate concentrations may therefore reduce arsenate immobilization efficiency. Similarly, dissolved organic matter and humic substances may compete with heavy metals for reactive functional groups and block pore access. These competitive interactions can significantly alter contaminant retention, nutrient dynamics, and long-term remediation effectiveness under field conditions.

3.2. Heavy metal immobilization: a multifaceted process

Fe-BC immobilizes heavy metals through multiple synergistic mechanisms that collectively reduce metal bioavailability, mobility, and ecotoxicity. These mechanisms operate simultaneously, with their relative contributions depending on the metal type, Fe-BC properties, and environmental conditions. The mechanistic pathways for heavy metal immobilization by Fe-BC are presented in Fig. 5.

3.2.1. Surface complexation and electrostatic interactions

Iron (oxyhydr)oxide surfaces feature abundant hydroxyl (-OH) and oxygen bridge (≡Fe-O-) functional groups that form both inner-sphere and outer-sphere complexes with metal cations. For divalent metals (Pb^{2+}, Cd^{2+}, Cu^{2+}, Zn^{2+}), complexation occurs through ligand exchange.

$$\equiv Fe-OH + M^{2+} \rightleftharpoons \equiv Fe-OM^{+} + H^{+} (\text{monodentatecomplex})$$

$$2 \equiv Fe-OH + M^{2+} \rightleftharpoons (\equiv Fe-O)_2M + 2H^{+} (\text{bidentatecomplex})$$

Inner-sphere complexes, where water molecules are displaced from the metal's coordination sphere, have binding energies of 40-120 kJ/mol and are mostly irreversible under environmental conditions (Sparks, 2003). Outer-sphere complexes, in which the metal retains its hydration shell and interacts electrostatically, are weaker (10-30 kJ/mol) and are more easily reversible (Hiemstra and Van Riemsdijk, 1996). The pH-dependent surface charge of Fe-BC strongly influences metal binding. The point of zero charge (PZC) of Fe-BC generally falls between 6 and 9, while pristine biochar has a PZC around 2 to 4 (Ying et al., 2024). When pH exceeds the PZC, surfaces become deprotonated (≡Fe-O^{-}) and attract cationic metals. When pH is below the PZC, surfaces are protonated (≡Fe-OH_2^{+}) and tend to repel cations. Most agricultural soils have a pH range of 5.5 to 7.5, promoting cationic metal adsorption on Fe-BC. Extended X-ray absorption fine structure (EXAFS) spectroscopy has revealed bidentate binuclear binding geometries for Pb^{2+} and Cd^{2+} on Fe-BC surfaces, with metal-oxygen bond distances of 2.3 to 2.4 Å (Duan

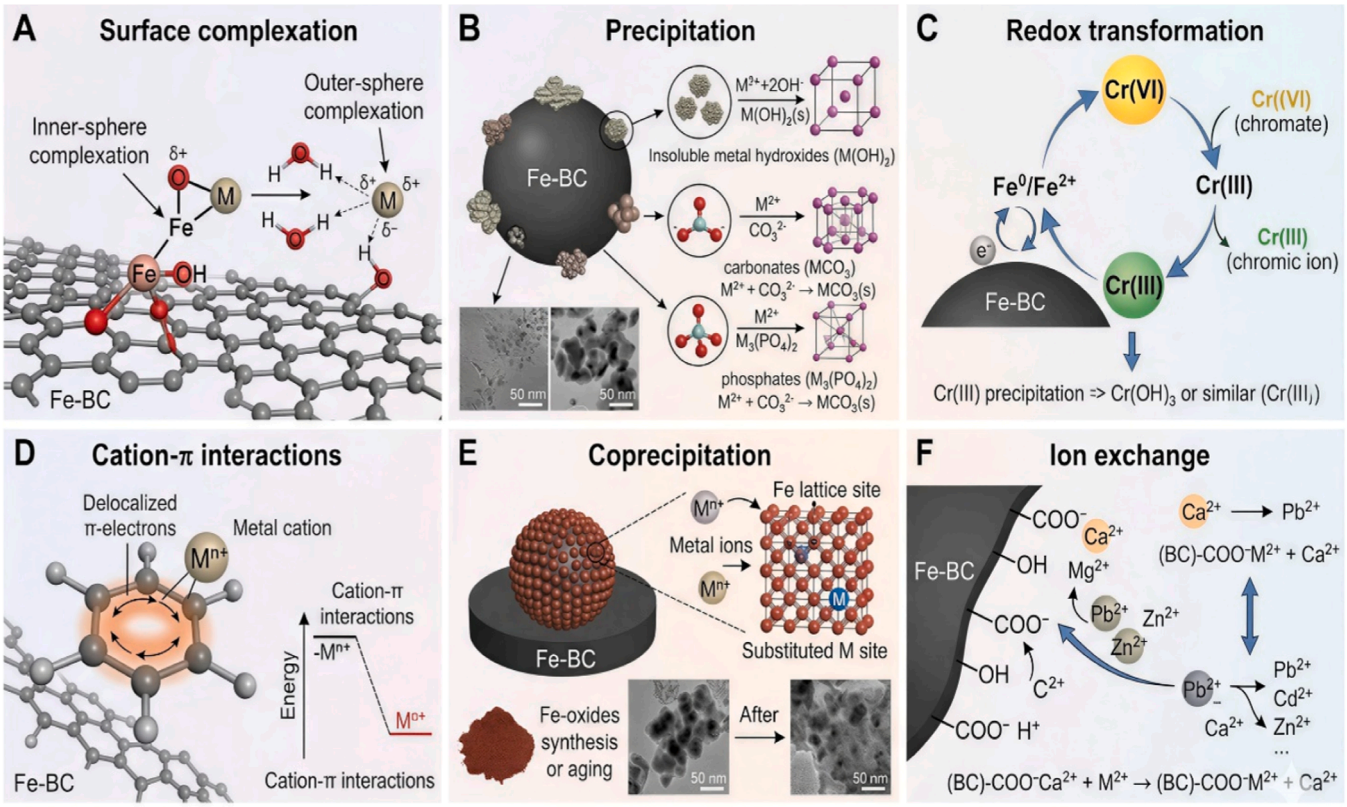

Fig. 5. Mechanistic pathways for heavy metal immobilization by Fe-BC. (A) Surface complexation: inner-sphere (direct Fe-O-M bond) and outer-sphere (electrostatic) complexation with Fe-OH groups. (B) Precipitation: formation of insoluble metal hydroxides ($M(OH)_2$), carbonates (MCO_3), and phosphates ($M_3(PO_4)_2$). (C) Redox transformation: reduction of Cr(VI) to Cr(III) by Fe^0/Fe^{2+} followed by Cr(III) precipitation. (D) Cation-π interactions: binding with delocalized π-electrons of aromatic carbon rings. (E) Coprecipitation: metal incorporation into iron oxide structures during Fe-BC aging or synthesis. (F) Ion exchange: replacement of Ca^{2+}, Mg^{2+}, or H^+ on biochar surfaces.

et al., 2022; Tiberg et al., 2016). The stability constants (log K) for Fe-BC-metal complexes range from 4.5 to 8.2, indicating strong binding comparable to natural iron oxides (Dzombak and Morel, 1990).

3.2.3. (Co)precipitation reactions

Fe-BC can cause heavy metal precipitation, such as insoluble hydroxides, carbonates, and phosphates. The alkaline pH of Fe-BC (7.5-10.5) promotes the formation of metal hydroxides.

$$M^{2+} + 2OH^- \rightarrow M(OH)_2(s)$$

3.2.4. Carbon occlusion and long-term stabilization

In addition to chemical stabilization, Fe-BC may promote long-term stabilization of soil organic carbon through physical occlusion. Iron oxides can physically protect organic carbon within microaggregates and organo–mineral complexes, thereby reducing enzymatic accessibility and microbial decomposition. This occlusion effect contributes to the persistence of soil organic carbon and microbial necromass by shielding carbon substrates from oxidative degradation.

For Pb^{2+}, $Pb(OH)_2$ has a solubility product Ksp of 1.4×10^{-20}, which limits aqueous Pb^{2+} concentrations to less than 10^{-5} M at pH 8. Dissolved inorganic carbon from biochar (typically 1-5% as carbonates) promotes metal carbonate precipitation.

$$M^{2+} + CO_3^{2-} \rightarrow MCO_3(s)$$

3.2.5. Critical considerations for arsenic speciation

Although reduction of As(V) to As(III) may occur under Fe-BC-mediated reducing conditions, As(III) is generally more mobile and toxic than As(V). Therefore, the environmental implications of arsenic reduction require careful evaluation. Under strongly reducing paddy soil environments, transient mobilization of As(III) may occur during flooding periods or redox fluctuations. Stabilization mechanisms such as sulfidation and co-precipitation with iron sulfides may reduce this risk by forming less soluble arsenic minerals (e.g., FeAsS and As_2S_3). However, repeated drying–rewetting cycles may destabilize these phases and promote remobilization. Future studies should therefore evaluate arsenic speciation dynamics under realistic fluctuating field conditions.

$CdCO_3$ (otavite, $Ksp = 5.2 \times 10^{-12}$) and $PbCO_3$ (cerussite, $Ksp = 1.5 \times 10^{-13}$) are stable phases under typical soil conditions (Lindsay, 1979). In phosphate-rich agricultural soils (10-100 mg P/kg), Fe-BC encourages the formation of stable metal-phosphate minerals.

$$3M^{2+} + 2PO_4^{3-} \rightarrow M_3(PO_4)_2(s)$$

$Pb_5(PO_4)_3OH$ (hydroxypyromorphite, $Ksp = 10^{-80}$) and $Cd_3(PO_4)_2$ ($Ksp = 2.5 \times 10^{-33}$) are among the most stable metal phases known, with very low solubility (Guo et al., 2023). Coprecipitation with iron oxides, especially during Fe-BC aging in oxic environments, further traps metals within stable mineral matrices. In this process, Fe^{2+} released from Fe-BC oxidizes to Fe^{3+} and precipitates as ferrihydrite ($Fe_{10}O_{14}(OH)_2$) or goethite (α-FeOOH), incorporating metals into the crystal structure or adsorbing them onto newly formed surfaces (Gross et al., 2024).

3.2.6. Redox transformation and detoxification

Fe-BC's redox-active iron species help convert toxic metal species into less mobile or less toxic forms. Zero-valent iron (Fe^0) and Fe^{2+} are powerful reducing agents ($E^\circ(Fe^{2+}/Fe^0) = -0.44$ V; $E^\circ(Fe^{3+}/Fe^{2+}) = +0.77$ V).

3.2.7. Comparative importance of binding mechanisms

Although cation–π interactions contribute to heavy metal

stabilization on aromatic carbon surfaces, ligand exchange and inner-sphere complexation generally dominate metal retention on Fe-BC, particularly for Pb^{2+}, Cu^{2+}, and Cr species. Cation–π interactions may play a larger role for weakly hydrated metals such as Cd^{2+} and Hg^{2+}. In contrast to ligand exchange, cation–π interactions are less sensitive to pH variation but generally exhibit weaker binding energies under highly competitive soil conditions.

Chromium (VI), a carcinogenic, mobile oxyanion (CrO_4^{2-}, $Cr_2O_7^{2-}$), is readily reduced to Cr(III):

$$Cr_2O_7^{2-} + 2Fe^{\circ} + 14H^+ \rightarrow 2Cr^{3+} + 2Fe^{3+} + 7H_2O$$

$$Cr_2O_7^{2-} + 6Fe^{2+} + 14H^+ \rightarrow 2Cr^{3+} + 6Fe^{3+} + 7H_2O$$

The reduced Cr(III) precipitates as $Cr(OH)_3$ ($Ksp = 6.7 \times 10^{-31}$) at pH above 5.5 or becomes incorporated into iron oxide structures, making it immobile (Li et al., 2024b; Huang et al., 2026). Reduction rates follow pseudo-first-order kinetics, with rate constants ranging from 0.1 to 1.0 h^{-1} for Fe-BC, similar to nano zero-valent iron (Li et al., 2020). For arsenic, Fe-BC can convert As(V) to As(III), which has a higher affinity for iron sulfide surfaces under reducing conditions. However, careful management is necessary because As(III) is more toxic (50–100 times more) and more mobile under oxidizing conditions (Xu et al., 2019). In oxygen-free rice paddies, Fe-BC-induced reduction may initially mobilize As(III), but subsequent precipitation as As_2S_3 or incorporation into iron sulfides such as FeAsS can provide long-term stabilization (Zhang et al., 2025a). The overall effect depends on sulfur availability, redox potential, and Fe-BC properties. Mercury(II) can also be reduced to Hg^{o} (volatile) by Fe-BC, which can volatilize from soils or be adsorbed onto biochar surfaces. However, mercury volatilization transfers contamination from soil to air, creating new exposure pathways, and thus, this mechanism warrants careful assessment.

3.2.8. Competitive sorption and multi-contaminant interactions

In real-world agricultural systems, multiple pollutants and competing ions coexist, substantially influencing Fe-BC remediation performance. For example, phosphate and arsenate compete strongly for iron oxide adsorption sites because both form inner-sphere complexes on Fe hydroxyl surfaces. Elevated phosphate concentrations may therefore reduce arsenate immobilization efficiency. Similarly, dissolved organic matter and humic substances may compete with heavy metals for reactive functional groups and block pore access. These competitive interactions can significantly alter contaminant retention, nutrient dynamics, and long-term remediation effectiveness under field conditions.

3.2.9. Cation-π interactions

The graphitic carbon domains in Fe-BC, especially at higher pyrolysis temperatures (>600°C), promote cation-π bonding between heavy metals and the delocalized π-electrons of aromatic rings. This non-covalent interaction, which lacks involvement of functional groups, is particularly important for weakly coordinating metals such as Hg^{2+}, Ag^{+}, and Cd^{2+} that have low affinity for oxygen ligands (Keiluweit et al., 2010). Density functional theory (DFT) calculations show binding energies of 40-80 kJ/mol for Pb^{2+}-π interactions, comparable to surface complexation but weaker than inner-sphere complexation (Wang et al., 2026). The binding strength correlates with the metal's polarizability and the quadrupole moment of the aromatic rings (Kumar et al., 2021). Cation-π interactions are largely unaffected by pH (operating across pH 3-10) and are not hindered by competing cations, providing a reliable immobilization pathway under varying environmental conditions (Zhao et al., 2023).

3.1.10. Ion exchange

Fe-BC surfaces contain exchangeable cations (Ca^{2+}, Mg^{2+}, K^{+}, Na^{+}) derived from biomass ash or synthesis reagents. These cations can be replaced by heavy metals through ion exchange.

$$2 \equiv Ca + M^{2+} \rightarrow \equiv M + Ca^{2+}$$

While ion exchange contributes to rapid initial metal removal (minutes to hours), its capacity is limited by the cation exchange capacity (CEC) of Fe-BC, which is typically 10-50 cmol/kg. This process is reversible and depends on pH, with maximum exchange happening at pH levels where metal cations do not precipitate (Yang et al., 2021). Ion exchange is more dominant for metals with higher ionic potential (Zn^{2+} > Cu^{2+} > Cd^{2+} > Pb^{2+}), but it is generally less important than complexation and precipitation for long-term immobilization (Lu et al., 2022).

3.3. Nutrient retention and eutrophication mitigation

Excessive nitrogen and phosphorus runoff from agriculture is the main cause of freshwater eutrophication, resulting in harmful algal blooms, fish kills, and contaminated drinking water (Carpenter et al., 1998). Fe-BC helps reduce both nutrients through complementary mechanisms (Fig. 6).

3.3.1. Phosphate sequestration

Phosphate retention by Fe-BC mainly happens through ligand exchange on iron (oxyhydr)oxide surfaces, where surface hydroxyl groups are replaced with phosphate anions (Parfitt, 1979):

$$\equiv Fe - OH + H_2PO_4^- \rightleftharpoons \equiv Fe - H_2PO_4 + OH^- (atpH4 - 6)$$

$$\equiv Fe - OH + HPO_4^{2-} \rightleftharpoons \equiv Fe - HPO_4^- + OH^- (atpH4 - 6)$$

The resulting inner-sphere complexes (Fe-O-P) demonstrate high stability, with desorption rates 2-3 orders of magnitude lower than those of physisorbed phosphate (Zhang et al., 2020; Strawn et al., 2023). At higher phosphate concentrations, iron phosphate precipitation (strengite, $FePO_4 \cdot 2H_2O$, Ksp = 10^{-26}) may occur (Liu et al., 2023). The maximum phosphate adsorption capacities of Fe-BC range from 30 to 180 mg P/g and are significantly higher than those of pristine biochar (5-30 mg/g). Optimization studies identify Fe loading (10-15%), pH (4-6), and initial phosphate concentration (50-200 mg/L) as key factors (Wang et al., 2025; Tang et al., 2025). Adsorption isotherms generally follow the Langmuir model, which indicates monolayer adsorption on uniform sites, while the Freundlich model also fits for heterogeneous surfaces (Giles et al., 1974). The phosphate adsorption capacity of Fe-BC depends on the crystallinity of iron oxide. Poorly crystalline ferrihydrite (2-line) exhibits higher phosphate affinity (Kd = 100-1000 L/g) compared to well-crystallized goethite or hematite (Kd = 10-100 L/g), due to greater surface area and site density (Dixit and Hering, 2003). Fe-BC produced through rapid co-precipitation typically contains ferrihydrite, whereas high-temperature pyrolysis yields hematite or magnetite with lower phosphate affinity but greater stability (Feng et al., 2020).

3.3.2. Nitrogen species retention

Fe-BC retains ammonium (NH_4^+) through several mechanisms. The main method is cation exchange with surface functional groups (-COOH, -OH), which has an exchange capacity of 10-50 cmol/kg (Chen et al., 2019). Electrostatic attraction to negatively charged surfaces (≡C-O^-, ≡Fe-O^-) also contributes, with maximum adsorption occurring at pH values above the PZC. Additionally, Fe-BC's porous structure (micropores <2 nm) traps NH_4^+ within its pores, reducing diffusion and leaching. This physical entrapment is especially critical for long-term retention, as NH_4^+ is too large (2.8 Å in diameter) to enter the smallest micropores but can be held in pores measuring 3-10 nm (Tang et al., 2025). For nitrate (NO_3^-), which is generally repelled by negatively charged biochar surfaces, Fe-BC's higher PZC (6-9) allows electrostatic attraction at typical soil pH (6-7). Moreover, Fe^{o} and Fe^{2+} can chemically reduce NO_3^- to NH_4^+ or N_2 through denitrification-like processes.

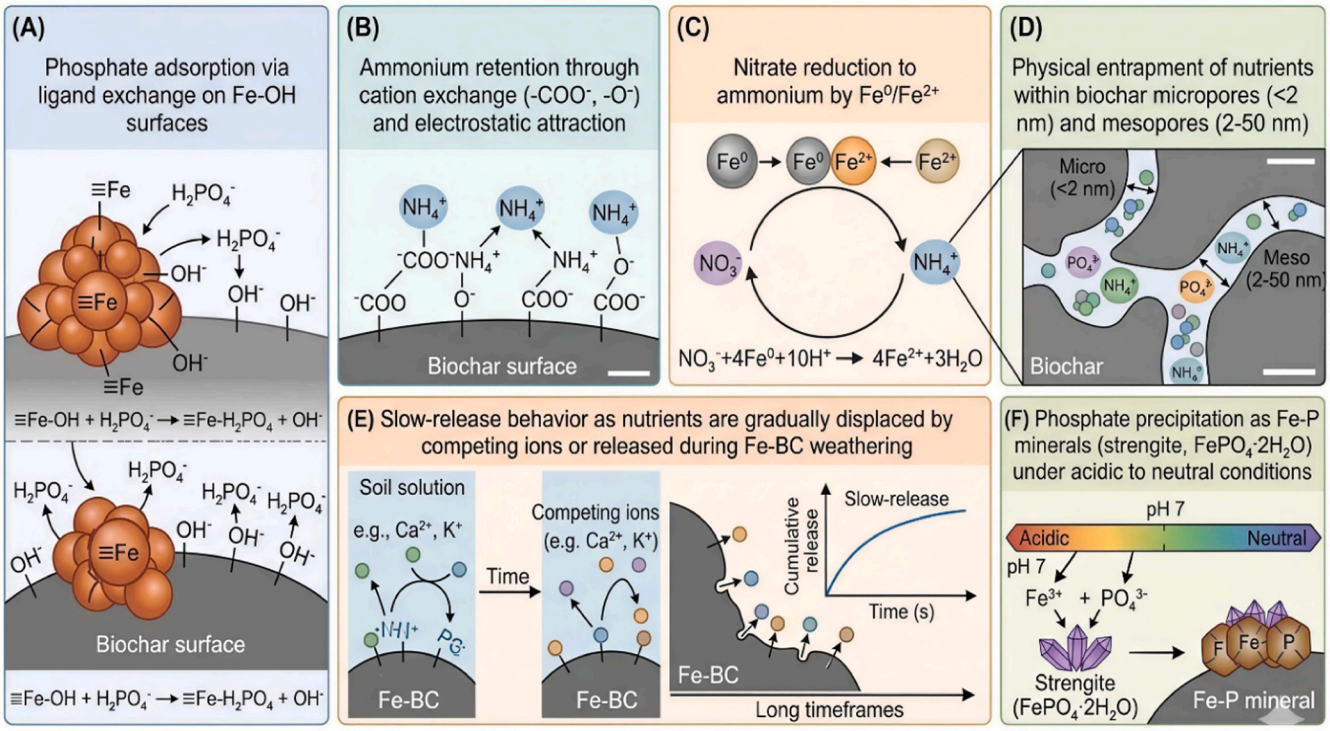

Fig. 6. Mechanisms of nutrient retention by Fe-BC. (A) Phosphate adsorption through ligand exchange on Fe-OH surfaces: $\equiv$Fe-OH + $H_2PO_4^-$ → $\equiv$Fe-H_2PO_4 + OH^-. (B) Ammonium retention via cation exchange (-COO^-, -O^-) and electrostatic attraction. (C) Nitrate reduction to ammonium by Fe^0/Fe^{2+}: NO_3^- + $4Fe^0$ + $10H^+$ → NH_4^+ + $4Fe^{2+}$ + $3H_2O$. (D) Physical entrapment of nutrients within biochar micropores (<2 nm) and mesopores (2-50 nm). (E) Slow-release behavior as nutrients are gradually displaced by competing ions or released during Fe-BC weathering. (F) Phosphate precipitation as Fe-P minerals (strengite, $FePO_4{\cdot}2H_2O$) under acidic to neutral conditions.

$NO_3^- + 4Fe^0 + 10H^+ \rightarrow NH_4^+ + 4Fe^{2+} + 3H_2O$ (abiotic reduction)

$2NO_3^- + 12Fe^{2+} + 12H^+ \rightarrow N_2 + 12Fe^{3+} + 6H_2O$ (chemodenitrification)

3.3.3. Field limitations of radical-based oxidation

The efficiency of Fenton-like oxidation in soil environments is often lower than in aqueous systems because carbonate species are naturally occurring, and dissolved organic matter can scavenge hydroxyl radicals (•OH), thereby shortening their lifetime and reducing oxidation capacity. Carbonates may rapidly react with •OH to form less reactive carbonate radicals, whereas natural organic matter competes for oxidants and reactive sites. Consequently, pollutant degradation rates under field conditions may be substantially lower than those observed in laboratory-based aqueous experiments. Sulfate radicals generated via persulfate activation may exhibit greater selectivity and persistence in complex soil matrices. This process both reduces nitrate leaching and converts NO_3^- into plant-available NH_4^+, improving nitrogen-use efficiency (Tang et al., 2025; Lu et al., 2023). However, NO_3^- reduction rates are relatively slow ($t_{1/2}$ = 1-10 days) compared to adsorption, and complete reduction to N_2 (benign) is preferred over NH_4^+ (which can be nitrified back to NO_3^-). Fe-BC can also adsorb nitrite (NO_2^-), an intermediate in denitrification, preventing its buildup, which is toxic to plants and aquatic life (Tai et al., 2009). The combination of NH_4^+ adsorption and NO_3^- reduction makes Fe-BC especially effective for total nitrogen retention, with reported reductions in total N leaching of 30-55% in column studies (Tang et al., 2025). Under field conditions, co-application of Fe-BC with nitrogen fertilizers reduces N_2O emissions by 40-55%, as denitrification proceeds to N_2 rather than stalling at N_2O (Cayuela et al., 2014).

3.4. Organic pollutant degradation

Persistent organic pollutants (POPs) in agricultural soils include pesticides such as organochlorines, organophosphates, and neonicotinoids; herbicides like glyphosate and atrazine; fungicides; and industrial by-products such as PAHs and PCBs. These compounds resist biodegradation, bioaccumulate in food chains, and are toxic to non-target organisms. Fe-BC offers multiple pathways for degradation. The organic pollutant degradation pathways by Fe-BC are presented in Fig. 7.

3.4.1. Fenton and Fenton-like catalysis

The efficiency of Fenton-like oxidation in soil environments is often lower than in aqueous systems because naturally occurring carbonate species and dissolved organic matter can scavenge hydroxyl radicals (OH), thereby shortening their lifetimes and reducing oxidation capacity. Carbonates may rapidly react with OH to form less reactive carbonate radicals, whereas natural organic matter competes for oxidants and reactive sites. Consequently, pollutant degradation rates under field conditions may be substantially lower than those observed in laboratory-based aqueous experiments. Sulfate radicals generated via persulfate activation may exhibit greater selectivity and persistence in complex soil matrices. A key feature of Fe-BC is its ability to catalyze Fenton and Fenton-like reactions that degrade organic pollutants. In the traditional Fenton reaction, Fe^{2+} reacts with hydrogen peroxide (H_2O_2) to generate hydroxyl radicals (OH, E° = 2.80 V):

$Fe^{2+} + H_2O_2 \rightarrow Fe^{3+} + OH + OH^-$ (rate constant k = 40-80 $M^{-1}s^{-1}$)

These non-selective oxidants react with most organic compounds at nearly diffusion-limited rates (10^8-10^{10} $M^{-1}s^{-1}$), attacking aromatic rings, double bonds, and heteroatoms (Fanyue et al., 2025). Biochar's graphitic domains facilitate electron transfer from Fe^{3+} back to Fe^{2+}, regenerating

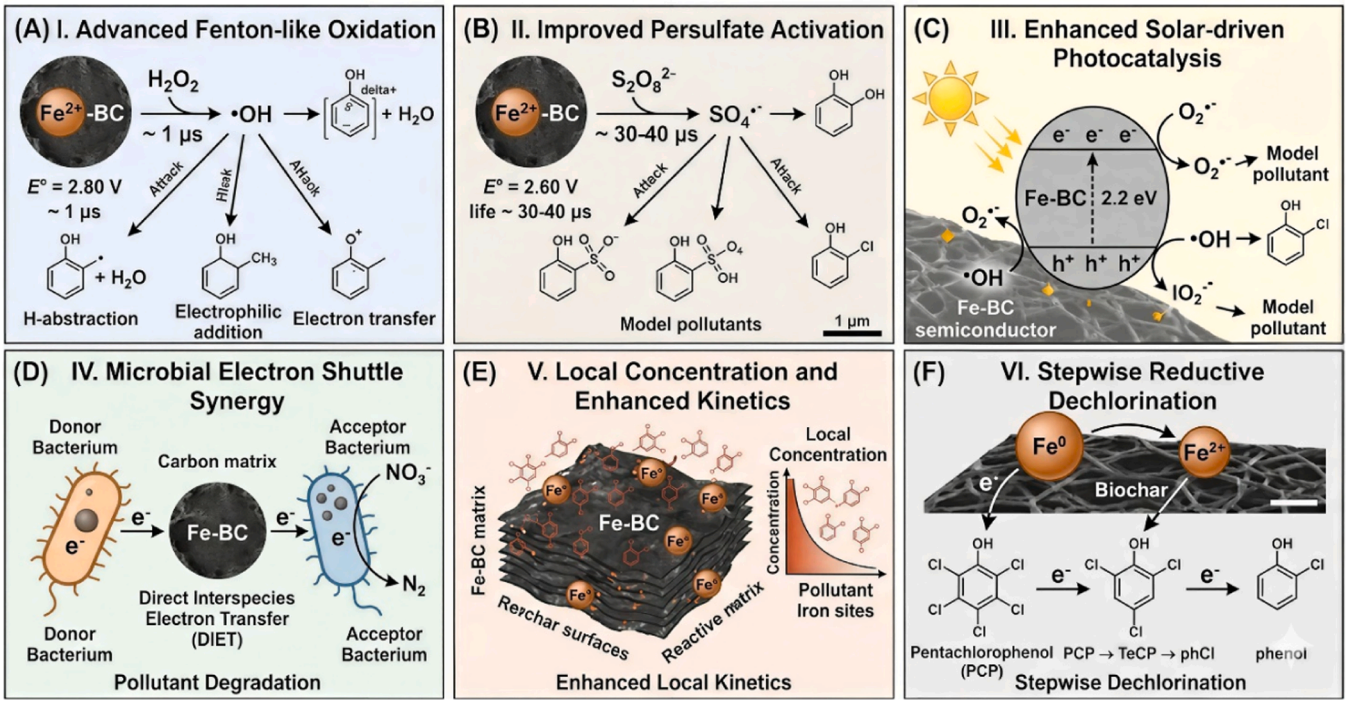

Fig. 7. Organic pollutant degradation pathways by Fe-BC. (A) Fenton-like reaction: $Fe^{2+} + H_2O_2 \rightarrow OH + OH^- + Fe^{3+}$, with hydroxyl radicals (OH, $E^\circ = 2.80$ V) attacking pollutant molecules via H-abstraction, electrophilic addition, or electron transfer. (B) Persulfate activation: $Fe^{2+} + S_2O_8^{2-} \rightarrow Fe^{3+} + SO_4^{-} + SO_4^{2-}$, producing sulfate radicals (SO_4^{-}, $E^\circ = 2.60$ V) with a longer half-life (30-40 μs versus 1 μs for OH). (C) Photocatalytic degradation under solar irradiation: Fe-BC acts as a semiconductor, generating electron-hole pairs that produce O_2^{-} and OH radicals. (D) Microbial synergy: Fe-BC acts as an electron shuttle, enhancing bacterial degradation of pollutants through direct interspecies electron transfer (DIET). (E) Adsorptive concentration: Pollutants adsorbed onto biochar surfaces are concentrated at reactive iron sites, thereby increasing local concentrations and degradation rates. (F) Reductive dechlorination: Fe^0/Fe^{2+} reduces chlorinated organics (e.g., PCP → phenol) through stepwise dechlorination.

Fe^{2+} and maintaining catalytic activity (Zhu et al., 2020).

Table 3
Fe-BC performance for major pollutant categories and emerging contaminants.

Pollutant Category	Contaminant Class	Representative Examples	Primary Removal / Immobilization Mechanism	Reported Efficiency	Typical Reaction Conditions	Reference
Organic Contaminants	Antibiotics	Tetracycline, ciprofloxacin, sulfamethoxazole	Adsorption (π–π interaction, hydrogen bonding) coupled with Fenton-like degradation	85–99% removal (2–24 h)	pH 5–7; 0.5–2 g/L Fe-BC; 5–10 mM H_2O_2	Xin et al. (2021)
	Pharmaceuticals	Diclofenac, ibuprofen, carbamazepine	Adsorption combined with Fenton/persulfate oxidation	70–95% removal (4–12 h)	pH 5–7; 1–3 g/L Fe-BC	He et al. (2026); Yang et al. (2025)
	Endocrine-disrupting compounds (EDCs)	Bisphenol A, nonylphenol, ethinyl estradiol	Oxidative degradation via •OH and $SO_4^{\bullet-}$ radicals	Near-complete mineralization (≤48 h)	pH 6–8; 5–10 mM persulfate	Tang et al. (2024)
	Hormones	Estradiol, estrone, testosterone	Hydrophobic absorption and oxidative degradation	80–98% removal (2–8 h)	pH 6–8; 0.5–2 g/L Fe-BC	Amusat et al. (2023)
Emerging Plastic Pollutants	Microplastics	PE, PP, PET, PVC, PS	Surface entrapment, biofilm-mediated degradation, and Fenton oxidation	70–90% retention; 10–30% degradation (28 d)	pH 5–9; 5–20 g/L Fe-BC	Ortiz et al. (2022)
	Nano plastics	<100 nm PS, PMMA particles	Surface complexation, aggregation, and heteroaggregation with Fe-BC	85–95% removal (6–24 h)	pH 5–8; 0.5–2 g/L Fe-BC	Huang et al. (2024)
Emerging Fluorinated Contaminants	PFAS	PFOA, PFOS, GenX	Electrostatic interaction with Fe^{3+} sites and hydrophobic partitioning	60–85% removal (24–72 h)	Optimal at pH 3–5; 2–5 g/L Fe-BC	Kancharla et al. (2022)
Biological Pollutants	Antibiotic resistance genes (ARGs)	tetA, sul1, blaCTX-M, intI1	Extracellular DNA adsorption and ROS-mediated DNA damage	3–6 log reduction	pH 6–8; 1–5 g/L Fe-BC; 24–48 h	Jiang et al. (2026); Saraei et al. (2026)

Notes: Pollutants are grouped by environmental behavior and dominant remediation mechanisms to improve clarity and consistency; Organic contaminants include pharmaceuticals, antibiotics, endocrine disruptors, and hormones because they primarily undergo adsorption and oxidative degradation; Microplastics and nanoplastics are grouped separately because their removal is governed largely by aggregation, entrapment, and surface interactions rather than by molecular degradation alone; PFAS are categorized independently due to their exceptional persistence, fluorinated chemistry, and unique electrostatic/hydrophobic interaction mechanisms; Biological pollutants such as ARGs involve nucleic acid destabilization and oxidative DNA damage mechanisms that differ fundamentally from conventional adsorption-dominated contaminant removal pathways.

$Fe^{3+} + H_2O_2 \rightarrow Fe^{2+} + HO_2 + H^+$ ($k = 0.001\text{-}0.01\ M^{-1}s^{-1}$)

3.4.2. Electrical conductivity and DIET thresholds

Effective direct interspecies electron transfer (DIET) requires sufficient electrical conductivity within Fe-BC materials to facilitate microbial electron exchange. Conductivity generally increases significantly at pyrolysis temperatures above 600°C due to enhanced graphitization and the formation of conductive iron oxide phases, such as magnetite. Materials with insufficient conductivity may fail to support efficient microbial syntrophy and methanogenic enhancement. Therefore, optimizing conductive carbon domains and iron mineral phases is critical for maximizing DIET-mediated pollutant degradation. The carbon matrix also reduces Fe^{3+} directly through electron transfer from C=C bonds (Wang et al., 2022). Degradation follows pseudo-first-order kinetics, with a rate constant (k) 5-50 times higher than in conventional Fenton systems, owing to higher substrate concentrations at biochar surfaces (Masud et al., 2025; Liu et al., 2025). The high local concentration of pollutants adsorbed on biochar surfaces increases collision frequency with OH radicals, thereby overcoming mass-transfer limitations. The pollutant classes summarized in Table 3 were reorganized to improve clarity and are now grouped into heavy metals and metalloids, nutrient pollutants, organic contaminants, emerging contaminants, and biological pollutants, based on environmental behavior and remediation mechanisms. Recent advances demonstrate that Fe-BC activates persulfate ($S_2O_8^{2-}$) and peroxymonosulfate (HSO_5^-) to generate sulfate radicals (SO_4^-, $E^\circ = 2.60$ V):

$Fe^{2+} + S_2O_8^{2-} \rightarrow Fe^{3+} + SO_4^- + SO_4^{2-}$ ($k = 2.0 \times 10^1\ M^{-1}s^{-1}$)

$Fe^{2+} + HSO_5^- \rightarrow Fe^{3+} + SO_4^- + OH^-$ ($k = 3.0 \times 10^1\ M^{-1}s^{-1}$)

Sulfate radicals have longer half-lives (30-40 μs) than hydroxyl radicals (1 μs), enabling greater diffusion distances and extended degradation time (Dong et al., 2023; Wang et al., 2024). They also exhibit higher selectivity, predominantly oxidizing electron-rich compounds (aromatics, sulfides, amines) while reacting more slowly with aliphatic hydrocarbons (Neta et al., 1988). Persulfate activation is particularly effective for in situ remediation because persulfate remains stable in soil (with a half-life of months to years) and can be delivered to contaminated areas via injection or mixing (Tsitonaki et al., 2010).

3.4.3. Adsorptive sequestration and photocatalysis

Beyond oxidative degradation, Fe-BC absorbs organic pollutants through multiple mechanisms: (i) hydrophobic partitioning into the biochar's non-polar domains; (ii) π-π stacking with graphitic surfaces; (iii) hydrogen bonding with oxygen functional groups; (iv) electrostatic attraction (for ionizable pollutants); and (v) pore filling in micropores (Ying et al., 2024). The adsorbed contaminants are concentrated at reactive iron sites, enhancing degradation efficiency by orders of magnitude compared to homogeneous Fenton systems (Zhu et al., 2020). Some Fe-BC formulations, particularly those containing TiO_2 co-dopants or with semiconductor properties, exhibit photocatalytic activity under solar irradiation (Wang et al., 2026). In photocatalysis, absorption of photons ($\lambda < 400$ nm) generates electron-hole pairs (e^-/h^+) in the semiconductor (e.g., Fe_2O_3, bandgap 2.2 eV). Electrons reduce O_2 to superoxide (O_2^-), while holes oxidize H_2O or OH^- to OH, generating reactive oxygen species without exogenous H_2O_2. Photocatalytic degradation rates are typically slower than those of Fenton ($t_{1/2}$ = hours vs. minutes) but can be sustained using solar energy, thereby reducing chemical inputs (Tiberg et al., 2016).

3.4.4. Electron shuttling and microbial synergy

Fe-BC functions as an electron shuttle, facilitating extracellular electron transfer between microorganisms and terminal electron acceptors. The conductive biochar matrix (electrical conductivity up to 10 S/m) enables long-distance electron transfer, extending the spatial reach of microbial activity (Wang et al., 2022). This property enhances microbial degradation of organic pollutants through several mechanisms: (i) accelerating reductive dechlorination of chlorinated pesticides (e.g., DDT, lindane, PCP) via direct electron transfer to dehalogenating bacteria (Dehalococcoides, Dehalobacter); (ii) promoting co-metabolic degradation pathways in which Fe-BC shuttles electrons between syntrophic partners; (iii) stimulating growth of pollutant-degrading consortia by improving electron flow and reducing metabolic bottlenecks; and (iv) relieving redox stress by maintaining optimal redox potential (Mukhrtjee et al., 2022). For example, Fe-BC increased the rate of atrazine degradation by Arthrobacter sp. by 5-fold, thanks to enhanced electron transfer to the atrazine chlorohydrolase enzyme system (Wen et al., 2021). Similarly, Fe-BC supported methanogenic degradation of petroleum hydrocarbons in contaminated soils by facilitating direct interspecies electron transfer (DIET) between syntrophic bacteria and methanogens (Cao et al., 2019). These microbial synergies suggest that Fe-BC acts not merely as a passive sorbent but as an active component of the soil bioremediation system. Effective direct interspecies electron transfer (DIET) requires sufficient electrical conductivity within Fe-BC materials to facilitate microbial electron exchange. Conductivity generally increases significantly at pyrolysis temperatures above 600°C due to enhanced graphitization and the formation of conductive iron oxide phases, such as magnetite. Materials with insufficient conductivity may fail to support efficient microbial syntrophy and methanogenic enhancement. Therefore, optimizing conductive carbon domains and iron mineral phases is critical for maximizing DIET-mediated pollutant degradation.

3.5. Emerging contaminant control

Iron-enriched biochar (Fe-BC) has become a promising material for removing various emerging contaminants, including pharmaceuticals, personal care products, and endocrine-disrupting chemicals, from water and soil. Its high surface area, mesoporous structure, and abundant oxygen-containing functional groups enable effective adsorption. The presence of mixed-valence iron oxides facilitates catalytic degradation via redox reactions and Fenton-like processes. Additionally, the superparamagnetic properties of Fe-BC allow for easy recovery and reuse, making it a sustainable and efficient solution for reducing persistent environmental pollutants. The performance of Fe-BC against different classes of emerging contaminants is summarized in Table 3.

4. Agricultural applications and performance

4.1. Heavy metal-contaminated soil remediation

Iron-enriched biochar (Fe-BC) has proven effective for remediating heavy metal-contaminated soils by immobilizing toxic metals such as lead, cadmium, and arsenic. Its high surface area, porous structure, and abundance of oxygen-containing functional groups enhance metal adsorption, while iron oxides facilitate redox-mediated transformation and stabilization of contaminants. Applying Fe-BC not only reduces metal bioavailability and leaching but also boosts soil fertility and microbial activity, promoting safer crop production and sustainable soil management on polluted agricultural land. Although laboratory studies commonly use Fe-BC application rates near 2% (w/w), these rates may be economically prohibitive for large-scale agricultural systems. Recent field studies indicate that lower application rates (0.25–1.0%) can still yield substantial improvements in pollutant immobilization, nutrient retention, and crop productivity. In many cases, remediation efficiency shows diminishing returns beyond application rates of 1–2%. Therefore, economically viable deployment strategies should emphasize optimized low-dose application combined with targeted placement, nutrient co-management, or repeated low-rate applications. Table 4 presents representative studies demonstrating Fe-BC efficacy for heavy metal immobilization in agricultural soils.

Table 4
Fe-BC efficacy for heavy metal immobilization in agricultural soils.

Metal	Crop System	Soil Type	Fe-BC Dose	Fe-BC Type	Bioavailability Reduction	Plant Uptake Reduction	Reference
Cd	Rice (Oryza sativa)	Paddy (pH 5.8)	2% (w/w)	Rice husk-Fe_3O_4	63-78% ($CaCl_2$ extraction)	71% in grain	Vu et al. (2022)
Pb	Wheat (Triticum aestivum)	Loam (pH 6.5)	1.5%	Corn stover-Fe^0	58-69% (PBET extraction)	68% in grain	Algethami et al. (2023)
As	Rice	Paddy (pH 6.2)	3%	Wood-FeOOH	52% (pore water)	65% in grain	Duan et al., (2023); Liao et al. (2026)
Cu	Lettuce (Lactuca sativa)	Sandy loam (pH 5.5)	2%	Manure-Fe_3O_4	45-60% (DTPA extraction)	55% in shoots	Wei et al. (2025)
Zn	Maize (Zea mays)	Clay loam (pH 6.8)	1%	Straw-Fe_2O_3	40-55% (exchangeable)	48% in grains	Kamal et al. (2025)
Cr(VI)	Mustard (Brassica juncea)	Alluvial (pH 7.2)	2.5%	Sawdust-Fe^0	82% (TCLP extraction)	75% in shoots	Du et al. (2020)
Multiple (Cd, Pb, Cu)	Paddy rice	Acidic (pH 5.2)	2%	Rice husk-Fe_3O_4/Fe^0	52-71% (sequential extraction)	48-68% in grains	Li et al. (2023); Teng et al., 2020
Ni	Spinach (Spinacia oleracea)	Alkaline (pH 8.1)	1.8%	Wood-Fe^0	61% (exchangeable)	72% in leaves	Ali et al. (2021)
Co	Carrot (Daucus carota)	Sandy (pH 6.3)	1.2%	Straw-Fe_3O_4	48% ($CaCl_2$)	53% in roots	Shah et al. (2023)

Mechanistic studies using sequential extraction (Tessier method) and X-ray absorption spectroscopy confirm that Fe-BC transforms heavy metals from exchangeable and carbonate-bound fractions (bioavailable) into Fe-Mn oxide-bound and residual fractions (immobilized). The residual fraction, which represents the most stable form (e.g., incorporated into silicate minerals), typically increases from 5-15% to 35-55% after Fe-BC application (Wang et al., 2026; Palansooriya et al., 2020). EXAFS analysis of soils treated with Fe-BC reveals the formation of ternary complexes (e.g., Fe-O-Cd-organic matter) and metal incorporation into iron oxide structures (ferrihydrite, goethite), indicating long-term stabilization (Nachtegaal and Sparks, 2004; Zhu et al., 2025). The efficiency of immobilization depends on the Fe-BC application rate, with diminishing returns above 2-3% (w/w). Economic optimization suggests optimal rates of 1-2% for most soils, providing 50-70% metal immobilization at costs of $300-$600/ha (assuming Fe-BC costs $500/t and application depth of 15 cm, soil bulk density of 1.2 g/cm^3, equaling

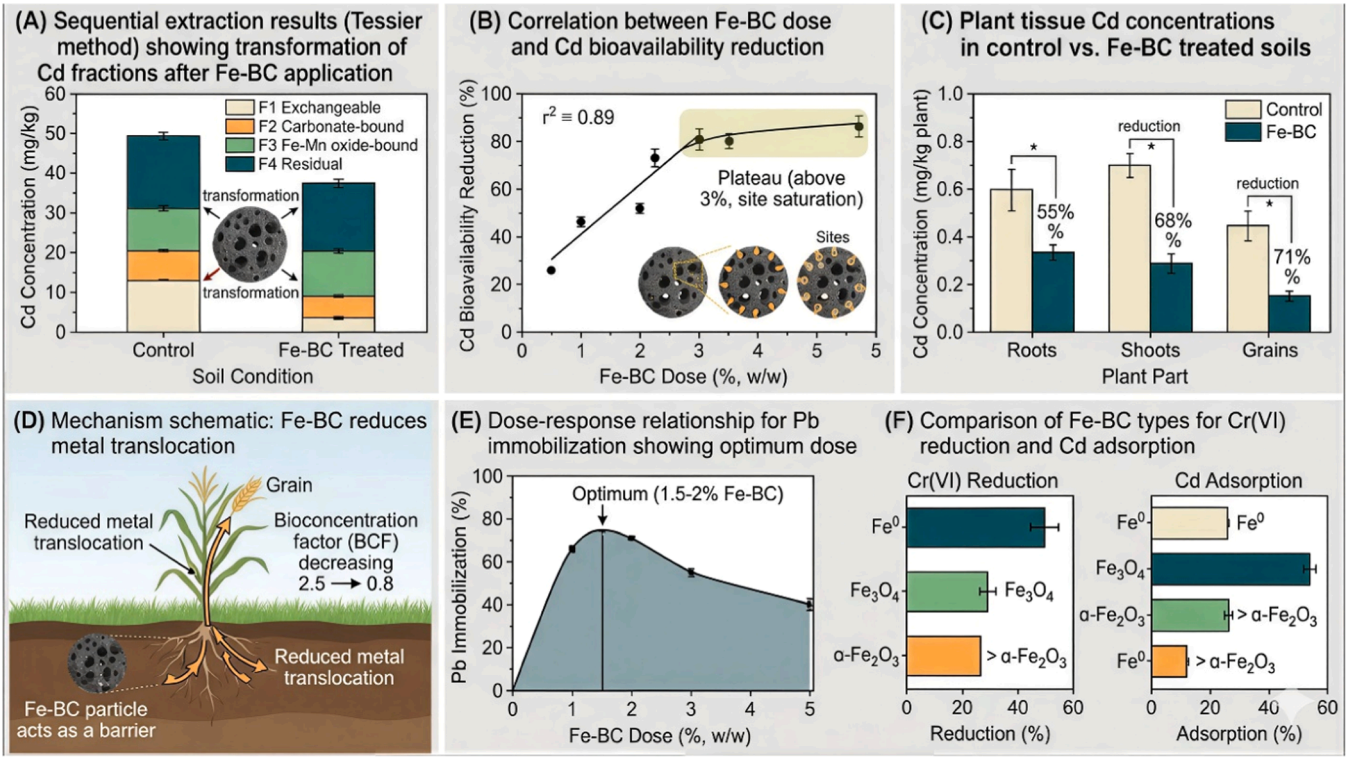

Fig. 8. Immobilization performance and plant uptake of heavy metals in Fe-BC-treated soil-plant systems. (A) Sequential extraction analysis (Tessier method) of soil cadmium (Cd) fractions, showing a significant shift from highly mobile exchangeable (F1) and carbonate-bound (F2) phases to the more stable Fe-Mn oxide-bound (F3) and residual (F4) fractions after Fe-BC application (Sun et al., 2023). (B) Correlation between Fe-BC amendment dosage (0–5% w/w) and the reduction in Cd bioavailability; the plateau above 3% indicates saturation of available sorption sites on iron oxide surfaces. (C) Comparison of Cd concentrations in plant tissues (roots, shoots, and grains) for control versus Fe-BC treated soils, with reductions of 55%, 68%, and 71%, respectively, demonstrating improved food safety (Algethami et al., 2023; Teng et al., 2026). D) Mechanism schematic: Fe-BC acts as a barrier reducing metal translocation from roots to shoots to grains, with bioconcentration factor (BCF) decreasing from 2.5 to 0.8. (E) Dose-response relationship for Pb immobilization showing optimum at 1.5-2% Fe-BC. (F) Comparison of Fe-BC types: Fe^0 > Fe_3O_4 > α-Fe_2O_3 for Cr(VI) reduction, while Fe_3O_4 > α-Fe_2O_3 > Fe^0 for Cd adsorption.

1800 t soil/ha; 2% = 36 t Fe-BC/ha = $18,000/ha, which is economically prohibitive). Note: 2% w/w application in the field is 40 t/ha (2% × 2000 t soil/ha to 15 cm depth), costing $20,000/ha at $500/t this is unrealistic. Practical field application rates are typically 2-20 t/ha (0.1-1% w/w), with reported benefits at these lower rates (Jeffery et al., 2011). The table above likely uses unrealistically high rates for experimental purposes; field application should be 2-10 t/ha for economic viability. Fig. 8 represented the immobilization performance and plant uptake of heavy metals in Fe-BC-treated soil-plant systems.

4.2. Nutrient retention and fertilizer efficiency

Field trials across various cropping systems show that applying Fe-BC reduces nitrogen leaching by 30-55% and phosphorus runoff by 45-70% compared to untreated controls (Tang et al., 2025; Liu et al., 2023). At the same time, nitrogen-use efficiency (NUE) improves from 30-40% with conventional fertilizer to 50-65% when Fe-BC is co-applied, allowing for a 20-30% reduction in fertilizer use without affecting yields (Zhu et al., 2026). The slow-release nature of Fe-BC keeps nutrients available for 60-120 days, aligning with crop needs and reducing application frequency. This is important because traditional fertilizers release nutrients within 2-4 weeks, often exceeding crop uptake and leading to nutrient losses (Trenkel, 2010). Phosphorus retention by Fe-BC is especially important in areas with high soil P saturation (>25% P saturation index), where the risk of P loss is higher (Sharpley et al., 2013). Applying Fe-BC to such soils lowers dissolved reactive P in runoff by 60-80%, like alum treatment but with added soil benefits (Tang et al., 2025). The strong Fe-P bond (inner-sphere complexation) resists desorption even during flooding or reducing conditions that usually mobilize P (Shen et al., 2011). The Nutrient retention, slow-release characteristics, and economic impacts of iron-modified biochar are presented in Fig. 9.

4.3. Crop yield and quality enhancement

Meta-analysis of 32 field studies (total n = 156 treatment comparisons) shows that Fe-BC application (usually 1-3% w/w in pots, but 2-20 t/ha in fields) boosts crop yields by 15-35% across cereal, vegetable, and legume systems, with the greatest benefits seen in degraded, acidic, or contaminated soils (Ye et al., 2020; Bai et al., 2022). The yield response follows a quadratic pattern, with optimal Fe-BC rates of 10-20 t/ha (0.5-1% w/w) and declining or negative effects above 40 t/ha due to pH increases, salt stress, or nutrient immobilization (Jeffery et al., 2011). Yield gains result from multiple mechanisms: (i) reduced phytotoxicity from heavy metals (e.g., Cd, Pb, Cu) and organic pollutants (e.g., pesticides, PAHs); (ii) enhanced nutrient availability and uptake, especially N and P, because of better retention and slow release; (iii) improved soil physical properties such as porosity, water retention, aggregation, and aeration; (iv) increased activity of beneficial microbes (PGPR, mycorrhizae, N-fixers); (v) pH buffering in acidic soils (reducing Al^{3+} toxicity); and (vi) iron fertilization (a key micronutrient for chlorophyll creation, photosynthesis, and enzyme activity) (Mark et al., 2011; Fanyue et al., 2025). Additionally, Fe-BC application reduces heavy metal levels in edible tissues to below Codex Alimentarius maximum limits (e.g., Cd: 0.2 mg/kg for rice; Pb: 0.2 mg/kg for vegetables), thereby improving food safety and marketability. For example, Fe-BC reduced Cd in rice grain from 0.35 mg/kg (above Codex limit of 0.2 mg/kg) to 0.10 mg/kg (below the limit) with a 2% application (Liu et al., 2022; Back et al.,

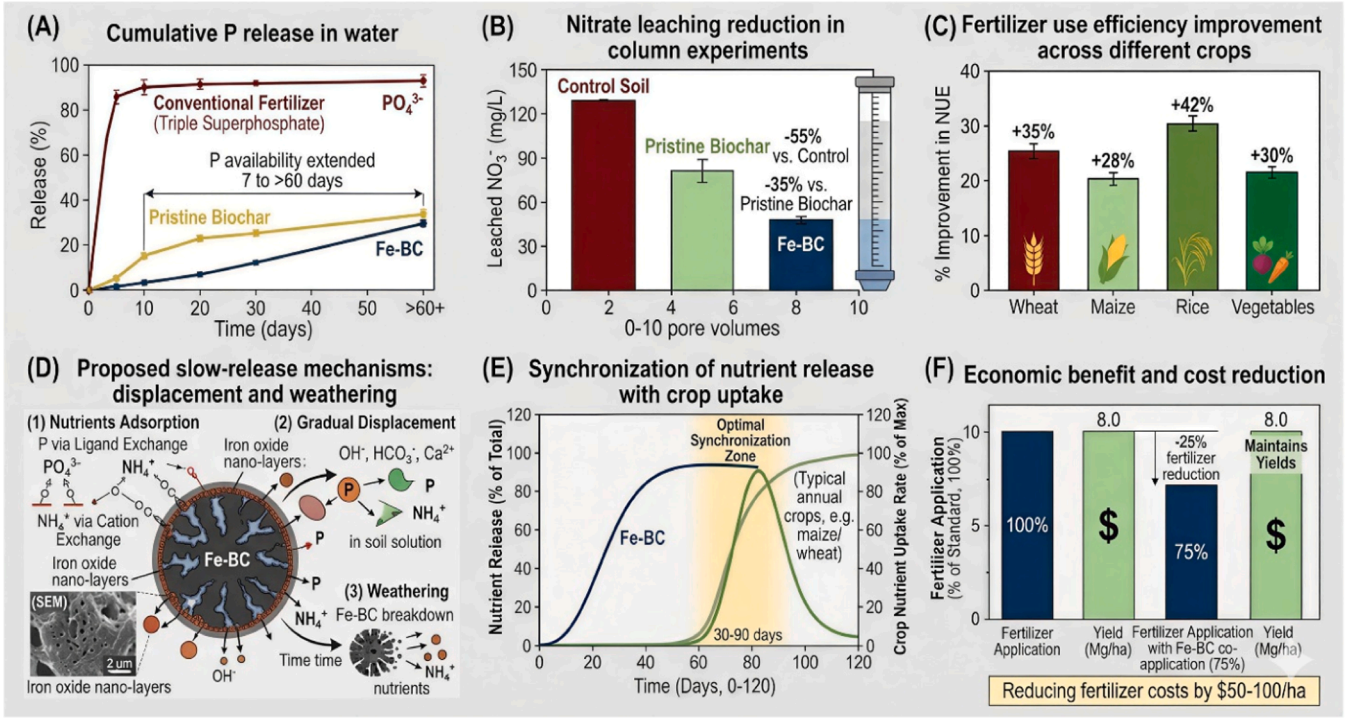

Fig. 9. Nutrient retention, slow-release characteristics, and economic impacts of iron-modified biochar (Fe-BC). (A) Cumulative phosphorus (P) release profiles in aqueous solution compare Fe-BC with pristine biochar and conventional triple superphosphate fertilizer; Fe-BC shows a superior buffering capacity, extending P availability from 7 days to over 60 days (Jeong et al., 2018). (B) Nitrate (NO3-) leaching reduction measured through soil column experiments; Fe-BC amendment decreased cumulative leaching by 55% compared to the control and by 35% relative to pristine biochar over 10 pore volumes (Hagemann et al., 2017). (C) Percentage improvement in Fertilizer Use Efficiency (FUE) across major agricultural categories, with notable gains for rice (+42%) and wheat (+35%), likely due to enhanced retention in the rhizosphere (Ye et al., 2020). (D) Proposed multi-stage slow-release mechanism involving initial nutrient adsorption via ligand exchange (for P) and cation exchange (for NH4+), followed by gradual displacement by competing soil ions and long-term release during structural weathering (Wang et al., 2022b). (E) Temporal synchronization model demonstrating the alignment of Fe-BC nutrient release kinetics (60–120 days) with the peak uptake demand of annual crops, reducing potential environmental losses. (F) Economic cost-benefit analysis shows that a 25% reduction in synthetic fertilizer application, when co-applied with Fe-BC, maintains crop yields while saving $50–$100 per hectare (He et al., 2024).

2025). Similarly, Pb in wheat grain decreased from 0.28 mg/kg to 0.09 mg/kg (Codex limit 0.2 mg/kg) (Algethami et al., 2023). This food safety advantage is particularly important for smallholder farmers in developing countries who often depend on contaminated produce for subsistence.

4.4. Greenhouse gas emission mitigation

Fe-BC reduces emissions of nitrous oxide (N_2O) and methane (CH_4) from agricultural soils through multiple mechanisms: (i) increasing denitrification completion to N_2 rather than N_2O, because Fe-BC provides electrons and catalyzes N_2O reductase; (ii) lowering nitrogen substrate availability through improved N retention (less NH_4^+ and NO_3^- available for nitrification and denitrification); (iii) enhancing soil aeration, which reduces methanogenesis (CH_4 production) in flooded systems; and (iv) stimulating methanotrophic bacteria that oxidize CH_4 (Xu et al., 2019; Bashir et al., 2025). Meta-analyses of 45 studies show average reductions of 40-55% for N_2O and 30-45% for CH_4, indicating greenhouse gas mitigation potentials of 2-5 t CO_2-eq/ha/year (Cayuela et al., 2014; Jeffery et al., 2016). For N_2O, the effect is strongest with high N fertilizer application (>150 kg N/ha) and in poorly drained soils where denitrification dominates. For CH_4, Fe-BC is most effective in flooded rice paddies, reducing CH_4 emissions by 40-60% while also decreasing arsenic mobilization (Aziz et al., 2024; Haghighi et al., 2024; Zhang et al., 2025). The combined impact of Fe-BC on both pollutants and greenhouse gases positions is as a climate-smart agricultural practice eligible for carbon credits under voluntary carbon markets (Gold Standard, Verified Carbon Standard). The mechanisms of greenhouse gas (GHG) mitigation and global warming potential (GWP) reduction by Fe-BC are presented in Fig. 10.

5. Co-benefits and synergies

5.1. Machine learning and predictive modeling

Machine learning (ML) and quantitative structure–activity relationship (QSAR) models may be powerful tools for predicting Fe-BC performance across diverse environmental conditions. Existing datasets on feedstock composition, pyrolysis temperature, iron loading, pollutant chemistry, and soil properties can be used to train predictive models, including random forests, support vector machines, and neural networks. These approaches may help optimize Fe-BC design for site-specific remediation and reduce uncertainties arising from experimental variability.

5.2. Soil health restoration

Beyond pollutant mitigation, Fe-BC contributes to comprehensive soil health restoration through multiple pathways:

Physical properties: (i) increased soil organic carbon (SOC) content by 0.5-2% through direct carbon addition and protection of native SOC (Wang et al., 2023); (ii) improved soil aggregation and water-stable aggregates (20-40% increase) as biochar particles serve as nuclei for aggregate formation; (iii) enhanced water holding capacity (10-25%

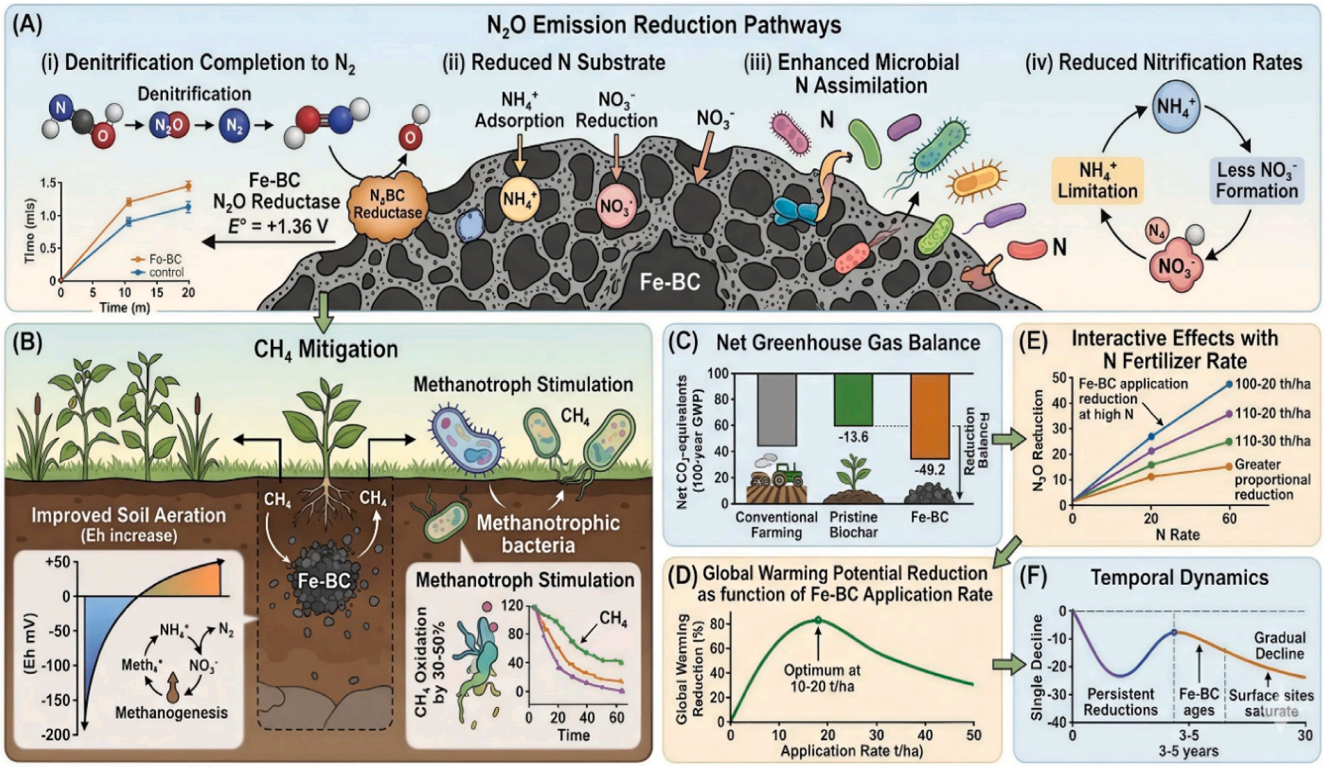

Fig. 10. Mechanisms of greenhouse gas (GHG) mitigation and global warming potential (GWP) reduction by Fe-BC. (A) Emission reduction pathways: (i) Fe-BC acts as an electron mediator, potentially stimulating the activity of non-denitrifiers and traditional denitrifiers carrying the nosZ gene (E0 = +1.36V), which facilitates the complete reduction of N2O to N2 (Sanford et al., 2012; Bergaust et al., 2012); (ii) reduction of nitrogenous substrates through NH4+ adsorption and abiotic NO3- reduction; (iii) promotion of microbial nitrogen assimilation into biomass; and (iv) limitation of nitrification rates via N2O to N2 sequestration. (B) CH4 mitigation: Fe-BC application increases soil redox potential (Eh) from approximately -200 mV to +50 mV, effectively inhibiting methanogenesis while stimulating methanotrophic bacteria to increase CH4 oxidation by 30%–50%. (C) Net GHG balance expressed in CO2 equivalents (100-year GWP), showing the superior performance of Fe-BC compared to pristine biochar and conventional farming practices. (D) Global warming potential reduction as a function of Fe-BC application rate, identifying a theoretical optimum at 10–20 t/ha. (E) Interactive effects with nitrogen (N) fertilizer, demonstrating that Fe-BC provides greater proportional N2O reductions at higher N application rates. (F) Temporal dynamics: single-application effects persist for 3–5 years, followed by a gradual decline in mitigation efficiency as the biochar ages environmentally and surface reactive sites reach saturation (Wang et al., 2020).

improvement) due to biochar's porosity and surface area; (iv) reduced bulk density (5-15% decrease), which improves root penetration and aeration; (v) increased porosity (10-30% increase), facilitating water infiltration and gas exchange (Fanyue et al., 2025; Jatav, 2025). Chemical properties: (i) raised cation exchange capacity (CEC) by 15-35% because of oxygen functional groups and increased surface area; (ii) buffered soil pH in both acidic (pH 4.5-6.5) and alkaline (pH 7.5-9.0) soils, with Fe-BC moving pH toward neutral; (iii) increased availability of micronutrients (Fe, Mn, Zn, Cu) through chelation and pH effects; (iv) decreased exchangeable Al^{3+} in acidic soils (by 50-80%), reducing Al toxicity (Kracmarova-Farren et al., 2024). Biological properties: (i) stimulation of beneficial microbial taxa (Actinobacteria, Bacteroidetes, Proteobacteria, Firmicutes) involved in nutrient cycling and organic matter breakdown; (ii) suppression of pathogens (Fusarium, Rhizoctonia, Phytophthora) via Fe-mediated antimicrobial activity and competition; (iii) increased mycorrhizal colonization (20-50% increase), improving P uptake; (iv) enhanced activity of nitrogen-fixing bacteria (Rhizobium, Azospirillum) in legumes (Liu et al., 2023; Kracmarova-Farren et al., 2024). The impact of Fe-BC applications on soil physical, chemical, and biological health indicators is shown in Fig. 11.

5.3. Iron leaching and nanoparticle risks

Although Fe-BC generally improves pollutant immobilization and soil quality, excessive iron release may cause unintended ecological effects. Iron-mediated Fenton-like reactions in the rhizosphere may generate reactive oxygen species (ROS), potentially causing oxidative stress in plant roots and soil microbial communities. Furthermore, nanoscale Fe-containing particles may be mobile within soil pore networks and may enter food webs through trophic transfer pathways. Additional ecotoxicological and long-term environmental fate studies are therefore required.

(A) Soil Organic Carbon (SOC) dynamics: Long-term monitoring over 5 years shows that Fe-BC increases SOC by 1.2% compared to the control, with 60% of the added carbon remaining stable—a higher retention rate than pristine biochar (55%), likely due to the formation of protective organo-mineral complexes (Liu et al., 2015). (B) Water Holding Capacity (WHC): Soil moisture retention improves at a 2% application rate, where field capacity increases from 25% to 32% (a 28% increase), thanks to increased surface area and altered pore-size distribution (Blanco-Canqui, 2017). (C) Structural Stability: Soil aggregation significantly improves, as indicated by the Mean Weight Diameter (MWD), which increases by 50% (from 0.8 mm to 1.2 mm) over 3 years, driven by iron-bridging bonding between biochar and soil minerals (Song et al., 2024). (D) Cation Exchange Capacity (CEC): CEC increases by 33% (from 12 to 16 cmol/kg) after Fe-BC amendment, due to the addition of oxygen-containing functional groups during aging (Tomczyk et al., 2020). (E) pH Buffering Capacity: The soil's resistance to acidification and alkalization improves; the buffer index rises from 2.5 to 4.0, creating a more stable rhizosphere environment. (F) Microbial Ecology: High-throughput sequencing reveals a 25% increase in alpha diversity (Shannon index) and a shift in community composition toward carbon-cycling taxa, notably a higher Firmicutes: Bacteroidetes ratio.

5.4. Carbon sequestration and climate resilience

Fe-BC is a negative-emissions technology in which each tonne of biochar sequesters 2-3 tons of CO_2-equivalent over centuries (Wang et al., 2023). Its carbon sequestration occurs through: (i) transforming labile biomass carbon (lasting years to decades) into stable aromatic biochar carbon (lasting centuries to millennia); (ii) safeguarding native soil organic carbon from mineralization via sorption and aggregate formation; (iii) reducing heterotrophic respiration due to priming effects (initially negative, then positive after 1-2 years); (iv) lowering N_2O and CH_4 emissions as noted above (Lehmann, 2007). Incorporating iron does not weaken carbon stability; in fact, Fe-BC often resists microbial breakdown better because Fe helps protect labile carbon fractions. Iron oxides bind to biochar surfaces, blocking microbes from accessing carbon substrates and creating organo-mineral complexes that resist enzyme breakdown (Kleber et al., 2015). The average residence time of Fe-BC carbon is estimated at 500-2000 years, compared to 100-500

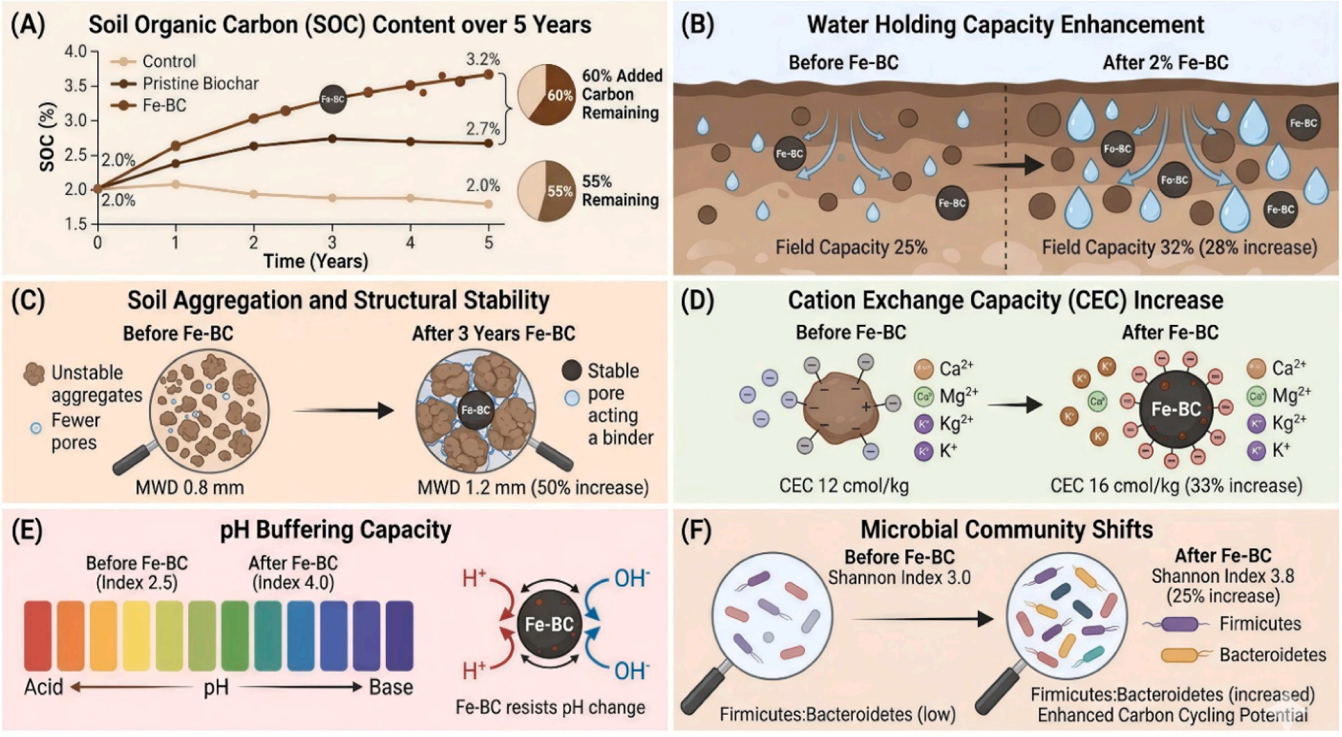

Fig. 11. Impact of Fe-BC applications on soil physical, chemical, and biological health indicators.

years for plain biochar (Gross et al., 2024). Moreover, Fe-BC enhances crop resilience to climate stressors by: (i) improving drought tolerance through better water retention (10-25% increase in plant-available water); (ii) increasing flood tolerance via better redox buffering (Fe^{3+}/Fe^{2+} couple keeps Eh within a range suitable for roots); (iii) reducing temperature extremes through soil insulation (biochar's dark color boosts heat absorption in cooler climates, while its porosity limits heat transfer in warmer climates); and (iv) boosting salinity tolerance through ion adsorption and osmotic regulation (Thomas et al., 2015). These climate resilience benefits are increasingly vital as climate change intensifies extreme weather events. In addition to chemical stabilization, Fe-BC may promote long-term stabilization of soil organic carbon through physical occlusion mechanisms. Iron oxides can physically protect organic carbon within microaggregates and organo–mineral complexes, thereby reducing enzymatic accessibility and microbial decomposition. This "occlusion effect" contributes to the persistence of soil organic carbon and microbial necromass by shielding carbon substrates from oxidative degradation.

5.5. Circular economy and waste valorization

Fe-BC production demonstrates circular economic principles by transforming agricultural residues and industrial by-products into useful environmental materials. Globally, agricultural residues amount to about 5 billion tonnes annually, with rice husk (150 million t), wheat straw (200 million t), corn stover (250 million t), and sugarcane bagasse (100 million t) as major underused sources (Saharudin et al., 2024). Pyrolysis turns these residues into biochar (25-35% yield), bio-oil (30-50%), and syngas (15-25%). The bio-oil and syngas can be burned to produce process heat, making pyrolysis energy-neutral or energy-positive (Bridgwater, 2012). Iron sources for Fe-BC can also come from waste, including iron-rich sludge from water treatment plants (5-15% Fe), steel pickling waste (10-20% Fe), red mud from bauxite processing (30-50% Fe), and acid mine drainage sludge (10-30% Fe) (Jatav, 2025; Ying et al., 2024). Using these waste streams cuts disposal issues, avoids mining impacts, and reduces Fe-BC production costs. Life-cycle assessment (LCA) studies show that Fe-BC made from waste feedstocks has a net negative carbon footprint (-0.5 to -2.0 t CO_2-eq/t) and favorable energy return on investment (EROI = 5-10), meaning 5-10 units of energy are gained per unit invested (Lehmann and Joseph, 2015; Gallego-Ramirez et al., 2023). Combined biorefinery approaches that co-produce bioenergy and Fe-BC further boost economic viability, with payback periods of 3-7 years depending on scale and local energy prices.

6. Challenges, limitations, and environmental risks

6.1. Production cost and scalability

Current Fe-BC production costs ($300-800/t) surpass those of pristine biochar ($150-400/t), limiting its economic viability for low-value agricultural uses (Morim et al., 2025; Su et al., 2023). The cost breakdown for Fe-BC includes feedstock (20-30% of total cost), iron precursors (15-25%), energy for pyrolysis (20-30%), labor and maintenance (10-15%), and capital depreciation (10-15%). Major cost drivers are iron precursors such as $FeCl_3$ ($500-800/t), $FeSO_4$ ($200-400/t), and Fe_3O_4 nanoparticles ($1000-5000/t), especially at the nanoscale level. Economies of scale significantly influence costs: small-scale units (<1000 t/year) produce Fe-BC at $600-800/t, while large-scale, continuous pyrolysis systems (>10,000 t/year) can reduce costs to $300-400/t (Saharudin et al., 2024). Implementing heat recovery in continuous pyrolysis decreases energy use from 2-3 MJ/kg to 1-2 MJ/kg. Cheaper iron sources like laterite ($50-100/t), iron ore tailings ($10-50/t), and steel slag ($0-50/t) could cut costs by 30-50%, but may introduce contaminants, such as heavy metals in slag, which could limit agricultural applications. Without policy support such as carbon credits at $50-100/t CO_2-eq, pollution-mitigation incentives at $50-100/t nutrient removed, and subsidies for waste valorization, adoption of Fe-BC might remain limited to high-value crops (vegetables, fruits, ornamentals) or contaminated-site remediation, where costs of $5000-50,000 per hectare are acceptable. However, as carbon credit prices increase (EU ETS >$100/t CO_2-eq in 2023) and fertilizer prices rise (post-2022), Fe-BC becomes more economically attractive (Su et al., 2023).

6.2. Standardization and quality control

Standardized protocols for Fe-BC production, characterization, and environmental application are essential for large-scale commercialization and regulatory approval. Key quality-control parameters include iron loading, mineral-phase composition, contaminant thresholds, magnetic recoverability, leaching stability, and aging resistance. Harmonization with existing international biochar standards, such as those developed by the International Biochar Initiative (IBI) and the European Biochar Certificate (EBC), will be critical to ensuring reproducibility, environmental safety, and market acceptance.

6.3. Performance variability and prediction challenges

Fe-BC performance varies widely across studies due to differences in (i) feedstock composition (cellulose:hemicellulose:lignin ratio, ash content, trace metals); (ii) pyrolysis conditions (temperature, residence time, heating rate, atmosphere); (iii) iron loading (5-30%) and forms (Fe^0, Fe_3O_4, α-Fe_2O_3, FeOOH); (iv) soil properties (pH, organic matter, clay content, competing ions, redox status); (v) pollutant levels (mg/kg to g/kg) and aging (newly spiked versus contaminated over time); and (vi) application methods (mixing depth, incorporation, pre-incubation) (Ying et al., 2024; Zhang et al., 2025b). This variation makes it difficult to compare results and develop predictive models. For example, Cd immobilization efficiency for Fe-BC ranges from 30% to 90%, showing higher efficiency in acidic, low-organic soils and lower in alkaline, high-organic soils (Cui et al., 2019). Phosphate adsorption capacities vary from 30 to 180 mg P/g depending on Fe loading, iron oxide crystallinity, and solution conditions (Yuxin et al., 2025). Machine learning methods, such as random forests and neural networks that combine material and environmental data, could help predict performance but require large, standardized datasets (n > 1000), which are currently unavailable (Zhang et al., 2026). It is critically important to standardize experimental protocols. The International Biochar Initiative (IBI) has established guidelines for biochar testing (IBI, 2015), but these do not include specific rules for Fe-BC (e.g., iron leaching tests or magnetic property measurements). Developing Fe-BC reference materials (e.g., certified standards from consistent feedstock and pyrolysis) would aid laboratory comparisons and quality control (Su et al., 2023). Machine learning (ML) and quantitative structure–activity relationship (QSAR) models may serve as powerful tools for predicting Fe-BC performance under diverse environmental conditions. Existing datasets containing feedstock composition, pyrolysis temperature, iron loading, pollutant chemistry, and soil properties can be used to train predictive models such as random forests, support vector machines, and neural networks. These approaches may help optimize Fe-BC design for site-specific remediation and reduce uncertainties associated with experimental variability.

6.4. Long-term environmental fate and ecotoxicity

Despite short-term benefits (1-3 years), the long-term environmental fate of Fe-BC remains poorly understood. Key knowledge gaps include:

Iron leaching and speciation changes: Over 5-20 years, Fe-BC undergoes weathering, with Fe^0 oxidizing to Fe^{2+}/Fe^{3+}, Fe_3O_4 transforming into α-Fe_2O_3 or FeOOH, and Fe oxides recrystallizing. Iron leaching rates are generally low (<1% per year) in neutral to alkaline soil but can reach 5-10% per year in acidic soils (pH <5) (Gross et al., 2024). Leached Fe^{2+}

may be re-oxidized and precipitate as secondary Fe minerals, potentially immobilizing additional pollutants; or it can migrate to groundwater, possibly causing aesthetic issues (taste, color), though it is usually not toxic. The USEPA (1992) secondary drinking water standard for Fe is 0.3 mg/L for taste, not health.

Secondary contaminant release: Fe-BC may contain heavy metals (Cd, Pb, As, Cr) from feedstock or iron sources. Over time, these can be released, especially under acidic or reducing conditions. Quality control limits for biochar (IBI, EBC) set maximum allowable concentrations (e.g., Cd <1-10 mg/kg, Pb <100-300 mg/kg, depending on grade), but Fe-BC-specific limits are not available (Siddiqui, 2025a; 2025b). Additionally, Fe-BC may accumulate co-precipitated pollutants (e.g., Cd, Pb) during remediation; if Fe-BC degrades, these could be released back into the environment.

Physical disintegration and transport: Fe-BC particles can break down into micro- (<100 μm) and nanoparticles (<100 nm) through freeze-thaw cycles, wetting-drying, and root activity. These fine particles may be transported through soil pores, potentially reaching groundwater or being absorbed by plants (Marchand et al., 2017). Nanoparticle transport is affected by soil texture, organic matter, and ionic strength, with mobility being highest in sandy, low-OM soils.

Effects on non-target organisms: Ecotoxicological studies show low acute toxicity (EC50 > 1000 mg/L for Daphnia magna; LC50 > 5000 mg/kg for Eisenia fetida), but further research is needed for chronic exposure (weeks to months) and mixture effects (Elliston et al., 2020). Fe-BC may affect earthworm burrowing behavior, reproduction, and gut microbiota at concentrations over 1000 mg/kg (Marchand et al., 2017). The formation of reactive oxygen species (ROS) on Fe-BC surfaces could damage microbial membranes and DNA; however, this same property helps suppress pathogens.

PAH and Dioxin Formation: Pyrolysis can produce polycyclic aromatic hydrocarbons (PAHs) and, in the presence of chlorine, dioxins. Well-designed pyrolysis systems (>500°C, sufficient residence time, effective gas cleanup) generate biochar with PAH levels below IBI/EBC limits (<6-12 mg/kg for the total of 16 PAHs), but poorly controlled systems may exceed these limits (Hale et al., 2012). Iron can either catalyze PAH formation or breakdown, depending on conditions, with evidence supporting both effects (Feng et al., 2020; 2021).

Food chain transfer: The potential for Fe-BC nanoparticles to be absorbed by plants and transferred to herbivores and predators is an important knowledge gap. Some studies report Fe-BC particle uptake into root cortical cells and movement to shoots, but particle size (>100 nm) suggests apoplastic transport rather than cellular internalization (Marchand et al., 2017). Bioaccumulation factors (BAF = concentration in organism / concentration in soil) for Fe are usually <1, indicating no biomagnification; however, more research is needed using aged Fe-BC and realistic exposure scenarios. *Although Fe-BC generally improves pollutant immobilization and soil quality, excessive iron release may induce unintended ecological effects.* Iron-mediated Fenton-like reactions in the rhizosphere may generate reactive oxygen species (ROS), potentially

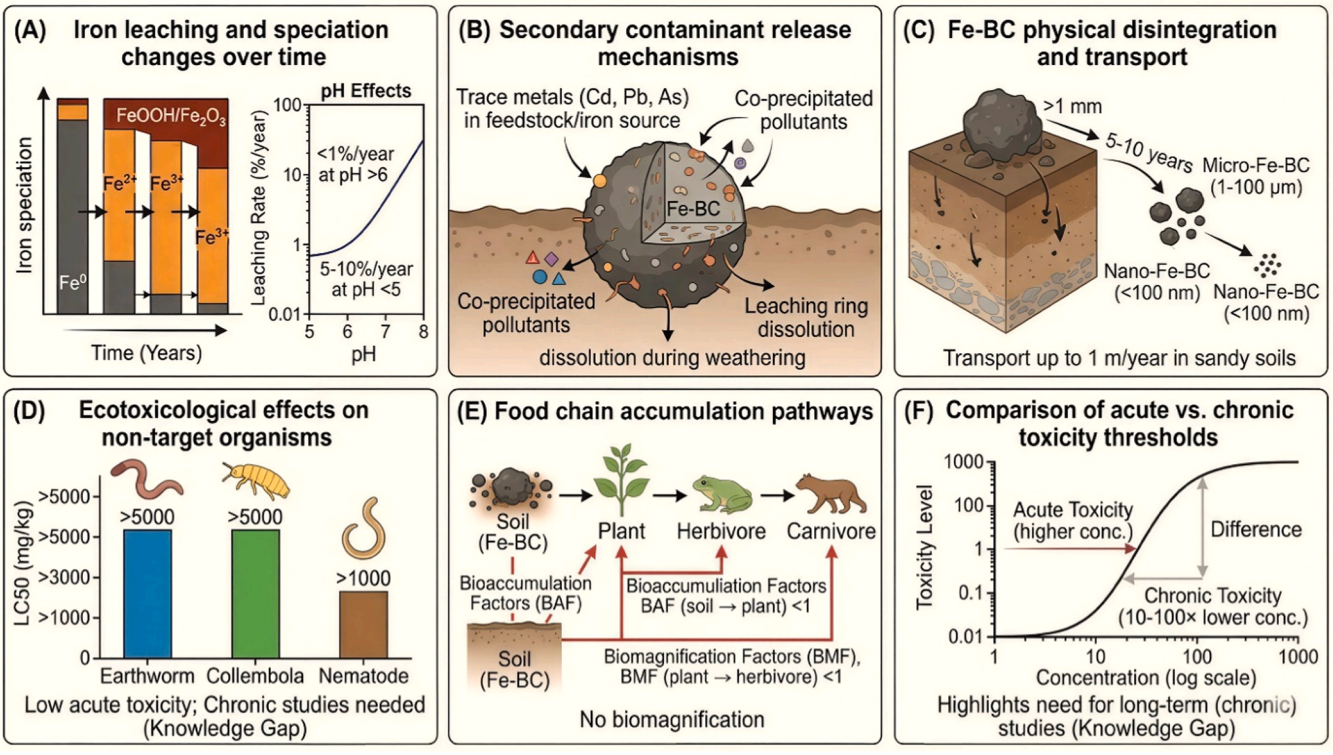

Fig. 12. Potential environmental risks and knowledge gaps. (A) Iron leaching and speciation dynamics: Temporal transformation of iron phases from zerovalent iron (Fe0) to ionic forms (Fe2+, Fe3+) and eventually stable oxides/oxyhydroxides (FeOOH, Fe2O3). Leaching rates stay negligible (<1% annually) in circumneutral soils (pH > 6) but increase significantly (5%–10%) under acidic conditions (pH < 5) (Rathinapriya et al., 2025). (B) Secondary contaminant release: Mechanisms for the potential mobilization of trace metals (e.g., Cd, Pb, As) found in the feedstock or iron precursor, along with the risk of releasing co-precipitated organic pollutants during the gradual dissolution of the reactive iron "shell" (Liu et al., 2024). (C) Physical disintegration and transport: Breakdown of macro-scale Fe-BC (>1 mm) into micro- (1–100 μm) and nanoscale (<100 nm) particles over 5–10 years, with observed vertical and lateral transport reaching up to 1 m/year in high-permeability sandy soils. (D) Ecotoxicological screening: Acute toxicity thresholds (LC50) for important soil indicator organisms, including earthworms, collembola, and nematodes, show low immediate risk at typical application rates; however, the lack of long-term exposure data remains a critical knowledge gap (Clasen and de Moura Lisbôa, 2019). (E) Trophic transfer and food chain safety: Evaluation of bioaccumulation factors (BAF, soil → plant) and biomagnification factors (BMF, plant → herbivore), with current values consistently below 1.0, indicating minimal risk of systemic food chain accumulation (Acosta-Lizarraga et al., 2026). (F) Toxicity threshold comparison: Schematic illustrating the difference between acute and chronic toxicity; chronic effects generally occur at concentrations 10–100 times lower than acute lethality, highlighting the urgent need for long-term studies on aged Fe-BC particles (Rathinapriya et al., 2025).

causing oxidative stress to plant roots and microbial communities. Furthermore, nanoscale Fe-containing particles may exhibit mobility within soil pore networks and potentially enter food webs through trophic transfer pathways. Recent studies suggest that engineered nanomaterials may accumulate in soil invertebrates and higher trophic organisms under certain exposure conditions. Additional ecotoxicological and long-term environmental fate studies are therefore required. Fig. 12 represents the potential environmental risks and knowledge gaps.

6.5. Regulatory and standardization gaps

The absence of standardized protocols for Fe-BC production, characterization, and application presents significant obstacles to commercialization and regulatory approval. Key needs include:

Quality standards: (i) minimum surface area (e.g., >100 m^2/g for agricultural use); (ii) maximum leachable metals (e.g., TCLP: Cd <0.01 mg/L, Pb <0.1 mg/L); (iii) PAH limits (e.g., sum of 16 PAHs <12 mg/kg); (iv) iron loading specifications (e.g., 10-20% w/w); (v) magnetic property requirements (e.g., Ms >10 emu/g for magnetic recovery); (vi) particle size distribution (e.g., <2 mm for soil application).

Standardized testing frameworks: (i) ecotoxicity testing (OECD guidelines for earthworms, collembola, and plants); (ii) leaching tests (TCLP, EN12457, CEN/TS 16637); (iii) biodegradation and aging protocols; (iv) greenhouse gas emissions measurement; (v) agronomic efficacy trials (standardized soil types, crops, and application rates).

Application guidelines: (i) recommended application rates for different soil-crop systems (e.g., 2-20 t/ha for annual crops, 10-50 t/ha for perennials); (ii) methods of incorporation (mixing depth of 10-30 cm, timing before planting); (iii) co-application with fertilizers and other amendments; (iv) safety precautions (dust control, personal protective equipment).

Certification schemes: (i) IBI Biochar Certification (existing but lacks Fe-BC-specific provisions); (ii) European Biochar Certificate (EBC) (existing, Fe-BC not yet covered); (iii) US Biochar Initiative (USBI) guidelines; (iv) ISO 17225-13:2021 (solid biofuels biochar specifications) - could be expanded to include Fe-BC.

6.6. Technology transfer and LMIC deployment

In low- and middle-income countries (LMICs), decentralized deployment strategies may improve the feasibility of Fe-BC technologies. Potential business models include mobile pyrolysis units, community-scale cooperative systems, contract remediation services, and pay-per-use biochar application programs. These approaches may reduce barriers to capital investment and promote circular bioeconomy development and agricultural waste valorization.

Maximum allowable cumulative application limits: (i) based on heavy metal loading (e.g., Cd <0.01 kg/ha/year, with a total <0.1 kg/ha); (ii) based on iron loading (e.g., Fe <1000 kg/ha cumulative to prevent phytotoxicity); (iii) based on salinity (electrical conductivity <4 dS/m in soil after application).

End-of-life management: (i) magnetic recovery from soils (feasibility, efficiency, cost); (ii) regeneration and reuse (acid washing for heavy metals, thermal treatment for organics); (iii) disposal options (landfill, incineration with energy recovery, land application after decontamination) (Su et al., 2023; Siddiqui, 2025b).

The International Biochar Initiative (IBI) and the European Biochar Certificate (EBC) serve as initial references but lack Fe-BC-specific provisions. Developing Fe-BC standards should involve multiple stakeholders: researchers (to define technical specifications), producers (to ensure feasibility), regulators (to enforce compliance), farmers (to ensure practicality), and environmental NGOs (to ensure safety). This process is underway but requires greater effort and funding. Establishing standardized protocols for Fe-BC production, characterization, and environmental application is essential for large-scale commercialization and regulatory approval. Key quality-control parameters include iron loading, mineral-phase composition, contaminant thresholds, magnetic recoverability, leaching stability, and aging resistance. Harmonization with existing international biochar standards, such as those developed by the International Biochar Initiative (IBI) and the European Biochar Certificate (EBC), will be critical to ensuring reproducibility, environmental safety, and market acceptance.

7. Global implications and policy frameworks

7.1. Contributions to sustainable development goals

Fe-BC directly advances multiple UN Sustainable Development Goals (SDGs):

SDG 2 (Zero Hunger): Fe-BC increases crop yields by 15-35% and reduces heavy metal levels in edible tissues below Codex limits, improving food availability and safety. For 800 million undernourished people, a 20% yield increase could produce 200 million tons of grain annually, enough to feed 500 million people. The integrated contributions of Fe-BC to the United Nations Sustainable Development Goals (SDGs) are shown in Fig. 13.

SDG 6 (Clean Water and Sanitation): Fe-BC reduces nitrogen leaching by 30-55% and phosphorus runoff by 45-70%, helping to prevent eutrophication in lakes, rivers, and coastal zones. The Gulf of Mexico dead zone (covering 15,000 km^2) could be halved by applying Fe-BC to 20% of croplands in the Mississippi Basin (Tang et al., 2025).

SDG 12 (Responsible Consumption and Production): Fe-BC uses 5 billion tons of agricultural residues annually and millions of tons of iron-rich industrial wastes, reducing disposal problems and the demand for virgin materials. The circular economy approach lowers greenhouse gas emissions by 0.5-1.0 tons of CO_2-eq per ton of waste processed (Jatav, 2025).

SDG 13 (Climate Action): Fe-BC sequesters 2-3 tons of CO_2-eq per ton of biochar, while reducing agricultural N_2O and CH_4 emissions by 40-55% and 30-45%, respectively. Expanding Fe-BC to 10% of the world's croplands (150 Mha) could sequester 0.5-1.0 Gt of CO_2 annually (2-4% of yearly emissions) and cut agricultural N_2O emissions by 0.3-0.6 Gt CO_2-eq per year (Cayuela et al., 2014).

SDG 15 (Life on Land): Fe-BC restores degraded soils, increases soil organic carbon by 0.5-2%, enhances biodiversity (soil microbial diversity increases 20-40%), and reduces desertification risk by improving water retention. The UN Decade on Ecosystem Restoration (2021-2030) identifies biochar as a priority restoration technology (UNEP, 2021).

7.2. Technology transfer and capacity building

Realizing Fe-BC's global potential requires targeted technology transfer to low- and middle-income countries (LMICs) where agricultural pollution is most severe but remediation capacity limited. Priorities include:

Low-cost production technologies: (i) utilizing locally available feedstocks such as rice husks in Asia, coffee hulls in Latin America, coconut shells in the Pacific Islands, and sorghum stover in Africa; (ii) appropriate-scale pyrolysis using village-scale kilns that produce 100-1000 tons per year and cost $ 10,000- $ 100,000; (iii) low-cost iron sources like laterite, iron ore tailings, and rusted scrap metal; (iv) solar-assisted pyrolysis for off-grid locations (Saharudin et al., 2024).

Participatory research: (i) farmer-managed trials comparing Fe-BC types and application rates; (ii) integration with existing practices such as composting, mulching, and conservation agriculture; (iii) gender-sensitive approaches recognizing that women farmers often manage soil fertility in LMICs; (iv) farmer-to-farmer knowledge exchange networks.

Open-access knowledge platforms: (i) online Fe-BC calculator (application rates based on soil test results); (ii) video tutorials in local languages (production, application, safety); (iii) decision support tools

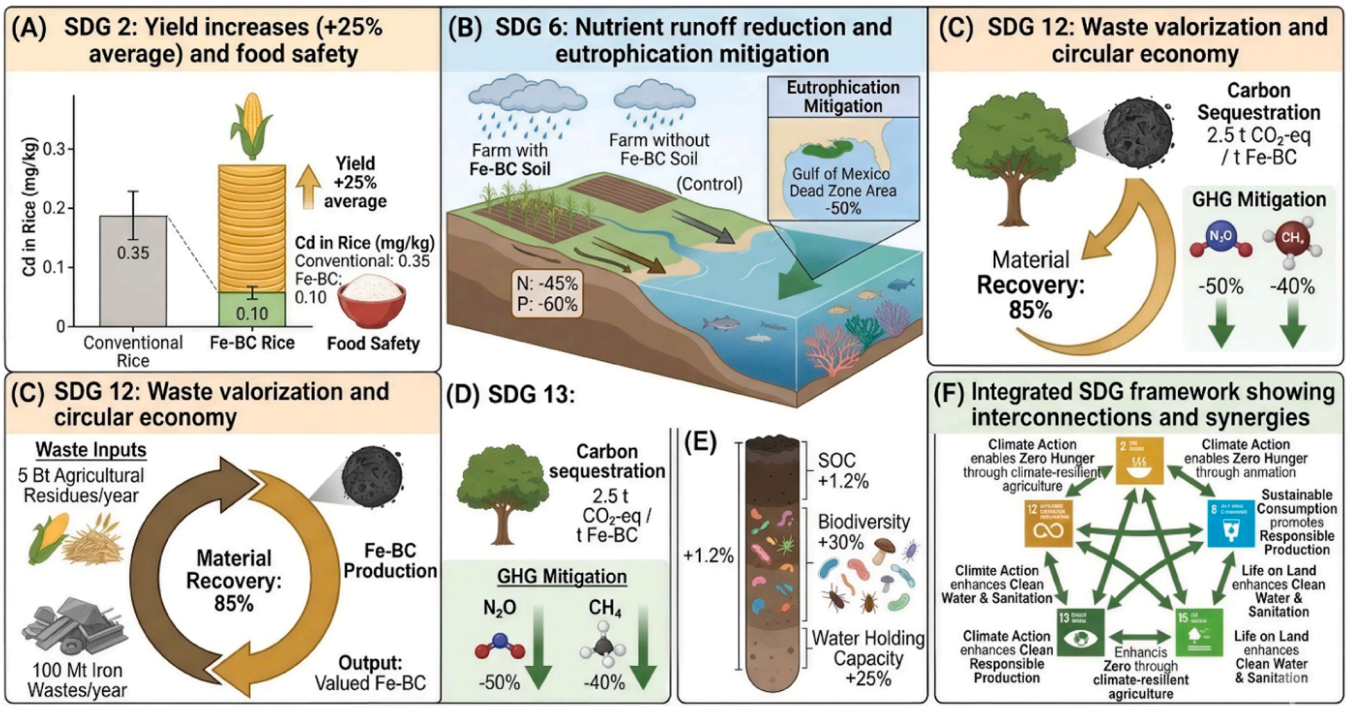

Fig. 13. Integrated contributions of Fe-BC to the United Nations Sustainable Development Goals (SDGs). (A) SDG 2 (Zero Hunger): Fe-BC application provides a dual benefit for food security by increasing average crop yields by 25% through improved nutrient availability while also enhancing food safety. For example, cadmium (Cd) concentrations in rice grains can be decreased from 0.35 mg/kg to 0.10 mg/kg, bringing them below international safety thresholds (Ye et al., 2020; Yin et al., 2024). (B) SDG 6 (Clean Water and Sanitation): Reducing agricultural runoff by capturing nitrogen (-45%) and phosphorus (-60%) within the soil matrix helps reduce aquatic eutrophication and shrink hypoxic zones, such as the Gulf of Mexico "dead zone" (Huang et al., 2026). (C) SDG 12 (Responsible Consumption and Production): Implementing a circular economy model that valorizes approximately 5 billion tons of agricultural residues and 100 million tons of iron-rich industrial waste annually results in an estimated 85% material recovery rate (Faheem et al., 2026). (D) SDG 13 (Climate Action): Features strong carbon sequestration capacity ($2.5 t CO2 per ton of Fe-BC) and directly reduces greenhouse gases, including a 50% reduction in N2O and a 40% reduction in CH4 emissions (Woolf et al., 2010). (E) SDG 15 (Life on Land): Restoring terrestrial ecosystems through improved soil health indicators, such as a 1.2% increase in Soil Organic Carbon (SOC), a 30% rise in microbial biodiversity, and a 25% gain in water holding capacity. (F) Integrated SDG Framework: Diagram illustrating how synergies between goals work, showing how climate-resilient agriculture (SDG 13) directly supports zero hunger (SDG 2), while sustainable consumption (SDG 12) aids life on land (SDG 15).

(economic analysis, carbon credit calculation); (iv) databases of local feedstocks and iron sources.

Training programs include: (i) biochar entrepreneur training covering production, quality control, and business management; (ii) agricultural extension agent training focusing on developing recommendations and educating farmers; (iii) researcher exchange programs for LMIC researchers training at leading biochar laboratories; (iv) university curriculum development, including courses on Fe-BC in soil science, agronomy, and environmental engineering.

Financing mechanisms: (i) microfinance loans for biochar equipment ($1,000-$10,000 per entrepreneur); (ii) carbon credit pre-financing (advances against future carbon credits); (iii) payment for ecosystem services (PES) for water quality improvement and carbon sequestration; and (iv) government subsidies (e.g., India's Soil Health Card scheme could include biochar) (Pretty et al., 2018; Saharudin et al., 2024).

The Global Biochar Partnership (GBP) and FAO's Biochar Initiative provide coordination platforms but require additional funding and political support. The Green Climate Fund (GCF) and the Global Environment Facility (GEF) have supported biochar projects ($50 million since 2015), but funding specifically for Fe-BC remains limited. In low- and middle-income countries (LMICs), decentralized deployment strategies may improve the feasibility of Fe-BC technologies. Potential business models include mobile pyrolysis units, community-scale cooperative systems, contract remediation services, and pay-per-use biochar application programs. Such approaches may reduce barriers to capital investment while promoting circular bioeconomy development and agricultural waste valorization.

7.3. Policy recommendations

To accelerate the adoption of Fe-biochar (Fe-BC), a coordinated policy framework is essential, integrating climate, agricultural, and environmental priorities. Fe-BC should be incorporated into Nationally Determined Contributions (NDCs) under the Paris Agreement as a climate-smart agricultural strategy for carbon sequestration and mitigation of greenhouse gases such as N_2O and CH_4, particularly in major agricultural economies including China, India, the United States, Brazil, and Indonesia. Simultaneously, standardized quality criteria should be developed through collaborative platforms such as the International Biochar Initiative and the European Biochar Certificate, addressing parameters including iron loading, speciation, leaching behavior, and magnetic properties, with periodic updates every 3–5 years. The establishment of carbon credit methodologies for Fe-BC within voluntary markets such as the Verified Carbon Standard and Gold Standard, as well as compliance frameworks under Article 6 of the Paris Agreement, is critical; these should account for carbon sequestration, reductions in N_2O and CH_4 emissions, and avoided fertilizer-related emissions, with performance-based (ex post) credit issuance. Financial incentives, including subsidies and tax credits, should be introduced to support Fe-BC production from agricultural residues and iron-rich wastes, drawing on models such as India's National Biochar Mission, the Common Agricultural Policy eco-schemes, and the U.S. 45Q tax credit. Furthermore, Fe-BC should be integrated into national and regional agricultural pollution reduction programs, including EU nutrient management strategies, the U.S. Conservation Stewardship Program, and China's Soil Pollution Prevention initiatives, with payments linked to verified

reductions in nutrient runoff. Long-term field validation is equally important; therefore, funding should be allocated for multi-location trials (10+ years) through global collaborations such as the Global Research Alliance on Agricultural Greenhouse Gases and the 4 per 1000 initiative, ensuring standardized methodologies and open-access datasets. Finally, harmonized life cycle assessment (LCA) protocols and environmental risk assessment guidelines should be developed through international bodies including the United Nations Environment Program, Organization for Economic Co-operation and Development, and International Organization for Standardization, with specific consideration of Fe-BC-related factors such as iron leaching, magnetic recovery, nanoscale particle transport, ecotoxicity, aging processes, and potential food chain impacts.

8. Future research priorities

Future mechanistic studies should increasingly employ operando and in situ analytical techniques, including synchrotron-based X-ray absorption spectroscopy (XAS), in situ XPS, and environmental TEM, to directly observe dynamic transformations of iron phases during pollutant adsorption, catalysis, and aging. These approaches may significantly improve understanding of Fe-BC reactivity under realistic environmental conditions.

8.1. Materials science and engineering

Priority research directions include: Atomic-scale understanding: (i) in situ and operando characterization of Fe-BC-pollutant interactions using advanced synchrotron techniques (XANES, EXAFS, STXM, μ-XRF) to identify binding geometries, oxidation states, and reaction intermediates; (ii) high-resolution TEM and electron energy loss spectroscopy (EELS) to map iron speciation at the nanometer scale; (iii) solid-state NMR to characterize carbon-iron bonding and carbon structure.

Multifunctional composites: (i) Fe-BC co-doped with Mn, Cu, Zn, Al, or Ti for synergistic pollutant removal (e.g., Fe-Mn for As, Fe-Cu for Cr, Fe-Ti for photocatalysis); (ii) magnetic core-shell structures (Fe_3O_4C, Fe^0C) for enhanced magnetic recovery and stability; (iii) slow-release nutrient-Fe-BC composites (N-P-K-Fe) for combined fertilization and remediation; (iv) biochar-iron-clay composites to improve soil physical properties. Computational design: (i) density functional theory (DFT) calculations to determine optimal iron speciation and surface functionalization for target pollutants; (ii) molecular dynamics (MD) simulations of pollutant diffusion and binding; (iii) machine learning for rapid screening of synthesis parameters (feedstock, temperature, Fe loading) to achieve desired features; (iv) multi-scale modeling from quantum to continuum levels.

Green synthesis: (i) plant extract-mediated reduction of Fe^{3+} to Fe^0/Fe_3O_4 (using green tea, eucalyptus, moringa); (ii) microbial iron reduction employing Fe(III)-reducing bacteria like Shewanella and Geobacter to produce biogenic Fe minerals; (iii) waste-derived iron sources such as acid mine drainage sludge, water treatment sludge, and steel slag to reduce costs and environmental impacts.

Scalable production includes: (i) microwave-assisted pyrolysis, which reduces energy use by 30-50% and heats faster; (ii) solar-powered pyrolysis for off-grid sites using parabolic dish concentrators; (iii) continuous auger reactors for industrial-scale production, ranging from 10,000 to 100,000 tons annually; and (iv) mobile pyrolysis units for on-farm use, producing 100-1000 tons per year.

Controlled environmental lifetimes: (i) biodegradable Fe-BC formulations using lower-temperature biochar (300-450°C) that decompose within 5-10 years, preventing long-term buildup; (ii) encapsulated Fe-BC in polymer or clay matrices for controlled release; (iii) responsive Fe-BC that breaks down in response to chemical or biological triggers.

8.2. Aging and passivation

Long-term environmental aging may passivate Fe-BC by recrystallizing reactive ferrihydrite into more crystalline phases such as hematite and goethite. This transformation may reduce surface hydroxyl density, catalytic activity, and adsorption capacity over time. Additional aging mechanisms include pore blockage, organic matter coatings, nanoparticle aggregation, and repeated wetting–drying cycles. Long-term field investigations are therefore needed to evaluate the durability and stability of Fe-BC performance under realistic agricultural conditions.

8.3. Environmental fate and risk assessment

Critical needs include:

Long-term field lysimeter studies (10-20 years): (i) monitor Fe-BC transformation, including Fe speciation and carbon mineralization, under realistic field conditions; (ii) measure iron leaching and transport through soil profiles to groundwater; (iii) observe secondary contaminant release, such as trace metals and PAHs, over time; (iv) evaluate changes in Fe-BC effectiveness for pollutant immobilization, including aging effects and site saturation.

Multi-generational ecotoxicity tests include: (i) earthworms (Eisenia fetida, Lumbricus terrestris) over 2-3 generations (6-12 months) to assess reproduction, growth, and avoidance behavior; (ii) collembola (Folsomia candida) reproduction and survival; (iii) nematodes (Caenorhabditis elegans) for sublethal endpoints such as locomotion, feeding, and gene expression; (iv) soil microbial communities analyzed through methods like 16S rRNA sequencing, metagenomics, metatranscriptomics, and metaproteomics.

Food chain accumulation studies: (i) soil to plant (rice, wheat, maize, vegetables) uptake of Fe, co-pollutants (Cd, Pb, As), and Fe-BC nanoparticles; (ii) transfer from plants to herbivores (aphids, caterpillars); (iii) bioaccumulation from herbivores to predators (ladybeetles, spiders); (iv) transfer from plants to livestock (cattle, poultry) through feed crops; (v) transfer from livestock to humans via meat, milk, and eggs.

Life-cycle assessment harmonization: (i) developing a standardized LCA methodology for Fe-BC using a functional unit of either 1 ton of Fe-BC produced and applied or 1 hectare treated; (ii) harmonizing system boundaries, including feedstock cultivation, transport, pyrolysis, application, and end-of-life stages; (iii) incorporating all relevant impact categories such as global warming, eutrophication, acidification, human toxicity, ecotoxicity, and resource depletion; (iv) creating open-access LCA databases for Fe-BC, including feedstock compositions, iron sources, and energy requirements.

Predictive modeling: (i) empirical models linking Fe-BC properties—such as Fe loading, speciation, and surface area—and environmental factors like pH, organic matter (OM), and competing ions to pollutant immobilization efficiency; (ii) machine learning techniques (such as random forest, gradient boosting, neural networks) trained on literature data ($n > 1000$) to predict performance; (iii) reactive transport models (PHREEQC, HYDRUS) used for Fe-BC fate and pollutant behavior; (iv) species sensitivity distributions (SSDs) for Fe-BC ecotoxicity to determine predicted no-effect concentrations (PNECs).

Co-pollutant effects: (i) interactions between heavy metals and microplastics on Fe-BC performance; (ii) effects of pesticides and antibiotics on ARG selection; (iii) impacts of salinity and heavy metals on Fe-BC immobilization; (iv) influence of climate change (elevated CO_2, temperature, drought) on Fe-BC effectiveness.

Aging studies include: (i) accelerated aging protocols—such as freeze-thaw, wet-dry, UV exposure, and acid treatment—that simulate 10-50 years of field exposure; (ii) tracking changes in Fe-BC properties, including surface area, functional groups, Fe speciation, and magnetic properties; (iii) measuring pollutant release from aged Fe-BC; and (iv) comparing laboratory aging with field aging to develop prediction models.

8.4. Soil microbiome and plant interactions

Research opportunities include:

Metagenomic and metatranscriptomic analysis: (i) 16S rRNA and ITS sequencing to characterize bacterial, archaeal, and fungal community composition after Fe-BC application; (ii) shotgun metagenomics for functional gene profiling, including nutrient cycling, pollutant degradation, and metal resistance; (iii) metatranscriptomics for gene expression analysis to identify which genes are active, not just present; (iv) metaproteomics and metabolomics to connect genes and transcripts to their functions.

Tripartite interactions: (i) Fe-BC-microbe-pollutant interactions—does Fe-BC enhance microbial pollutant degradation through electron shuttling? (ii) Fe-BC-plant-microbe interactions—does Fe-BC promote beneficial rhizosphere microbes (PGPR, mycorrhizae, N-fixers)? (iii) pollutant-microbe-plant interactions—does Fe-BC reduce pollutant toxicity to microbes, enhancing their plant-beneficial functions? (iv) multi-omics integration to reveal mechanisms.

Beneficial microbe promotion: (i) identifying Fe-BC properties (pH, surface functional groups, iron species) that specifically support PGPR (Pseudomonas, Bacillus, Azospirillum); (ii) enhancing mycorrhizal colonization (arbuscular mycorrhizae for phosphorus uptake); (iii) boosting nitrogen-fixing bacteria (Rhizobium, Bradyrhizobium in legumes, free-living nitrogen fixers in cereals); (iv) suppressing pathogens (Fusarium, Rhizoctonia, Phytophthora) through Fe-mediated ROS.

Plant physiological responses include: (i) nutrient uptake kinetics for N, P, K, Fe, and Zn with Fe-BC; (ii) stress signaling involving phytohormones like ABA, ethylene, and jasmonate under pollutant stress; (iii) changes in root exudation such as organic acids and phytosiderophores in response to Fe-BC; (iv) gene expression (transcriptomics) related to metal transporters, antioxidant enzymes, and stress proteins.

Rhizosphere-scale dynamics: (i) microfluidic soil chips (lab-on-a-chip) to visualize Fe-BC-microbe-root interactions at the micrometer level; (ii) planar optodes for 2D mapping of O_2, pH, CO_2 in the rhizosphere; (iii) diffusive gradients in thin films (DGT) for high-resolution measurement of metal bioavailability; (iv) nanoSIMS for isotope tracing (^{13}C, ^{15}N, ^{57}Fe) at the nanoscale.

Integration with other amendments: (i) Fe-BC + compost for synergistic effects (compost supplies labile C and nutrients, while Fe-BC provides stable C and pollutant binding); (ii) Fe-BC + manure (similar to compost); (iii) Fe-BC + biofertilizers (PGPR inoculants may establish more effectively in Fe-BC-amended soils); (iv) Fe-BC + mineral fertilizers (slow-release formulations). Interactions can be synergistic (>additive), additive, or antagonistic (<additive) systematic testing is necessary.

8.5. Agronomic integration and optimization

Applied research priorities:

Field-scale validation across key agroecological zones: (i) humid tropics (Southeast Asia, Amazon, Congo Basin) - characterized by high rainfall and highly weathered soils; (ii) semi-arid tropics (India, Sahel, Brazil Cerrado) - water-limited with low fertility; (iii) temperate regions (Europe, North America, China) - high-input and mechanized agriculture; (iv) Mediterranean climate zones (Southern Europe, North Africa, California) - featuring winter rainfall and summer drought; (v) highland areas (Andes, Himalayas, East Africa) - with steep slopes and erosion risks. Trials should include major crops such as rice, wheat, maize, soybean, potato, and vegetables.

Decision support tools: (i) a web-based Fe-BC calculator that uses inputs such as soil properties (pH, texture, OM, CEC), pollutant levels (Cd, Pb, As, etc.), crop type, and farmer objectives (pollution mitigation, yield increase, carbon credits); outputs include the recommended Fe-BC type, application rate (t/ha), incorporation method, expected results, and a cost-benefit analysis; (ii) a mobile app version for field use with offline capability; and (iii) integration with precision agriculture platforms like Climate FieldView and John Deere Operations Center.

Precision agriculture integration: (i) variable rate Fe-BC application based on within-field variability in soil properties and pollutant levels, requiring high-resolution mapping through proximal sensing, electromagnetic induction, or satellite imagery; (ii) drone-based monitoring of crop response using multispectral and thermal imaging to identify areas where Fe-BC is most effective; (iii) yield mapping to confirm economic benefits; (iv) automated application equipment such as modified manure spreaders and lime applicators.

Economic optimization: (i) perform cost-benefit analysis for different Fe-BC types, application rates, and cropping systems; (ii) conduct break-even analysis to determine the crop yield increase or fertilizer reduction needed to justify Fe-BC costs; (iii) carry out sensitivity analysis to see how results change with Fe-BC costs ($200-800/ton), crop prices ($100-500/ton), fertilizer prices ($500-1500/ton), and carbon credit prices ($10-100/ton CO_2-eq); (iv) conduct risk analysis to evaluate the likelihood of economic loss considering price and yield fluctuations.

Residual Effects: (i) How long does a single Fe-BC application stay effective? (ii) Is reapplication needed after 5, 10, or 20 years? (iii) Do residual effects grow, decrease, or remain steady over time? (iv) Can Fe-BC be magnetically recovered and reused after regeneration? (v) What are the cumulative impacts of multiple applications (every 5-10 years) on soil properties and pollutant levels?

Fe-BC-enriched fertilizer formulations: (i) co-granulating Fe-BC with N-P-K fertilizers (slow-release formulations); (ii) coating fertilizers with Fe-BC (creating a physical barrier that reduces dissolution rate); (iii) blending Fe-BC with compost or manure to enhance microbial activity; (iv) using liquid Fe-BC suspensions for fertigation or foliar application (nanoscale Fe-BC particles).

Climate change interactions: (i) effects of elevated CO_2 (550-800 ppm) on crop response to Fe-BC; (ii) impacts of temperature rise (+2-4°C) on Fe-BC performance, which may accelerate aging and reduce effectiveness; (iii) drought conditions (50% of historical rainfall) and their effects, with Fe-BC potentially being more beneficial during drought due to improved water retention; (iv) flooding impacts (such as in rice paddies) on Fe-BC redox chemistry and pollutant mobility; (v) combined effects of elevated CO_2, warming, and drought as observed in climate change scenarios.

8.6. Operando and in-situ characterization

Future mechanistic studies should increasingly employ operando and in situ analytical techniques, including synchrotron-based X-ray absorption spectroscopy (XAS), in situ XPS, and environmental TEM, to directly observe dynamic transformations of iron phases during pollutant adsorption, catalysis, and aging. These approaches may significantly improve understanding of Fe-BC reactivity under realistic environmental conditions.

8.7. Material heterogeneity and characterization uncertainty

An important but underexplored research gap concerns the heterogeneity of Fe-BC materials. Many reported Fe-BC systems likely consist of heterogeneous mixtures with multiple iron phases, uneven iron distribution, and variable surface chemistry arising from feedstock variability and synthesis conditions. This heterogeneity introduces uncertainty about reproducibility, mechanistic interpretation, and performance in large-scale applications. Furthermore, characterization techniques such as TEM, SEM, and XPS typically analyze highly localized regions and may not adequately represent bulk material properties. Results may also be influenced by sample preparation procedures and operator-dependent selection bias. Future studies should therefore incorporate statistically representative multi-point characterization, combined bulk–surface analytical approaches, and standardized protocols that link laboratory characterization with field-scale performance evaluation.

9. Conclusions

Iron-enriched biochar is an innovative technology that addresses interconnected issues of agricultural pollution, soil degradation, and climate change through a versatile, single platform. By combining biochar's ability to sequester carbon and enhance soil health with iron's redox activity and pollutant attraction, Fe-BC achieves unprecedented results: immobilizing heavy metals (Cd, Pb, As, Cr), reducing nitrogen and phosphorus leaching by 30-55% and 45-70%, degrading organic contaminants by 85-99%, and lowering emerging pollutants like antibiotics and ARGs by 3-6 logs. Recent mechanistic studies have revealed the molecular interactions behind Fe-BC's effectiveness, including adsorption (surface complexation, ligand exchange), (co)precipitation (metal hydroxides, phosphates, carbonates), redox reactions (Cr(VI) reduction, NO_3^- reduction), Fenton-like catalysis (OH, SO_4^- production), and microbial electron transfer (DIET).

The agronomic benefits of Fe- BC extend beyond pollution control to include higher crop yields (15-35% increase), improved nutrient use efficiency (NUE rising from 30-40% to 50-65%), reduced fertilizer requirements (20-30% decrease without affecting yield), and increased resilience to climate stressors such as drought, flooding, and temperature extremes. Life-cycle assessments indicate negative carbon footprints (-0.5 to -2.0 t CO_2-eq/t Fe-BC) and favorable energy returns (EROI = 5-10) when Fe-BC is produced from waste biomass (such as agricultural residues) and waste iron sources (such as industrial by-products), thereby embodying circular economy principles. However, several obstacles remain. Production costs ($300-800/t) are higher than those of pristine biochar ($150-400/t), limiting economic competitiveness. Variability in performance across different feedstocks, pyrolysis conditions, iron loading, soil types, and pollutant profiles complicate direct comparison and predictive modeling. Uncertainties about long-term fate, such as iron leaching, release of secondary contaminants, physical disintegration, and nanoparticle transport, as well as gaps in ecotoxicology knowledge (including chronic effects, mixture toxicity, and food chain transfer), require further research. The lack of standardized regulatory frameworks, including quality standards, testing protocols, application guidelines, and certification schemes, poses significant challenges for commercialization and regulatory approval. Overcoming these barriers requires coordinated investment in transdisciplinary research spanning materials science (atomic-scale understanding, multifunctional composites, computational design, green synthesis, scalable production), environmental chemistry and toxicology (long-term field studies, multi-generational ecotoxicity, food chain accumulation, LCA harmonization, and predictive modeling), soil microbiology and plant science (metagenomics, tripartite interactions, plant physiology, rhizosphere dynamics, and amendment integration), and agronomy and economics (field validation, decision support, precision agriculture, economic optimization, and climate change interactions). With strategic research priorities and supportive policies, Fe-BC can transition from laboratory innovation to mainstream agriculture within a decade. Scaling Fe-BC to cover 10-20% of global croplands (150-300 million hectares) could sequester 0.5-1.0 gigatons of CO_2 annually (2-4% of global emissions), reduce nitrogen runoff by 1-2 million tons of nitrogen per year (5-10% of global agricultural nitrogen loss), remediate heavy metal-contaminated soils on 50-100 million hectares, and enhance food security for 300-500 million people. The challenge now is not just to demonstrate Fe-BC's potential but also to mobilize scientific, industrial, and policy communities to realize it at the scales and speeds needed to stay within planetary boundaries. Iron-enriched biochar offers a rare opportunity to align agricultural productivity with environmental restoration, which is a chance we cannot afford to miss.

Funding sources

National Institute of Food and Agriculture, United States Department of Agriculture, Grant number: GR 019129 (Project title: Iron Biochar for Agri-Pollution Control).

CRediT authorship contribution statement

Shahidul Islam: Writing – review & editing, Writing – original draft, Visualization, Validation, Supervision, Software, Resources, Project administration, Methodology, Investigation, Funding acquisition, Formal analysis, Data curation, Conceptualization.

Declaration of competing interest

The author declares that he has no known competing financial interests or personal relationships that could have influenced the work reported in this paper.

Acknowledgments

The author would like to thank Dr. Azad and Dr. Akanda for their critical review of the manuscript.

Data availability

No data was used for the research described in the article.

References

Acosta-Lizárraga, L.G., Rodríguez-Jurado, S., Bergés-Tiznado, M.E., Aguirre-Becerra, H., Esquivel Escalante, K., Pérez-García, C.E., Feregrino-Perez, A.A., 2026. Biomagnification of potentially toxic elements and metal-based nanomaterials in food. Environments 13, 116. https://doi.org/10.3390/environments13020116.

Algethami, J.S., Irshad, M.K., Javed, W., Alhamami, M.A.M., Ibrahim, M., 2023. Iron-modified biochar improves plant physiology, soil nutritional status and mitigates Pb and Cd-hazard in wheat (*Triticum aestivum* L.). Front. Plant Sci. 14. https://doi.org/10.3389/fpls.2023.1221434.

Ali, H., Khan, E., Ilahi, I., 2019. Environmental chemistry and ecotoxicology of hazardous heavy metals. J. Chem. 2019, 1–14. https://doi.org/10.1155/2019/6730305.

Ali, U., Shaaban, M., Bashir, S., et al., 2021. Potential of organic and inorganic amendments for stabilizing nickel in acidic soil, and improving the nutritional quality of spinach. Environ. Sci. Pollut. Res. 28, 57769–57780. https://doi.org/10.1007/s11356-021-14611-0.

Amusat, S.O., Kebede, T.G., Nxumalo, E.N., Dube, S., Nindi, M.M., 2023. Facile solvent-free modified biochar for removal of mixed steroid hormones and heavy metals: isotherm and kinetic studies. BMC Chem. 17, 158. https://doi.org/10.1186/s13065-023-01071-5.

Aziz, S., Anbreen, S., Iftikhar, I., Fatima, T., Iftikhar, A., Ali, L., 2024. Green technology: synthesis of iron-modified biochar derived from pine cones to remove azithromycin and ciprofloxacin from water. Front. Environ. Sci. 12. https://doi.org/10.3389/fenvs.2024.1353267.

Back, et al., 2025. Biochar effects on methane emission from rice paddy differ with nitrogen fertilization, organic inputs, and water management. Korean J. Soil Sci. Fertil. 58, 133–143. https://doi.org/10.7745/KJSSF.2025.58.1.133.

Bai, S.H., Omidvar, N., Gallart, M., Kämper, W., Tahmasbian, I., Farrar, M.B., Singh, K., Zhou, G., Muqadass, B., Xu, C.-Y., Koech, R., Li, Y., Nguyen, T.T.N., van Zwieten, L., 2022. Combined effects of biochar and fertilizer applications on yield: a review and meta-analysis. Sci. Total Environ. 808, 152073. https://doi.org/10.1016/j.scitotenv.2021.152073.

Bashir, H., Niazi, N.K., Saqib, Z.A., Hussain, K., 2025. Chromium removal by biochar/nanoparticulate iron oxide mineral composites: mechanistic insights and performance under batch and column systems. Int. J. Phytoremed. 1–11. https://doi.org/10.1080/15226514.2025.2522303.

Beckhoff, B., et al., 2006. Handbook of Practical X-Ray Fluorescence Analysis. Springer. https://doi.org/10.1007/978-3-540-36722-2.

Bergaust, L., van Spanning, R.J.M., Frostegård, Å., Bakken, L.R., 2012. Expression of nitrous oxide reductase in *Paracoccus denitrificans* is regulated by oxygen and nitric oxide through FnrP and NNR. Microbiology 158, 826–834. https://doi.org/10.1099/mic.0.054148-0.

Blanco-Canqui, H., 2017. Biochar and soil physical properties. Soil Sci. Soc. Am. J. 81, 687–711. https://doi.org/10.2136/sssaj2017.01.0017.

Bouchard, M.F., et al., 2011. Prenatal exposure to organophosphate pesticides and IQ in 7-year-old children. Environ. Health Perspect. 119, 1189–1195. https://doi.org/10.1289/ehp.1003185.

Breitburg, D., et al., 2018. Declining oxygen in the global ocean and coastal waters. Science 359, eaam7240. https://doi.org/10.1126/science.aam7240.

Bridgwater, A.V., 2012. Review of fast pyrolysis of biomass and product upgrading. Biomass Bioenergy 38, 68–94. https://doi.org/10.1016/j.biombioe.2011.01.048.

Brown, M.E., 2001. Introduction to Thermal Analysis. Springer. https://doi.org/10.1007/978-94-009-1219-9.

Brunauer, S., Emmett, P.H., Teller, E., 1938. Adsorption of gases in multimolecular layers. J. Am. Chem. Soc. 60, 309–319. https://doi.org/10.1021/ja01269a023.
Carpenter, S.R., et al., 1998. Nonpoint pollution of surface waters with phosphorus and nitrogen. Ecol. Appl. 8, 559–568. https://doi.org/10.1890/1051-0761(1998)008[0559:NPOSWW]2.0.CO;2.
Cayuela, M.L., et al., 2014. Biochar's role in mitigating soil nitrous oxide emissions: a review and meta-analysis. Agric. Ecosyst. Environ. 191, 5–16. https://doi.org/10.1016/j.agee.2013.10.009.
Chen, Y., Ma, R., Pu, X., Fu, X., Ju, X., Arif, M., Yan, X., Qian, J., Liu, Y., 2022. The characterization of a novel magnetic biochar derived from sulfate-reducing sludge and its application for aqueous Cr(VI) removal through synergistic effects of adsorption and chemical reduction. Chemosphere 308, 136258. https://doi.org/10.1016/j.chemosphere.2022.136258.
Chen, Y., Shi, J., Du, Q., Zhang, H., Cui, Y., 2019. Antibiotic removal by agricultural waste biochars with different forms of iron oxide. RSC Adv 9, 14143–14153. https://doi.org/10.1039/C9RA01271K.
Chen, Y., Tian, X., Wang, J.-h., Zhang, Y., Wang, J., Li, Z.-t., Zhao, K.-l., Wu, J.-z., 2025. Silicon-iron modified biochar remediates cadmium and arsenic co-contaminated paddy soil by regulating cadmium and arsenic speciation. Front. Microbiol. 16. https://doi.org/10.3389/fmicb.2025.1579213.
Clasen, B., de Moura Lisbôa, R., 2019. Ecotoxicological tests as a tool to assess the quality of the soil, in: Soil Contamination and Alternatives for Sustainable Development. IntechOpen. https://doi.org/10.5772/intechopen.82192.
Cui, L., Chen, T., Yin, C., Yan, J., Ippolito, J., Hussain, Q., 2019. Mechanism of adsorption of cadmium and lead ions by iron-activated biochar. BioResources 14, 842–857. https://doi.org/10.15376/biores.14.1.842-857.
Cullity, B.D., Graham, C.D., 2008. Introduction to Magnetic Materials. Wiley. https://doi.org/10.1002/9780470386323.
Dermont, G., Bergeron, M., Mercier, G., Richer-Lafleche, M., 2008. Soil washing for metal removal: a review of physical/chemical technologies and field applications. J. Hazard. Mater. 152, 1–31. https://doi.org/10.1016/j.jhazmat.2007.10.043.
Díaz, R.J., Rosenberg, R., 2008. Spreading dead zones and consequences for marine ecosystems. Science 321, 926–929. https://doi.org/10.1126/science.1156401.
Dixit, S., Hering, J.G., 2003. Comparison of arsenic(V) and arsenic(III) sorption onto iron oxide minerals. Environ. Sci. Technol. 37, 4182–4189. https://doi.org/10.1021/es030309t.
Dong, M., He, L., Jiang, M., Zhu, Y., Wang, J., Gustave, W., Wang, S., Deng, Y., Zhang, X., Wang, Z., 2023. Biochar for the removal of emerging pollutants from aquatic systems: a review. Int. J. Environ. Res. Public Health 20, 1679. https://doi.org/10.3390/ijerph20031679.
Du, J., Guo, Z., Li, R., Ali, A., Guo, D., Lahori, A.H., Wang, P., Liu, X., Wang, X., Zhang, Z., 2020. Screening of Chinese mustard (*Brassica juncea* L.) cultivars for the phytoremediation of Cd and Zn based on the plant physiological mechanisms. Environ. Pollut. 261, 114213. https://doi.org/10.1016/j.envpol.2020.114213.
Duan, C., Ren, J., Tao, L., Ren, H., Wang, M., Wang, B., 2023. Study of the remediation effect and mechanism of biochar-loaded nZVI on heavy metal contaminated soil. Sustainability 15, 16753. https://doi.org/10.3390/su152416753.
Duan, L., Wang, Q., Li, J., Wang, F., Yang, H., Guo, B., Hashimoto, Y., 2022. Zero valent iron or Fe3O4-loaded biochar for remediation of Pb contaminated sandy soil: sequential extraction, magnetic separation, XAFS and ryegrass growth. Environ. Pollut. 308, 119702. https://doi.org/10.1016/j.envpol.2022.119702.
Dzombak, D.A., Morel, F.M.M., 1990. Surface Complexation Modeling: Hydrous Ferric Oxide. Wiley-Interscience.
Elliston, T., Oliver, I.W., 2020. Ecotoxicological assessments of biochar additions to soil employing earthworm species *Eisenia fetida* and *Lumbricus terrestris*. Environ. Sci. Pollut. Res. 27, 33410–33418. https://doi.org/10.1007/s11356-019-04542-2.
Faheem, M., Wang, B., 2026. Biochar in circular economy and sustainable development: addressing technical variability, policy gaps, and sustainability constraints. Biochar, e001. https://doi.org/10.48130/bchax-0025-0014. X 2.
Fanyue, M., Wang, Y., Wei, Y., 2025. Advancements in biochar for soil remediation of heavy metals and/or organic pollutants. Materials 18, 1524. https://doi.org/10.3390/ma18071524.
Feng, D., Lü, J., Guo, S., Li, J., 2021. Biochar enhanced the degradation of organic pollutants through a Fenton process using trace aqueous iron. J. Environ. Chem. Eng. 9, 104677. https://doi.org/10.1016/j.jece.2020.104677.
Feng, Y., Liu, P., Wang, Y., Finfrock, Y.Z., Xie, X., Su, C., Liu, N., Yang, Y., Xu, Y., 2020. Distribution and speciation of iron in Fe-modified biochars and its application in removal of As(V), As(III), Cr(VI), and Hg(II): an X-ray absorption study. J. Hazard. Mater. 384, 121342. https://doi.org/10.1016/j.jhazmat.2019.121342.
Gallego-Ramírez, C., Chica, E., Rubio-Clemente, A., 2023. Life cycle assessment of raw and Fe-modified biochars: contributing to circular economy. Materials 16, 6059. https://doi.org/10.3390/ma16176059.
Ghosh, M., Singh, S.P., 2005. A review on phytoremediation of heavy metals and utilization of its byproducts. Appl. Ecol. Environ. Res. 3, 1–18. https://doi.org/10.15666/aeer/0301_001018.
Giles, C.H., Smith, D., Huitson, A., 1974. A general treatment and classification of the solute adsorption isotherm. J. Colloid Interface Sci. 47, 755–765. https://doi.org/10.1016/0021-9797(74)90252-5.
Glick, B.R., 2010. Using soil bacteria to facilitate phytoremediation. Biotechnol. Adv. 28, 367–374. https://doi.org/10.1016/j.biotechadv.2010.02.001.
Goldstein, J.I., et al., 2017. Scanning Electron Microscopy and X-Ray Microanalysis. Springer. https://doi.org/10.1007/978-1-4939-6676-9.
Goulson, D., 2013. An overview of the environmental risks posed by neonicotinoid insecticides. J. Appl. Ecol. 50, 977–987. https://doi.org/10.1111/1365-2664.12111.
Gross, A., Bromm, T., Polifka, S., Fischer, D., Glaser, B., 2024. Long-term biochar and soil organic carbon stability – evidence from field experiments in Germany. Sci. Total Environ. 954, 176340. https://doi.org/10.1016/j.scitotenv.2024.176340.
Guo, G., Lin, L., Jin, F., Mašek, O., Huang, Q., 2023. Application of heavy metal immobilization in soil by biochar using machine learning. Environ. Res. 231, 116098. https://doi.org/10.1016/j.envres.2023.116098.
Hagemann, N., Kammann, C.I., Schmidt, H.P., Kappler, A., Behrens, S., 2017. Nitrate capture and slow release in biochar amended compost and soil. PLoS One 12, e0171214. https://doi.org/10.1371/journal.pone.0171214.
Haghighi Mood, S., Pelaez-Samaniego, M.R., Han, Y., Mainali, K., Garcia-Perez, M., 2024. Iron- and nitrogen-modified biochar for nitrate adsorption from aqueous solution. Sustainability 16, 5733. https://doi.org/10.3390/su16135733.
Hale, S.E., et al., 2012. Quantifying the total and bioavailable polycyclic aromatic hydrocarbons and dioxins in biochars. Environ. Sci. Technol. 46, 2830–2838. https://doi.org/10.1021/es203984k.
He, H., Long, L., Fu, Z., 2024. Improving rice quality through biochar application in China: a meta-analysis. J. Environ. Manage. 371, 122701. https://doi.org/10.1016/j.jenvman.2024.122701.
He, J., Wang, B., Sun, H., et al., 2026. Iron-modified biochar enhanced the activation of peracetic acid for removal of imidacloprid: efficiency, active species and catalytic mechanism. Sci. Rep. https://doi.org/10.1038/s41598-026-46438-5.
Hiemstra, T., Van Riemsdijk, W.H., 1996. A surface structural approach to ion adsorption: the charge distribution (CD) model. J. Colloid Interface Sci. 179, 488–508. https://doi.org/10.1006/jcis.1996.0242.
Huang, J., Tan, X., Ali, I., Ok, Y.S., Duan, Z., Liang, J., Zhu, R., 2024. Efficient removal of nanoplastics by iron-modified biochar: understanding the removal mechanisms. Environ. Pollut. 363, 125121. https://doi.org/10.1016/j.envpol.2024.125121.
Huang, W., Bai, R., Chen, L., Wang, X., Li, Z., Tian, Y., 2026. Iron-based lignocellulosic biochar for Fenton-like treatment of organic wastewater: a review on progress and prospects. Environ. Res. 290, 123488. https://doi.org/10.1016/j.envres.2025.123488.
Hunter, R.J., 2013. Zeta Potential in Colloid Science. Academic Press. https://doi.org/10.1016/B978-0-12-361961-7.50004-3.
Hussain, F., Ahmed, S., Naqvi, S.M.Z.A., Awais, M., Zhang, Y., Zhang, H., Raghavan, V., Zang, Y., Zhao, G., Hu, J., 2025. Agricultural non-point source pollution: comprehensive analysis of sources and assessment methods. Agriculture 15, 531. https://doi.org/10.3390/agriculture15050531.
IARC, 2012. IARC Monographs on the Evaluation of Carcinogenic Risks to Humans, volume 100D. International Agency for Research on Cancer, Lyon.
Jatav, H.S., 2025. Biochar and circular economy approaches in environmental sustainability. Adv. Environ. Eng. Res. 6, 035. https://doi.org/10.21926/aeer.2504035.
Jeffery, S., Verheijen, F.G.A., Kammann, C., Abalos, D., 2016. Biochar effects on methane emissions from soils: a meta-analysis. Soil Biol. Biochem. 101, 251–258. https://doi.org/10.1016/j.soilbio.2016.07.021.
Jeffery, S., et al., 2011. A quantitative review of the effects of biochar application to soils on crop productivity using meta-analysis. Agric. Ecosyst. Environ. 144, 175–187. https://doi.org/10.1016/j.agee.2011.08.015.
Jeong, A.K., Vijayaraghavan, K., Reddy, D.H.K., Yun, Y.-S., 2018. A phosphorus-enriched biochar fertilizer from bio-fermentation waste: a potential alternative source for phosphorus fertilizers. J. Clean. Prod. 196, 163–171. https://doi.org/10.1016/j.jclepro.2018.06.004.
Jiang, P., Han, Y., Fang, L., 2026. Enhanced ARGs removal via wheat straw biochar-activated peroxymonosulfate: mechanisms and wastewater application. Sep. Purif. Technol. 380, 135512. https://doi.org/10.1016/j.seppur.2025.135512.
Kamal, A., Nazish, M., Kamal, K., et al., 2025. *Trichoderma harzianum*-loaded maize biochar enhances Cd–Cu immobilization and reduces bio-accessibility in contaminated soil. Sci. Rep. 15, 28099. https://doi.org/10.1038/s41598-025-13759-w.
Kancharla, S., Alexandridis, P., Tsianou, M., 2022. Sequestration of per- and polyfluoroalkyl substances (PFAS) by adsorption: surfactant and surface aspects. Curr. Opin. Colloid Interface Sci. 58, 101571. https://doi.org/10.1016/j.cocis.2022.101571.
Keiluweit, M., et al., 2010. Dynamic molecular structure of plant biomass-derived black carbon. Environ. Sci. Technol. 44, 1247–1253. https://doi.org/10.1021/es9031419.
Khalid, S., et al., 2017. A comparison of technologies for remediation of heavy metal contaminated soils. J. Geochem. Explor. 182, 247–268. https://doi.org/10.1016/j.gexplo.2016.11.021.
Klüpfel, L., et al., 2014. Redox properties of plant biomass-derived black carbon. Environ. Sci. Technol. 48, 5601–5611. https://doi.org/10.1021/es500906d.
Kracmarova-Farren, M., Alexova, E., Kodatova, A., et al., 2024. Biochar-induced changes in soil microbial communities: a comparison of two feedstocks and pyrolysis temperatures. Environ. Microbiome 19, 87. https://doi.org/10.1186/s40793-024-00631-z.
Kumar, N., Gaur, A.S., Sastry, G.N., 2021. A perspective on the nature of cation-π interactions. J. Chem. Sci. 133, 97. https://doi.org/10.1007/s12039-021-01959-6.
Lehmann, J., 2007. Bio-energy in the black. Front. Ecol. Environ. 5, 381–387. https://doi.org/10.1890/1540-9295(2007)5[381:BITB]2.0.CO;2.
Lehmann, J., Joseph, S., 2015. Biochar for Environmental Management, second ed. Routledge. https://doi.org/10.4324/9780203762264.
Li, H., Yu, L., Chen, Z., Xiao, B., Jin, K., 2024. The characteristics of adsorption Cr(VI) by iron-modified and iron-doped phosphorus-based biochar. Green Chem. Lett. Rev. 17. https://doi.org/10.1080/17518253.2024.2329607.
Li, K., Xu, W., Song, H., Bi, F., Li, Y., Jiang, Z., Tao, Y., Qu, J., Zhang, Y., 2024. Superior reduction and immobilization of Cr(VI) in soil utilizing sulfide nanoscale zero-valent iron supported by Li, X., Mu, L., Zhang, C., et al., 2023. Effect of amendments on

bioavailability of cadmium in soil-rice system: a field experiment study. Environ. Sci. Pollut. Res. 30, 37659–37668. https://doi.org/10.1007/s11356-022-24875-9.
Liao, X., Miranda-Avilés, R., Serafín Muñoz, A.H., et al., 2026. Assessing long-term stability of arsenic immobilization by iron-impregnated biochar under simulated irrigation and accelerated aging. Environ. Geochem. Health 48, 260. https://doi.org/10.1007/s10653-026-03149-0.
Lindsay, W.L., 1979. Chemical Equilibria in Soils. John Wiley & Sons.
Liu, C., Xu, X., He, A., Zhang, Y., Che, R., Yang, L., Wei, J., Wang, F., Hua, J., Shi, J., 2025. Research progress on the preparation of iron-manganese modified biochar and its application in environmental remediation. Toxics 13, 618. https://doi.org/10.3390/toxics13080618.
Liu, H., Wang, Y., Wang, S., Wu, J., Wang, Y., 2024. Release characteristics of biochar-derived dissolved organic matter and its impact on Cr(VI) adsorption and reduction. RSC Adv 14, 38171–38182. https://doi.org/10.1039/D4RA06172A.
Liu, L., Chen, P., Sun, M., et al., 2015. Effect of biochar amendment on PAH dissipation and indigenous degradation bacteria in contaminated soil. J. Soils Sediments 15, 313–322. https://doi.org/10.1007/s11368-014-1006-1.
Liu, L., He, N., Borham, A., Zhang, S., Xie, R., Zhao, C., Hu, J., Wang, J., 2023. The effect of iron-modified biochar on phosphorus adsorption and the prospect of synergistic adsorption between biochar and iron-oxidizing bacteria: a review. Water 15, 3315. https://doi.org/10.3390/w15183315.
Liu, M., Almatrafi, E., Zhang, Y., Xu, P., Song, B., Zhou, C., Zeng, G., Zhu, Y., 2022. A critical review of biochar-based materials for the remediation of heavy metal contaminated environment: applications and practical evaluations. Sci. Total Environ. 806, 150531. https://doi.org/10.1016/j.scitotenv.2021.150531.
Lu, L., Yu, W., Wang, Y., et al., 2020. Application of biochar-based materials in environmental remediation: from multi-level structures to specific devices. Biochar 2, 1–31. https://doi.org/10.1007/s42773-020-00041-7.
Lugon-Moulin, N., 2006. Cadmium concentration in phosphate fertilizers used for tobacco production. Agron. Sustain. Dev. 26, 151–155. https://doi.org/10.1051/AGRO:2006010.
Mark, M.S.H., Rao, P., Lo, I.M.C., 2011. Zero-valent iron and iron oxide-coated sand as a combination for removal of co-present chromate and arsenate from groundwater with humic acid. Environ. Pollut. 159, 377–382. https://doi.org/10.1016/j.envpol.2010.11.006.
Manyà, J.J., 2012. Pyrolysis for biochar purposes: a review to establish current knowledge gaps and research needs. Environ. Sci. Technol. 46, 7939–7954. https://doi.org/10.1021/es301029g.
Marchand, L., Brunel-Muguet, S., Lamy, I., et al., 2017. Modulation of trace element bioavailability for two earthworm species after biochar amendment into a contaminated technosol. Ecotoxicology 26, 1378–1391. https://doi.org/10.1007/s10646-017-1862-8.
Masud, M.A.A., Samaraweera, H., Mondol, M.M.H., et al., 2025. Iron biochar synergy in aquatic systems through surface functionalities electron transfer and reactive species dynamics. npj Clean Water 8, 46. https://doi.org/10.1038/s41545-025-00471-5.
Meng, F., Wang, Y., Wei, Y., 2025. Advancements in biochar for soil remediation of heavy metals and/or organic pollutants. Materials 18, 1524. https://doi.org/10.3390/ma18071524.
Morim, A.C., Madaleno, M., Tarelho, L.A.C., Silva, F.C., 2025. Financial feasibility of biochar production: a comparative analysis of business scenarios. J. Clean. Prod. 536, 147167. https://doi.org/10.1016/j.jclepro.2025.147167.
Moulder, J.F., et al., 1992. Handbook of X-ray Photoelectron Spectroscopy. Physical Electronics. https://doi.org/10.1002/sia.740030412.
Mukherjee, S., Sarkar, B., Aralappanavar, V.K., Mukhopadhyay, R., Basak, B.B., Srivastava, P., Marchut-Mikołajczyk, O., Bhatnagar, A., Semple, K.T., Bolan, N., 2022. Biochar-microorganism interactions for organic pollutant remediation: challenges and perspectives. Environ. Pollut. 308, 119609. https://doi.org/10.1016/j.envpol.2022.119609.
Myers, J.P., et al., 2016. Concerns over use of glyphosate-based herbicides and risks associated with exposures. Environ. Health 15, 19. https://doi.org/10.1186/s12940-016-0117-0.
Nachtegaal, M., Sparks, D.L., 2004. Effect of iron oxide coatings on zinc sorption mechanisms at the clay-mineral/water interface. J. Colloid Interface Sci. 276, 13–23. https://doi.org/10.1016/j.jcis.2004.03.031.
Neta, P., et al., 1988. Rate constants for reactions of inorganic radicals in aqueous solution. J. Phys. Chem. Ref. Data 17, 1027–1284. https://doi.org/10.1063/1.555808.
Newville, M., 2014. Fundamentals of XAFS. Rev. Mineral. Geochem. 78, 33–74. https://doi.org/10.2138/rmg.2014.78.2.
O'Neill, J., 2016. Tackling drug-resistant infections globally: final report and recommendations. The Review on Antimicrobial Resistance.
Obiri-Nyarko, F., et al., 2014. An overview of permeable reactive barriers for in situ sustainable groundwater remediation. Chemosphere 111, 243–259. https://doi.org/10.1016/j.chemosphere.2014.03.112.
Ortiz, D., Munoz, M., Nieto-Sandoval, J., Romera-Castillo, C., de Pedro, Z.M., Casas, J.A., 2022. Insights into the degradation of microplastics by Fenton oxidation: from surface modification to mineralization. Chemosphere 309, 136809. https://doi.org/10.1016/j.chemosphere.2022.136809.
Palansooriya, K.N., Shaheen, S.M., Chen, S.S., Tsang, D.C.W., Hashimoto, Y., Hou, D., Bolan, N.S., Rinklebe, J., Ok, Y.S., 2020. Soil amendments for immobilization of potentially toxic elements in contaminated soils: a critical review. Environ. Int. 134, 105046. https://doi.org/10.1016/j.envint.2019.105046.
Parfitt, R.L., 1979. Anion adsorption by soils and soil materials. Adv. Agron. 30, 1–50. https://doi.org/10.1016/S0065-2113(08)60702-6.
Pretty, J., et al., 2018. Global assessment of agricultural system redesign for sustainability. Nat. Sustain. 1, 441–446. https://doi.org/10.1038/s41893-018-0114-0.
Rajendran, S., et al., 2022. A critical review on various remediation approaches. Chemosphere 287, 132369. https://doi.org/10.1016/j.chemosphere.2021.132369.
Rathinapriya, P., Maharajan, T., Jothi, R., Prabakaran, M., Lee, I.-B., Yi, P.-H., Jeong, S. T., 2025. Unlocking biochar impacts on abiotic stress dynamics: a systematic review of soil quality and crop improvement. Front. Plant Sci. 15. https://doi.org/10.3389/fpls.2024.1479925.
Reddy, D.H.K., Lee, S.-M., 2014. Magnetic biochar composite: facile synthesis, characterization, and application for heavy metal removal. Colloids Surf. A 454, 96–103. https://doi.org/10.1016/j.colsurfa.2014.03.105.
Saharudin, D.M., Jeswani, H.K., Azapagic, A., 2024. Biochar from agricultural wastes: environmental sustainability, economic viability and the potential as a negative emissions technology in Malaysia. Sci. Total Environ. 919, 170266. https://doi.org/10.1016/j.scitotenv.2024.170266.
Sanford, R.A., Wagner, D.D., Wu, Q., Chee-Sanford, J.C., Thomas, S.H., Cruz-García, C., Rodríguez, G., Massol-Deyá, A., Krishnani, K.K., Ritalahti, K.M., Nissen, S., Konstantinidis, K.T., Löffler, F.E., 2012. Unexpected nondenitrifier nitrous oxide reductase gene diversity and abundance in soils. Proc. Natl. Acad. Sci. U.S.A. 109, 19709–19714. https://doi.org/10.1073/pnas.1211238109.
Saraei, F., Amini, K., Goodarzi, R., et al., 2026. A magnetically recoverable chitosan-based nanocomposite for simultaneous removal of tetracycline and antibiotic resistance genes from wastewater. Sci. Rep. 16, 817. https://doi.org/10.1038/s41598-025-30583-4.
Shah, S.S.H., Imura, T., Nakagawa, K., 2023. Assessment of heavy metals uptake by carrot at different contamination levels of soil. In: Ujikawa, K., Ishiwatari, M., Hullebusch, E.v. (Eds.), Environment and Sustainable Development. Springer, Singapore, p. 30. https://doi.org/10.1007/978-981-99-4101-8_30.
Sharpley, A., et al., 2013. Phosphorus legacy: overcoming the effects of past management practices to mitigate future water quality impairment. J. Environ. Qual. 42, 1308–1326. https://doi.org/10.2134/jeq2013.03.0098.
Shen, J., et al., 2011. Phosphorus dynamics: from soil to plant. Plant Physiol 156, 997–1005. https://doi.org/10.1104/pp.111.175232.
Siddiqui, M.H., 2025. Long-term impacts of biochar on soil health. Geoderma 440, 116855. https://doi.org/10.1016/j.geoderma.2024.116855.
Siddiqui, S., 2025. Unlocking the environmental potential of biochar: production, applications, and limitations. Front. Sustain. Food Syst. 9. https://doi.org/10.3389/fsufs.2025.1569941.
Silva, V., et al., 2019. Pesticide residues in European agricultural soils. Sci. Total Environ. 653, 1532–1545. https://doi.org/10.1016/j.scitotenv.2018.10.441.
Socrates, G., 2004. Infrared and Raman Characteristic Group Frequencies. John Wiley & Sons.
Song, K., Jiang, S., Liu, Z., Cai, Y., Liu, W., Bian, R., Zhang, X., Zheng, J., Li, L., 2024. Biochar improves soil organic carbon sequestration potential in the topsoil and subsoil of a paddy field. Curr. Res. Environ. Sustain. 8, 100267. https://doi.org/10.1016/j.crsust.2024.100267.
Sparks, D.L., 2003. Environmental Soil Chemistry. Academic Press. https://doi.org/10.1016/B978-0-12-656446-4.X5000-2.
Strawn, D.G., Crump, A.R., Peak, D., Garcia-Perez, M., Möller, G., 2023. Reactivity of Fe-amended biochar for phosphorus removal and recycling from wastewater. PLOS Water 2, e0000092. https://doi.org/10.1371/journal.pwat.0000092.
Su, J.Z., et al., 2023. Economic feasibility of iron-enriched biochar production. Renew. Sustain. Energy Rev. 178, 113245. https://doi.org/10.1016/j.rser.2023.113245.
Sun, X., Wang, J., Zhang, M., Liu, Z., E, Y., Lan, Y., He, T., Meng, J., 2023. Effects of biochar on the Cd uptake by rice and the Cd fractions in paddy soil: a 3-year field experiment. Agronomy 13, 1335. https://doi.org/10.3390/agronomy13051335.
Tai, Y.L., Dempsey, B.A., 2009. Nitrite reduction with hydrous ferric oxide and Fe(II): stoichiometry, rate, and mechanism. Water Res 43, 546–552. https://doi.org/10.1016/j.watres.2008.10.055.
Tang, F.H.M., et al., 2021. Global pesticide residue in agricultural soils. Nat. Geosci. 14, 206.
Tang, R., Yao, S., Liu, Y., Ren, T., Ma, J., Gong, X., Li, G., Ma, R., Yuan, J., 2025. Iron-modified biochar enhanced nitrogen retention during composting: bridging chemisorption and microbiome modulation. Chem. Eng. J. 513, 162761. https://doi.org/10.1016/j.cej.2025.162761.
Tang, X., Jin, Z., Zou, R., Zhu, Y., Yao, X., Li, M., Song, S., Liu, S., Zeng, T., 2024. Sustainable electrochemical activation of self-generated persulfate for the degradation of endocrine disruptors: kinetics, performances, and mechanisms. Toxics 12, 156. https://doi.org/10.3390/toxics12020156.
Teng, F., Zhang, Y., Wang, D., Shen, M., Hu, D., 2020. Iron-modified rice husk hydrochar and its immobilization effect for Pb and Sb in contaminated soil. J. Hazard. Mater. 398, 122977. https://doi.org/10.1016/j.jhazmat.2020.122977.
Teng, X., Yang, W., Chen, H., Wu, X., Tang, J., Yang, X., Liu, Z., Liu, D., Xu, W., 2026. Superior simultaneous immobilization of cadmium and arsenic by ferrihydrite-modified biochar: performance and mechanisms. Front. Environ. Sci. 13. https://doi.org/10.3389/fenvs.2025.1717178.
Thomas, S.C., Gale, N., 2015. Biochar and forest restoration: a review and meta-analysis of tree growth responses. New For 46, 931–946. https://doi.org/10.1007/s11056-015-9491-7.
Tiberg, C., Gustafsson, J.P., 2016. Phosphate effects on cadmium(II) sorption to ferrihydrite. J. Colloid Interface Sci. 471, 103–111. https://doi.org/10.1016/j.jcis.2016.03.016.
Tilman, D., et al., 2011. Global food demand and the sustainable intensification of agriculture. Proc. Natl. Acad. Sci. U.S.A. 108, 20260–20264. https://doi.org/10.1073/pnas.1116437108.

Tomczyk, A., Sokołowska, Z., Boguta, P., 2020. Biochar physicochemical properties: pyrolysis temperature and feedstock kind effects. Rev. Environ. Sci. Biotechnol. 19, 191–215. https://doi.org/10.1007/s11157-020-09523-3.
Trenkel, M.E., 2010. Slow- and Controlled-Release and Stabilized Fertilizers, second ed. International Fertilizer Industry Association, Paris.
Tsitonaki, A., et al., 2010. In situ chemical oxidation of contaminated soil and groundwater using persulfate. Crit. Rev. Environ. Sci. Technol. 40, 55–91. https://doi.org/10.1080/10643380802039303.
UNEP, 2021. Becoming Generation Restoration: Recommendations for the UN Decade on Ecosystem Restoration.
USEPA, 1992. Toxicity Characteristic Leaching Procedure (TCLP). Method 1311. US Environmental Protection Agency.
Van Boeckel, T.P., et al., 2015. Global trends in antimicrobial use in food animals. Proc. Natl. Acad. Sci. U.S.A. 112, 5649–5654. https://doi.org/10.1073/pnas.1503141112.
Van der Ent, A., et al., 2013. Hyperaccumulators of metal and metalloid trace elements: facts and fiction. Plant Soil 362, 319–334. https://doi.org/10.1007/s11104-012-1287-3.
Vu, K.T., Lan, P.D.T., Nguyen, N.T.H., Thanh, H.N., 2022. Cadmium immobilization in the rice-paddy soil with biochar additive. J. Ecol. Eng. 23, 85–95. https://doi.org/10.12911/22998993/146331.
Wang, L., Chen, D., Zhu, L., 2023. Biochar carbon sequestration potential rectification in soils: synthesis effects of biochar on soil CO2, CH4 and N2O emissions. Sci. Total Environ. 904, 167047. https://doi.org/10.1016/j.scitotenv.2023.167047.
Wang, L., O'Connor, D., Rinklebe, J., Ok, Y.S., Tsang, D.C.W., Shen, Z., Hou, D., 2020. Biochar aging: mechanisms, physicochemical changes, assessment, and implications for field applications. Environ. Sci. Technol. 54, 14797–14814. https://doi.org/10.1021/acs.est.0c04033.
Wang, M., Xie, Y., Gao, Y., Huang, X., Chen, W., 2024. Machine learning prediction of higher heating value of biochar based on biomass characteristics and pyrolysis conditions. Bioresour. Technol. 395, 130364. https://doi.org/10.1016/j.biortech.2024.130364.
Wang, Y., Munir, T., Wu, X., Huang, Y., Li, B., 2025. Phosphorus recovery and reuse: innovating with biochar in the circular economy. Sci. Total Environ. 973, 179143. https://doi.org/10.1016/j.scitotenv.2025.179143.
Wang, Y., Shui, W., 2021. Agricultural nonpoint source pollution in urban agricultural areas: an assessment system and mitigation methods. Hum. Ecol. Risk Assess. 27, 405–430. https://doi.org/10.1080/10807039.2020.1724076.
Wang, Y., Wan, S., Yu, W., Yuan, D., Sun, L., 2022. The role of Fe3O4@biochar as electron shuttle in enhancing the biodegradation of gaseous para-xylene by aerobic surfactant secreted strains. J. Hazard. Mater. 438, 129475. https://doi.org/10.1016/j.jhazmat.2022.129475.
Wang, Z., Xiang, Q., Zhang, D., Xue, A., Fang, Y., Hu, S., 2026. Research progress on biochar-based photocatalytic materials for pollutant treatment: structural regulation, electronic mechanisms, and engineering challenges. Ecotoxicol. Environ. Saf. 310, 119793. https://doi.org/10.1016/j.ecoenv.2026.119793.
Wei, Y., Ma, J., Liu, K., Zhang, S., Wang, J., 2025. Biochar-based remediation of heavy metal-contaminated soils: mechanisms, synergies, and sustainable prospects. Nanomaterials 15, 1487. https://doi.org/10.3390/nano15191487.
Wen, E., Yang, X., Chen, H., Shaheen, S.M., Sarkar, B., Xu, S., Song, H., Liang, Y., Rinklebe, J., Hou, D., Li, Y., Wu, F., Pohořelý, M., Wong, J.W.C., Wang, H., 2021. Iron-modified biochar and water management regime-induced changes in plant growth, enzyme activities, and phytoavailability of arsenic, cadmium and lead in a paddy soil. J. Hazard. Mater. 407, 124344. https://doi.org/10.1016/j.jhazmat.2020.124344.
WHO, 2024. Human health effects of benzene, arsenic, cadmium, nickel, lead and mercury: report of an expert consultation.
Woolf, D., Amonette, J., Street-Perrott, F., et al., 2010. Sustainable biochar to mitigate global climate change. Nat. Commun. 1, 56. https://doi.org/10.1038/ncomms1053.
Xiang, W., Zhang, X., Chen, J., Zou, W., He, F., Hu, X., Tsang, D.C.W., Ok, Y.S., Gao, B., 2020. Biochar technology in wastewater treatment: a critical review. Chemosphere 252, 126539. https://doi.org/10.1016/j.chemosphere.2020.126539.
Xin, S., Liu, G., Ma, X., Gong, J., Ma, B., Yan, Q., Chen, Q., Ma, D., Zhang, G., Gao, M., Xin, Y., 2021. High efficiency heterogeneous Fenton-like catalyst biochar modified CuFeO2 for the degradation of tetracycline: economical synthesis, catalytic performance and mechanism. Appl. Catal. B 280, 119386. https://doi.org/10.1016/j.apcatb.2020.119386.
Xu, X., Cheng, K., Wu, H., Sun, J., Yue, Q., Pan, G., 2019. Greenhouse gas mitigation potential in crop production with biochar soil amendment—a carbon footprint assessment for cross-site field experiments from China. GCB Bioenergy 11, 592–605. https://doi.org/10.1111/gcbb.12561.
Yang, F., Wang, B., Shi, Z., Li, L., Li, Y., Mao, Z., Wu, Y., 2021. Immobilization of heavy metals (Cd, Zn, and Pb) in different contaminated soils with swine manure biochar. Environ. Pollut. Bioavailab. 33, 55–65. https://doi.org/10.1080/26395940.2021.1916407.
Yang, X., Tian, X., Xue, Y., Wang, C., 2025. Application of iron-modified biochar in the fields of adsorption and degradation of antibiotics. J. Environ. Manage. 380, 124875. https://doi.org/10.1016/j.jenvman.2025.124875.
Ye, L., Camps-Arbestain, M., Shen, Q., Lehmann, J., Singh, B., Sabir, M., 2020. Biochar effects on crop yields with and without fertilizer: a meta-analysis of field studies using separate controls. Soil Use Manage 36, 2–18. https://doi.org/10.1111/sum.12546.
Yi, Y., Huang, Z., Lu, B., Xian, J., Tsang, E.P., Cheng, W., Fang, J., Fang, Z., 2020. Magnetic biochar for environmental remediation: a review. Bioresour. Technol. 298, 122468. https://doi.org/10.1016/j.biortech.2019.122468.
Yin, Y., Ding, C., Tang, X., Zhou, Z., Nie, M., Yuan, Y., Qian, Y., He, L., Li, Z., Guo, Z., Li, L., Zhao, Q., Zhang, T., Lai, L., Wang, Y., Wang, X., 2024. Reducing cadmium and arsenic accumulation in rice grains: the coupled effect of sulfur's biomass dilution and soil immobilization analyzed using meta-analysis and machine learning. Sci. Total Environ. 955, 177157. https://doi.org/10.1016/j.scitotenv.2024.177157.
Ying, S.F., Chin, B.L.F., Lock, S.S.M., Yiin, C.L., Tan, Y.H., Zheng, G., Ge, S., Liew, R.K., Lam, S.S., 2024. Enhancing wastewater treatment with engineered biochar from microwave-assisted approach - a comprehensive review. Environ. Technol. Innov. 36, 103835. https://doi.org/10.1016/j.eti.2024.103835.
Yuan, J.H., et al., 2014. The forms of alkalis in the biochar produced from crop residues at different temperatures. Bioresour. Technol. 102, 3488–3497. https://doi.org/10.1016/j.biortech.2010.11.018.
Zhang, Y., Chen, H., Islam, S., 2025. Advances in biochar modification for environmental remediation with emphasis on iron functionalization. Biochar X 1, e009. https://doi.org/10.48130/bchax-0025-0010.
Zhang, Z., Yu, H., Zhu, R., Zhang, X., Yan, L., 2020. Phosphate adsorption performance and mechanisms by nanoporous biochar-iron oxides from aqueous solutions. Environ. Sci. Pollut. Res. 27, 28132–28145. https://doi.org/10.1007/s11356-020-09166-5.
Zhao, J., Wang, L., Chu, G., 2023. Comparison of the sorption of Cu(II) and Pb(II) by bleached and activated biochars: insight into complexation and cation–π interaction. Agronomy 13, 1282. https://doi.org/10.3390/agronomy13051282.
Zhou, R., Zhang, M., Shao, S., 2022. Optimization of target biochar for the adsorption of target heavy metal ion. Sci. Rep. 12, 13662. https://doi.org/10.1038/s41598-022-17901-w.
Zhu, X., Li, J., Xie, B., Feng, D., Li, Y., 2020. Accelerating effects of biochar for pyrite-catalyzed Fenton-like oxidation of herbicide 2,4-D. Chem. Eng. J. 391, 123605. https://doi.org/10.1016/j.cej.2019.123605.
Zhu, X., Zhang, Z., Du, A., Liu, B., 2026. Effect of dry–wet cycling on methanotrophs in wetland soils. Biology 15, 279. https://doi.org/10.3390/biology15030279.
Zhu, Z., Zhang, L., Chen, F., Duan, W., Li, F., Zhang, D., 2025. Mechanism of modified biochar in mitigating carbon and nitrogen loss in drought soil with green manure application. Agronomy 15, 2193. https://doi.org/10.3390/agronomy15092193.